THERMAL AND THERMOMECHANICAL PROPERTIES OF CLAY CONTAINING POLYMER NANOCOMPOSITES

By

MAMOOKHO ELIZABETH MAKHATHA (M.Sc.)

submitted in accordance with the requirements for the degree

PHILOSOPHIAE DOCTOR (Ph.D.)

in the

Department of Chemistry

Faculty of Natural and Agricultural Sciences

at the

UNIVERSITY OF THE FREE STATE (QWAQWA CAMPUS)

SUPERVISOR: PROF. A. S LUYT

CO-SUPERVISOR: PROF. S. SINHA RAY

DECEMBER 2009

DECLARATION

We, the undersigned, hereby declare that the research in this thesis is Mrs. Makhatha's own original work, which has not partly or fully been submitted to any other university in order to obtain a degree.

_____	_____
Mrs ME Makhatha	Prof AS Luyt
	_____
	Prof S Sinha Ray

DEDICATION

This work is dedicated to my husband **Tsietsi Shadrack Makhatha** and our lovely son **Lesedi Bokang Makhatha**.

ACKNOWLEDGEMENTS

Firstly, my utmost thanks to the Almighty God for the opportunity to undertake this study and for His grace, without which this study would not have been possible and the support, hard work and endless efforts of a large number of individuals and institutions.

I would like to thank my supervisor, **Prof. Adriaan Stephanus Luyt,** for his great efforts to explain things clearly and simply, and his guidance during my research. I express my deep sense of gratitude for his guidance, cloudless source of inspiration and constant support all through the course of the study. Throughout my thesis-writing period, he provided encouragement, sound advice, good teaching, good company, and lots of good ideas. His overly enthusiasm and integral view on research and his mission for providing 'only high-quality work and not less', has made a deep impression on me. I owe him lots of gratitude for having me shown this way of research not only now but since I was a second year at university. He could not even realize how much I have learned from him. He has not only been there as promoter but also as a father who wouldn't let his child miss directions. I am grateful to acknowledge **Prof. Luyt's** wife for understanding and the support that she gives him, especially throughout thethesis-writing period. I am really glad that I have come to know **Prof. Luyt** in my life.

I would like to gratefully thank my enthusiastic co-supervisor, **Assoc. Prof. S. Sinha Ray**, during this work, who shared with me a lot of his expertise and research insight. His thoughtful advice often served to give me a sense of direction during my PhD studies. This opportunity to work with him, his continued support, understanding and the encouragement during the course of these studies has made me succeed to this far.

I would like to express my sincere gratitude to Jayita Bandyopadhyay who endlessly helped me to discuss the results and contributed to this work in numerous ways. I couldn't have wished for better colleagues to work with. Special thanks are due to all my colleagues, the past and present associates and students in the National Centre for Nanostructured Materials (NCNSM) for their valuable discussions, help and for their awesome company (Dr. Sarah Mohlala, Nonhlanhla Cele, Letlhogonolo Mabena, Mpitloane Hato, Thabo Gcwabaza and James Ramontja).

I am tempted to individually thank all of my friends which, from my childhood until graduate school, have joined me in the discovery of what life is all about and how to make the best of it and for helping me get through the difficult times, for all the emotional support, entertainment, and caring they provided. However, because the list might be too long and by fear of leaving someone out, I simply say thank you very much to all of you. No matter where I go you will always remain in my heart.

Many thanks are due to my pride and joy, my family, my parents and in-laws who have nurtured my very existence with love (Nkupi P. Maloka, Halieo P. Maloka, Sekgalajwe M. Makhatha and Puseletso J. Makhatha). To them I dedicate this thesis.

I wish to thank my brothers (Maluke A., Geelbooi D., and Khotso J. Maloka), brothers in-law (Lehlohonolo M., and Ramotete A. Makhatha), sisters and sister in-law (Masehlomeng E.,Matsietsi A. Maloka and Ntswaki J. Makhatha) for providing a loving environment, for all the emotional support and for helping me get through the difficult times. Special thanks to Hlomi, "Matope" Keneuwe E., Modiehi "Manana" and Khotso Maloka and Enie Khaka) who would leave everything that makes them happy to come and help me when I needed them the most, they are the apple of my eye, and all my wonderful cousins.

I want to acknowledge the CSIR and the Department of Science and Technology (DST) for financial support, because without their support my work at the University of the Free State would remain just a dream.

Lastly, and most importantly, I would like to thank my husband, **Tsietsi S. Makhatha**, for God has given me the most precious person. He has loved me unconditionally and stood by my side like a rock. Most importantly, he has taken very good care of our son, **Lesedi Makhatha,** when times were hard in this project.

"Modimo o Lerato"

ABSTRACT

The main focus of this research project was to understand the effect of clay particles incorporation on the thermal and thermomechanical behaviour of biodegradable polymers. Clay minerals, due to their unique layered structure, rich intercalation chemistry and availability at low cost, are promising nano-particles reinforcement for polymers to manufacture low cost, light weight, and high performance nanocomposites. Up to this date very few attention has been given to using nano-dimentional clay particles as a means of increasing the crystallinity and improving the thermal and mechanical properties. Understanding the structure-property relationship in polymer-clay layered silicate nanocomposites is of fundamental importance in designing materials with desired properties. To understand the relations, in the case of poly(ethylene succinate) (PES), poly(butylene succinate) (PBS) and the organically modified layered silicates: montmorillonite (MMT) and synthetic fluorine mica (SFM), wide-angle x-ray diffraction (WAXRD), small-angle x-ray scattering (SAXS) and transmission electron microscopy (TEM) analyses were conducted for the structural and morphological analysis.

The PES/OMMT nanocomposite was prepared by a solution-intercalation-film-casting technique. SAXS and TEM observations show the homogeneous dispersion of silicate layers in the PES matrix. The crystallization and melting behaviour of the PES matrix in the presence of the dispersed silicate layers were studied by differential scanning calorimetry (DSC), polarized optical microscopy (POM), and WAXRD. The results show that the incorporation of OMMT stops the super-cooling effect and significantly accelerates the mechanism of nucleation and crystal growth of the PES matrix. The incorporation of OMMT also significantly improves the thermal stability of the PES.

The effect of the change of variables like temperature, time, and heating rate on the crystallization behaviour was studied. It was observed that the double melting behaviour of the PBS matrix is a function of these variables. Various models namely the Avrami method, the Ozawa method, and the combined Avrami-Ozawa method, were applied to describe the kinetics of the pure PBS and its nanocomposite samples during non-isothermal crystallization. The Ozawa equation did not provide an adequate description of the non-isothermal crystallization kinetics of PBS and its nanocomposite. In contrast, the Avrami analysis

modified by Jeziorny and the method developed by Liu et al. were successful in describing the non-isothermal crystallization kinetics of pure PBS and its nanocomposite. The results show that the crystal growth of the PBS matrix retards in the presence of dispersed intercalated organoclays and supports the reduced crystallization of the PBS matrix in the presence of Cloisite® 30B nanoclay.

The structure and morphology of the PBS nanocomposites, with three different weight ratios of organically modified synthetic fluorine mica (OMSFM) were also characterized. We observed the homogeneous dispersion of the intercalated silicate layers into the PBS matrix. The thermal properties of pure PBS and the nanocomposite samples were studied by both conventional and temperature modulated differential scanning calorimetry (DSC) analysis, which shows multiple melting behaviour of the PBS matrix. The investigation of the thermomechanical properties was performed by dynamic mechanical analysis (DMA). The results reveal a significant improvement in the storage modulus of the PBS in the presence of OMSFM. The tensile modulus of the PBS is also significantly increased in the presence of OMSFM. However, the yield strength and the elongation at break of the PBS systematically decrease with the loading of OMSFM. The thermal stability of the nanocomposites compared to that of the pure polymer sample was examined under both pyrolytic and thermo-oxidative environments. The thermal stability of PBS increased moderately in the presence of 3 wt% of OMSFM, but there is no significant effect on further silicate loading in the oxidative environment. In the nitrogen environment, however, the thermal stability systematically decreased with increasing clay loading.

PUBLICATIONS

I. **M.E. Makhatha**, S.Sinha Ray, J. Hato, A.S. Luyt, M. Bousmina. Thermal and thermomechanical properties of poly(butylene succinate) nanocomposites. Journal of Nanoscience and Nanotechnology 2007; 8:1679-1689 (DOI: 10.1166/jnn.2008.035).

II. **M.E. Makhatha**, S.Sinha Ray, A.S. Luyt. Unusual thermal properties of poly(ethylene succinate) nanocomposites. Division of Polymeric Materials: Science & Engineering; 236th ACS National Meeting, Philadelphia, PA, 2008.

III. S.Sinha Ray, **M.E. Makhatha**. Thermal properties of poly(ethylene succinate) nanocomposite. Polymer 2009; 50:4635-4643 (DOI: 10.1016/j.polymer.2009.07.025)

IV. **M.E. Makhatha**, S.Sinha Ray, A.S. Luyt. Crystallization kinetics and melting behaviour of a poly(butylene succinate)/clay nanocomposite. Journal of Nanoscience and Nanotechnology (Submitted December 2009).

PRESENTATIONS

I. Nano-Africa, Poster presentation, Council for Science and Industrial Research (CSIR), RSA, November 2009.

II. National Centre for Nano-structured Materials Colloquium, Oral presentation, CSIR, RSA, August 2008

III. American Chemical Society (ACS), Oral presentation, Philadelphia, Pennsylvania, USA, August 2008.

IV. International Centre for Materials Research (ICMR), Poster presentation, Richards Bay, RSA, July 2007.

V. Fiber reinforced composites, Poster presentation CSIR, Port Elizabeth, RSA, December 2007.

ABREVIATIONS

AAC	: Aliphatic-aromatic copolyesters
AFM	: Atomic force microscopy
AIBN	: Azobis(isobutyronitrile)
ALA	: Aminolauric acid
BAPs	: Biodegradable aliphatic polyesters
Bz	: Benzyl
C30B	: Cloisite 30B
CEC	: Cation-exchange capacity
DSC	: Differential scanning calorimetry
DMA	: Dynamic mechanical analysis
dTGA	: Derivative TGA
FTIR	: Fourier transform infrared spectroscopy
HAD	: Hexadecylamine
HDT	: Heat distortion temperature
HRR	: Heat release rate
HRTEM	: High resolution TEM
MAPP	: Maleinated polypropylene
MMT	: Montmorillonite
NMR	: Nuclear magnetic resonance
OMLS	: Organically modified layered silicates
OMMT	: Organically modified montmorillonite
OM-SFM	: Organically modified synthetic fluorine mica
o-PCL	: Oligo-poly(ε-caprolactone)
PAA	: Poly(acrylic acid)
PBAT	: Polybutylene adipate/terephthalate
PBS	: Poly(butylene succinate)
PBSA	: Polybutylene succinate adipate
PCL	: Polycaprolactone
PEO	: Poly(ethylene oxide)
PES	: Poly(ethylene succinate)
PET	: Polyethylene terephthalate

PHA : Polyhydroxyalkanoates
PHB : Polyhydroxybutyrate
PHH : Polyhydroxyhexanoate
PHV : Polyhydroxyvalerate
PLA : Polylactide
PLACNs : Polylactide/clay nanocomposites
PMMA : Poly(methylmethacrylate)
POM : Polarized optical microscope
PP : Polypropylene
PP-MA : PP-maleic anhydride
PS3Br : Poly(3-bromostyrene)
PS-PI : Polystyrene-polyisoprene
PTMAT : Polymethylene adipate/terephthalate
PVCH : Poly(vinylcyclohexane)
PVOH : Poly(vinyl alcohol)
PVP : Poly(vinylpyridine)
PVPyr : Poly(vinylpyrrolidone)
SANS : Small-angle neutron scattering
SAXS : Small-angle x-ray scattering
SBS : Styrene-butadiene-styrene
SEM : Scanning electron microscopy
SFC : Self-consistent field theory
SFM : Synthetic fluorine mica
TEM : Transmission electron microscopy
TGA : Thermogravimetric analysis
TMDSC : Temperature modulated DSC
USA : United states of America
WXRD : Wide-angle x-ray diffraction

CONTENTS

LIST OF TABLES

LIST OF FIGURES

CHAPTER 1

INTRODUCTION

1.1 Overview

This introductory chapter aims to provide a foundation and background covering the main aspects that are common throughout the separate projects detailed in this thesis. These underlying themes are polymers, nanocomposites, and clays. The idea and importance of nano-scale materials will be introduced. The theory of how and why the sizes of nanoparticles affect their properties will be discussed, along with potential applications. The existing general synthetic strategies for the formation of nanoparticles are outlined to provide context. Polymers will be defined and some fundamental properties explained. The history and importance of the production of polymeric materials will then be reviewed before the topic of blending nanoparticles into polymeric substrates is detailed in both *in-situ* and *ex-situ* terms. The final section aims to provide an understanding of the use and properties of nanocomposites, especially in relation to organically modified clay galleries, and to show how they can be used for the processing of polymers and the introduction of nanoparticles into host materials. As the separate projects covered in this thesis differ substantially in some areas (preparatory methods), this chapter provides only a brief introduction to some important topics. These will be expanded in greater detail in the specific chapter they relate to.

1.2 Nanocomposite materials

The definition [1] of a nano-composite material encompasses a large variety of systems such as one-dimensional, two-dimensional, three-dimensional and amorphous materials, made of distinctly dissimilar components and mixed at the nanometer scale. Nanocomposites are found in nature, for example in the structure of the abalone shell and bone. In the broadest sense this definition can include porous media, colloids, gels and copolymers, but is more usually taken to mean the solid combination of nano-dimensional phases differing in properties due to dissimilarities in structure and chemistry.

The general class of nanocomposite organic/inorganic materials is a fast growing area of research. Significant effort is focused [2] on the ability to obtain control of the nanoscale structures via innovative synthetic approaches. The properties of nano-composite materials depend not only on the properties of their individual parents, but also on their morphology and interfacial characteristics. This rapidly expanding field generates many exciting new materials with novel properties, derives by combining properties from the parent constituents into a single material. There is also the possibility of new properties which are unknown in the parent constituent materials.

The inorganic components can be three-dimensional framework systems such as zeolites, two-dimensional layered materials such as clays, metal oxides, metal phosphates, chalcogenides, and even one-dimensional and zero-dimensional materials such as $(Mo_3Se_3\text{-})_n$ chains and clusters [1-3]. Experimental work has generally shown that virtually all types and classes of nanocomposite materials lead to new and improved properties when compared to their microcomposite counterparts. Therefore, nanocomposites promise new applications in many fields such as mechanically reinforced lightweight components, non-linear optics, battery cathodes and ionics, nano-wires, sensors and other systems.

The general class of organic/inorganic nanocomposites may also be of relevance to bio-ceramics and biomineralization in which *in-situ* growth and polymerization of the biopolymer and inorganic matrix occurs. Lamellar nanocomposites represent an extreme case of a composite in which interface interactions between the two phases are maximized. Since the remarkable properties of conventional composites are mainly due to interfacial interactions, the nanocomposites could provide good model systems in which such interactions can be studied in detail using conventional bulk sample (as opposed to surface) techniques. By judiciously engineering the polymer-host interactions [4], nanocomposites may be produced with a broad range of properties.

There is a big variety of norganic layered materials. They possess well defined, ordered intralamellar spaces potentially accessible to foreign species. This ability enables them to act as matrices or hosts for polymers, yielding interesting hybrid nano-composite materials. The use of nanoparticle rich materials long predates the understanding of the physical and chemical nature of these materials. Jose-Yacaman *et al.* [3] investigated the origin of the depth of colour and the resistance to acids and bio-corrosion of Maya blue paint, attributing it

to a nanoparticle mechanism. From the mid 1950s nanoscale organo-clays have been used to control the flow of polymer solutions (e.g. as paint viscosifiers) or the constitution of gels (e.g. as a thickening substance in cosmetics, keeping the preparations in a homogeneous state). By the 1970s polymer/clay composites was the topic of textbooks [5], although the term "nanocomposites" was not in common use.

Lamellar nano-composites can be divided into two distinct classes, intercalated and exfoliated. In the former, the polymer chains alternate with the inorganic layers in a fixed compositional ratio and have a well defined number of polymer layers in the intralamellar space. In exfoliated nano-composites the number of polymer chains between the layers is almost continuously variable and the layers are separated by more than 100 Å. The intercalated nano-composites are also more compound-like because of the fixed polymer/layer ratio, and they are interesting for their electronic and charge transport properties. On the other hand, exfoliated nano-composites are more interesting for their superior mechanical properties [2-6].

1.3 Biodegradable polyesters

Polyesters play a predominant role as biodegradable plastics due to their potentially hydrolysable ester bonds. As shown in Figure 1, the polyester family is made up of two major groups – aliphatic and aromatic polyesters. The following biodegradable polyesters have been developed commercially, or are in commercial development:

PHA – polyhydroxyalkanoates	PHB - polyhydroxybutyrate
PHH – polyhydroxyhexanoate	PHV - polyhydroxyvalerate
PLA - polylactic acid	PCL - polycaprolactone
PBS - polybutylene succinate	PBSA – polybutylene succinate adipate
AAC - Aliphatic-Aromatic copolyesters	PET - polyethylene terephthalate
PBAT-polybutylene adipate/terephthalate	PTMAT-polymethylene adipate/terephthalate

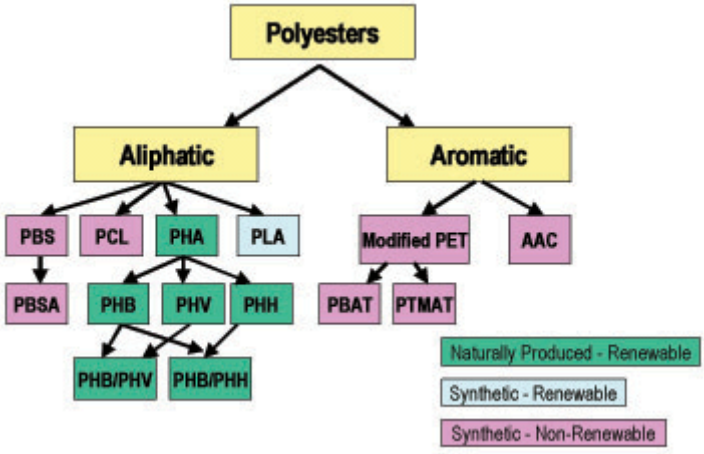

Figure 1.1 Biodegradable polyester family

While aromatic polyesters such as PET exhibit excellent material properties, they are almost totally resistant to microbial attack. Aliphatic polyesters on the other hand are readily biodegradable, but lack good mechanical properties that are critical for most applications. All polyesters degrade eventually, with hydrolysis (degradation induced by water) being the dominant mechanism. Synthetic aliphatic polyesters are synthesised from diols and dicarboxylic acids via condensation polymerisation, and are known to be completely biodegradable in soil and water. These aliphatic polyesters are, however, much more expensive and lack mechanical strength compared to conventional plastics such as polyethylene. Many of these polyesters are blended with starch based polymers for cost competitive biodegradable plastics applications. Aliphatic polyesters have better moisture resistance than starches, which have many hydroxyl groups.

It is well known that aliphatic polyesters have a high level of biodegradability. Aliphatic polyesters are usually synthesized by polycondensation or ring-opening polymerization of lactones. The low melting point of poly(caprolactone) (PCL) makes it undesirable for use in biodegradable plastics, and this gave rise to the development of various PCL copolymers and blends [7]. About 20 years ago Showa High Polymer commercialized aliphatic polyesters produced from aliphatic dicarboxylic acids and glycols [8]. They have excellent mechanical properties and biodegradability and are consequently well suited for biodegradable, single-use items such as plastic utensils, plates, paper coatings, milk jugs, shampoo bottles, and garbage bags. Such discarded plastics could be disposed of in composting facilities with yard waste instead of accumulating in landfills.

A drawback of the aliphatic polyesters is that they currently have a high cost compared with petroleum-based commodity plastics such as polyethylene and polystyrene. It has been found that layered silicate filled polymer composites often exhibit remarkable improvement in mechanical, thermal and physicochemical properties when compared with pure polymers and their conventional microcomposites, even at very low filler concentration due to the nano-level interactions with the polymer matrix [9]. These layered silicates attracted a lot of attention from researchers because of their low cost, abundance and high aspect ratio, which give greater possibility of energy transfer from one phase to another.

1.4 Clays

Clay minerals used for polymer nanocomposites can be classified into three groups. They are 2:1 types, 1:1 types, and layered silicic acids. Their structures (Figure 2) are briefly described as follows.

2:1 Type: The layered silicates used in the preparation of nanocomposites generally consist of phyllosilicates and more precisely 2:1 phyllosilicates [9-13]. The clay morphology consists of layers of tetrahedral silicate sheets (Si, Al) and octahedral hydroxide [$Mg(OH)_2$ or $Al(OH)_3$] sheets. The tetrahedral sheet consists of individual tetrahedral silica, which shares three out of four oxygen atoms, forming a plane sheet. The sheet composition can be represented as T_2O_5 where T indicates cations of Si and Al and at the same time Fe and B. The octahedral sheets consist of an individual octahedron sharing edges composed of oxygen and hydroxyl with positively charged species Al, Mg, Fe^{+++} and Fe^{++} which serve as coordinating cations. The layer thickness is around 1 nm whereas the lateral dimensions may vary from 300 nm to several microns depending upon the silicate structure [14].

1:1 Type: The clays consist of layers made up of one aluminium octahedron sheet and one silicon tetrahedron sheet. Each layer bears no charge due to the absence of isomorphic substitution in either the octahedron or tetrahedron sheet. Thus, except for water molecules, neither cations nor anions occupy the space between the layers, and the layers are held together by hydrogen bonding between the hydroxyl groups in the octahedral sheets and oxygen in the tetrahedral sheets of the adjacent layers.

Layered silicic acids: These clays consist mainly of silicon tetrahedron sheets with different layer thickness. Their basic structures are composed of layered silicate networks and interlayer hydrated alkali metal cations.

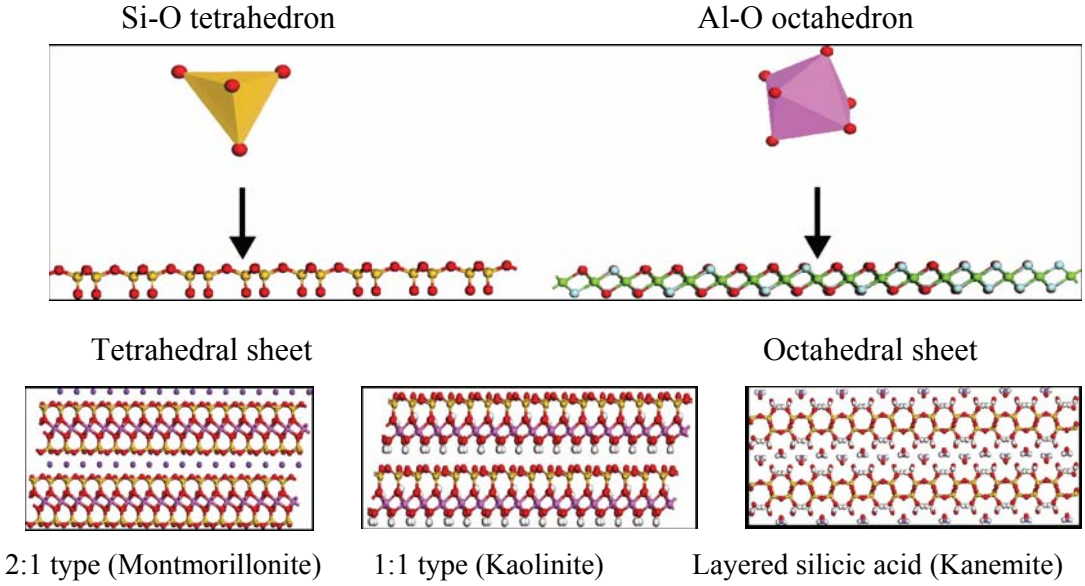

Figure 1.2 Structure of clay minerals represented by montmorillonite, kaolinite and kanemite. They are built up from combinations of tetrahedral and octahedral sheets whose basic units are usually Si–O tetrahedron and Al–O octahedron, respectively [15]

1.5 Hypothesis and objectives

The commercial importance of polymers has been driving intense applications in the form of composites in various fields, such as aerospace, automotive, marine, infrastructure, military etc. [16]. Performance during use is a key feature of any composite material, which decides the real fate of products during use in outdoor applications. Whatever the application, there is often a natural concern regarding the durability of polymeric materials, partly because of their useful lifetime, maintenance and replacement. The deterioration of these materials depends on the duration and the extent of interaction with the environment.

The amount of municipal and industrial waste has markedly increased throughout the world in the last few years. Waste disposal is becoming a serious environmental problem because of limited landfill capacity and incineration facilities. Environmental concern over solid waste

management has stimulated interest in biodegradable materials as alternatives to conventional nondegradable polymers such as polyethylene and polystyrene, which are widely used in disposable applications. The term biodegradable materials is used here to describe those materials which can be degraded by the enzymatic action of living organisms such as bacteria, yeasts and fungi, the ultimate end products of the degradation process being CO_2, H_2O, and biomass under aerobic conditions and hydrocarbons, methane, and biomass under anaerobic conditions [17].

The main objective of this study was to understand the effect of clay particles on the thermal and thermomechanical behaviour of biodegradable polymers upon nanocomposite formation with organically modified montmorillonite (OMMT) and organically modified synthetic fluorine mica (OM-SFM). The first part of this study has been devoted to the characterisation of nanocomposites by XRD and TEM and should provide an overview of the dispersion of silicate layers in polymer matrices. The influence of the silicate layers dispersion on the thermal and mechanical properties of neat PBS will also be discussed.

1.6 References

1. P.M. Ajayan, L.S. Schadler, P.V. Braun. Nanocomposite Science and Technology. Wiley VCH: Verlag GmbH & Co. KGaA, Weinheim (2003).
2. O. Kamigaito. What can be improved by nanometre composites? Journal of the Japan Society of Powder Metallurgy 1991; 38:315-321.
3. M. Jose-Yacaman, L. Rendon, J. Arenas, M.C Serra Puche. Maya blue paint: An ancient nanostructured material. Science 1996; 273:223-225 (DOI: 10.1126/science.273.5272.223).
4. B.K.G. Theng. Formation and properties of clay polymer complexes. Elsevier: New York (1979) (ISBN 978-0444417060).
5. E. Manias, A. Touny, L. Wu, K. Strawhecker, B. Lu, T.C. Chung. Polypropylene/montmorillonite nanocomposites. Review of the synthetic routes and materials properties. Chemistry of Materials 2001; 13:3516-3523 (DOI: 10.1021/cm0110627).
6. N. Herron, D.L Thorn. Nanoparticles: Uses and relationships to molecular clusters compounds. Advanced Materials 1998; 10:1173-1184 (DOI: 10.1002/(SICI)1521-4095(199810)10:15<1173::AID-ADMA1173>3.0.CO;2-6).

7. Y. Tokiwa, T. Suzuki. Hydrolysis of copolyesters containing aromatic and aliphatic ester blocks by lipase. Journal of Applied Polymer Science 1981; 26**:**441-448 (DOI: 10.1002/app.1981.070260206).
8. T. Fujimaki. Processability and properties of aliphatic polyesters, 'Bionolle', synthesized by polycondensation reaction. Polymer Degradation and Stability 1998; 59:209-214 (PII: S0141-3910(97)00220-6).
9. M. Alexandre, P. Dubois. Polymer-layered silicate nanocomposites: preparation, properties and uses of a new class of materials. Materials Science and Engineering 2000; R28:1-63 (PII:S0927-796X(00)00012-7).
10. C.O. Oriakhi, Polymer nanocomposition approach to advanced materials. Journal of Chemical Education 2000; 77:1138-1146.
11. D. Schmidt, D. Shah, E.P. Giannelis. New advances in polymer-layered silicate nanocomposites. Current Opinion in Solid State and Materials Science 2002; 6:205-212 (PII: S1359-0286(02)00049-9).
12. M. Biswas, S. Sinha Ray. Recent progress in synthesis and evaluation of polymer-montmorrillonite nanocomposites, in new polymerization techniques and synthetic methodologies. Advances in Polymer Science 2001; 155:167-221.
13. S. Sinha Ray, M. Okamoto. Polymer/layered silicate nanocomposites: a review from preparation to processing. Progress in Polymer Science 2003; 28:1539-1641 (DOI:10.1016/j.progpolymsci.2003.08.002).
14. M. Kawasumi. The discovery of polymer-clay hybrids. Journal of Polymer Science Part A: Polymer Chemistry 2004; 42:819-824 (DOI: 10.1002/pola.10961).
15. Q.H. Zeng, A.B. Yu, G.Q. (Max) Lu, D.R. Paul. Clay-based polymer nanocomposites: research and commercial development. Journal of Nanoscience and Nanotechnology 2005; 5:1574–1592 (DOI: 10.1166/jnn.2005.411).
16. J.K. Pandey, K.R. Reddy, A.P. Kumar, R.P. Singh. An overview on the degradability of polymer nanocomposites. Polymer Degradation and Stability 2005; 88:234-250 (doi:10.1016/j.polymdegradstab.2004.09.013).
17. S.W. Lim, I.K. Jung, K.H. Lee, B.S. Jin. Structure and properties of biodegradable gluten/aliphatic polyester blends. European Polymer Journal 1999; 35:1875-1881 (PII: S00 1 4- 30 5 7(98)0 02 7 3- 0).

CHAPTER 2

LITERATURE REVIEW

2.1 Overview

The focus of this chapter is on a literature review of clay-based polymer nanocomposites. Clay minerals have unique layered structures, rich intercalation chemistry and they are available at low cost. They are promising nanoparticle reinforcements for polymers to manufacture low-cost, light weight and high performance nanocomposites.

2.2 Science and technology of clay

Nanostructures are difficult to characterize because they are much smaller than visible light wavelengths and significantly larger than individual molecules. Simulation at the nanoscale is equally difficult, as the structures are mostly too small for range treatments and too large for simulations concerning individual atoms and molecules. Investigative tools have played a critical role in the advancement of the entire nano-field. These investigative tools may be grouped as (1) modeling and simulation, (2) testing and measurement, (3) information technology, and (4) reaction path ways and process control. Modeling and simulation is one of the investigative tools of the connection between structure, properties, functions and processing. They use atom-based quantum mechanics, molecular dynamics and macromolecular approaches [1].

Nanoparticles are currently made out of a wide variety of materials [2]. Nanoparticles include carbon nanotubes, metal nanowires, semiconductor quantum dots and other nanoparticles produced from a variety of substances. The most common of the new generation of nanoparticles are the ceramics. They can be divided into metal oxide ceramics, such as titanium, zinc aluminum and iron oxides. Silicate, or silicon oxide, particles are also ceramic and they are generally in the form of nanoscale flakes of clay [3]. Silicate nanoparticles currently in use are flakes about 1 nm thick and 100 to 1000 nm across. They have been produced for many years now, and the most common type of clay used is montmorillonite (MMT) (Figure 2.1).

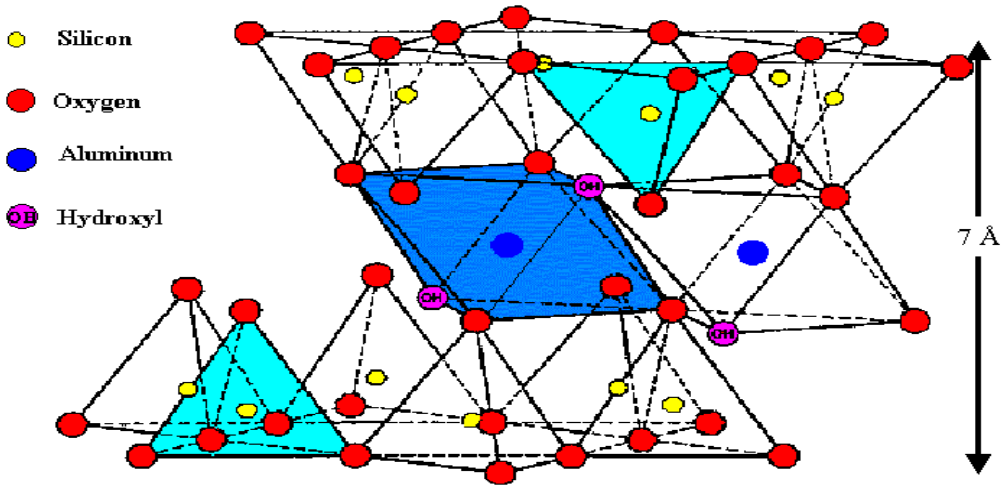

Figure 2.1 Single crystal structure of montmorillonite MMT [3]

2.2.1 Structure and properties of layered silicate (MMT)

Silicates used in preparing layered silicate/polymer nanocomposites belong to the 2:1 layered structure type. MMT is one of the most interesting and widely investigated silicates and belong to the general family of 2:1 layered or phyllosilicates. The chemical formula of MMT silicate is $NaO_{.33}$ $(Al1_{.67}Mg0_{.33})$ Si_4O_{10} $(OH)_2$ nH_2O. The crystal structure of MMT consists of two silicates tetrahedrally fused to an edge shared octahedral sheet of either aluminium or magnesium (Figure 2.2). Each layer is composed of a sheet of octahedral aluminium or magnesium sandwiched between two sheets of tetrahedral SiO_4, which has a unit cell structure consisting of 20 oxygen atoms and 4 OH groups [4]. These layers are continuous and are stacked one above the other. Stacking of the layers leads to a regular van der Waals gap between the layers, called the interlayer or gallery. They have a stiffness of approximately 170 GPa (25 Msi), and have aspect ratios in the range of 100–1500. Each layer is approximately 1 nm thick, while the diameter may vary from 30 nm to several microns or larger. This provides a large surface area, approximately 700-800 m^2 per gram of silicate material. The silicate layers have a specific gravity of 2.5. The layer spacing (d-spacing) prior to processing with a polymer is 1.2 nm [5]. Hundreds or thousands of these layers are stacked together with weak Van der Waals forces to form a silicate particle. Isomorphic substitution within the layers (for example, Al^{3+} replaced by Mg^{2+} or by Fe^{2+}, or Mg^{2+} replaced by $Li^{+)}$ generates excess negative charges, naturally balanced by exchangeable inorganic cations. The

polar Si-O groups at the MMT surface impart a hydrophilic nature which results in an affinity of MMT for polar molecules [6]. MMT need to be treated from its hydrophilic silicate state to an organophilic state to render miscibility with most polymer matrices. Generally this can be done by ion-exchange reactions.

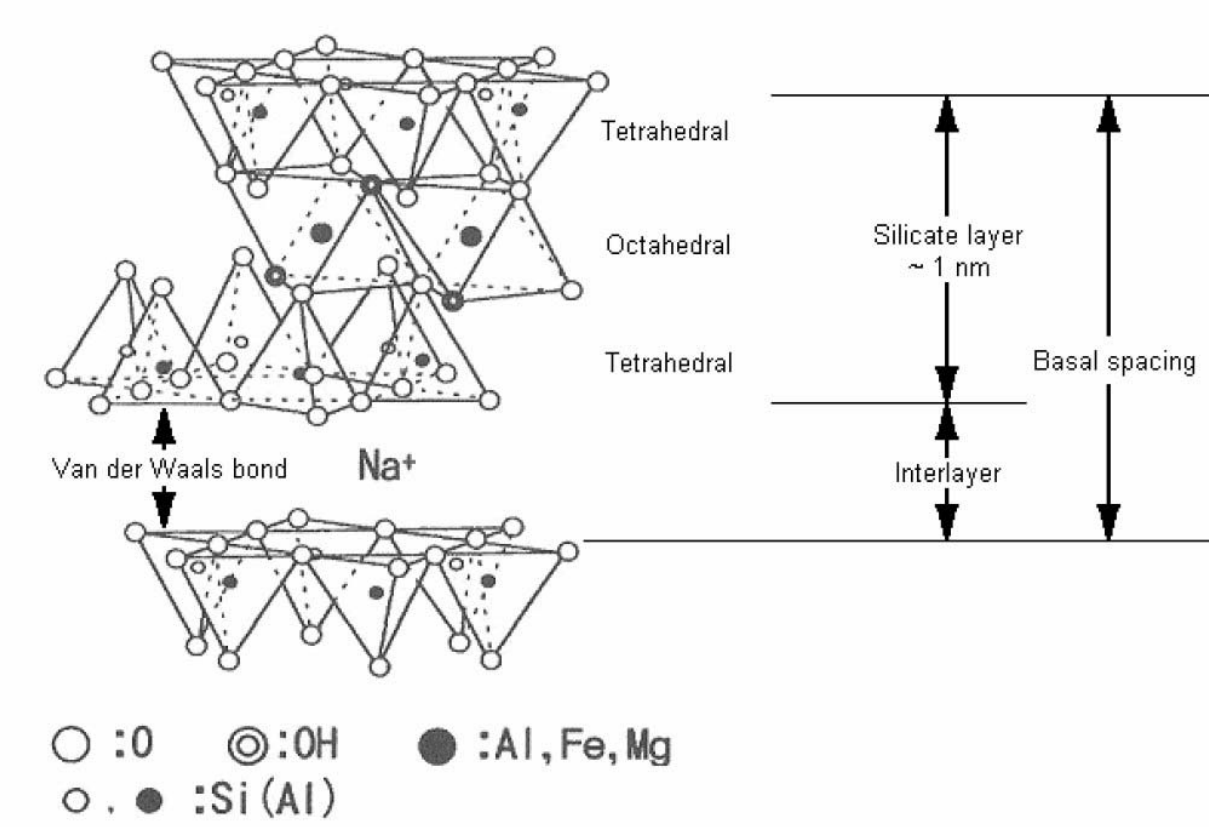

Figure 2.2 Schematic illustration of the atomic arrangement in a typical MMT layer [7]

2.2.2 Organically modified silicates

MMT is used in polymer nanocomposites due to its swellable layered structure. However, the charged nature of the sheets in the silicate makes them incompatible with hydrophobic polymers. The lack of affinity between a hydrophilic silicate and a hydrophobic polymer tends to agglomeration of the mineral within the polymer matrix [8]. In this case, pre-treatment of the silicates is necessary. Pristine layered silicates (MMT) usually contain hydrated Na^+ or K^+ cations. They can be replaced through an ion exchange reaction with cationic surfactants, including amino acids, organic ammonium salts, or tetra organic phosphoniums, to render the normally hydrophilic silicate surfaces as organophilic [9]. The most popular cationic surfactant is the alkylammonium ion, because it can be easily

exchanged with the ions situated between the silicate layers. Depending on the layer charge density of the silicate, the alkylammonium ions adopt different structures between the silicate layers. The modified silicate, known as organically modified montmorillonite (OMMT), is organophilic and it is more compatible with organic polymers. In this way the polymer molecules may be able to intercalate within the clay galleries Figure 2.3. The role of the alkylammonium cations in the organosilicate is to lower the surface energy of the inorganic host and to improve its wetting with the polymer. This increases the interlayer spacing and provides better compatibility with the polymer. The basal spacing can be changed depending on the nature of the exchanged cations and/or the size of the organic molecule [10].

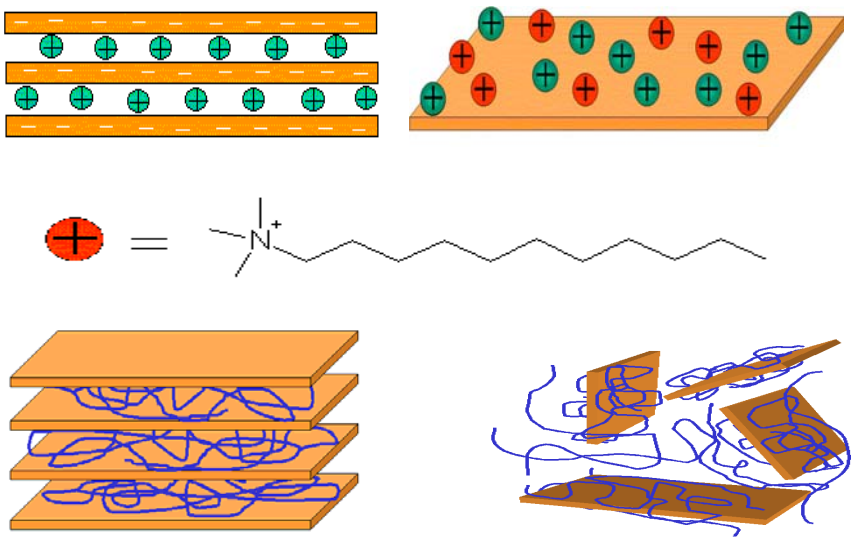

Figure 2.3 Modification of clay surfaces through an ion exchange reaction by replacing the Na+ cations with a cationic surfactant [3]

For a given silicate, the maximum number of exchangeable interlayer cations is known as the cation-exchange capacity (CEC), and it is usually described in milli-equivalents per gram (meq/g) or more frequently in milliequivalents per 100 g (meq/100g). The CEC of MMT varies from 80 to 150 meq/100 g [11]. The exchange of inorganic cations by organic surfactant ions in the silicate galleries not only makes the organosilicate surface compatible with a monomer or a polymer matrix, but it also decreases the interlayer cohesive energy by expanding the d-spacing. The orientation of the surfactant in the galleries depends on its chemical structure, the cation-exchange capacity and charge density of the silicate [12]. This means that the length of the surfactant chain determines the distance between the layers. The adsorbed organic cations in swelled silicates (e.g. montmorillonite) may adopt several

configurations in the interlayers. Some possible configurations, such as a flat monolayer, bilayer, pseudo-trilayer, and inclined paraffin structure, are shown in Figure 2.4. At lower charge densities, the surfactant packs in monolayers and as the charge density increases, bilayers and trilayers can form. At very high CECs (≥120 meq/100 g) and long surfactants (>15 carbons), the packing can be ordered in a paraffin-type structure [7].

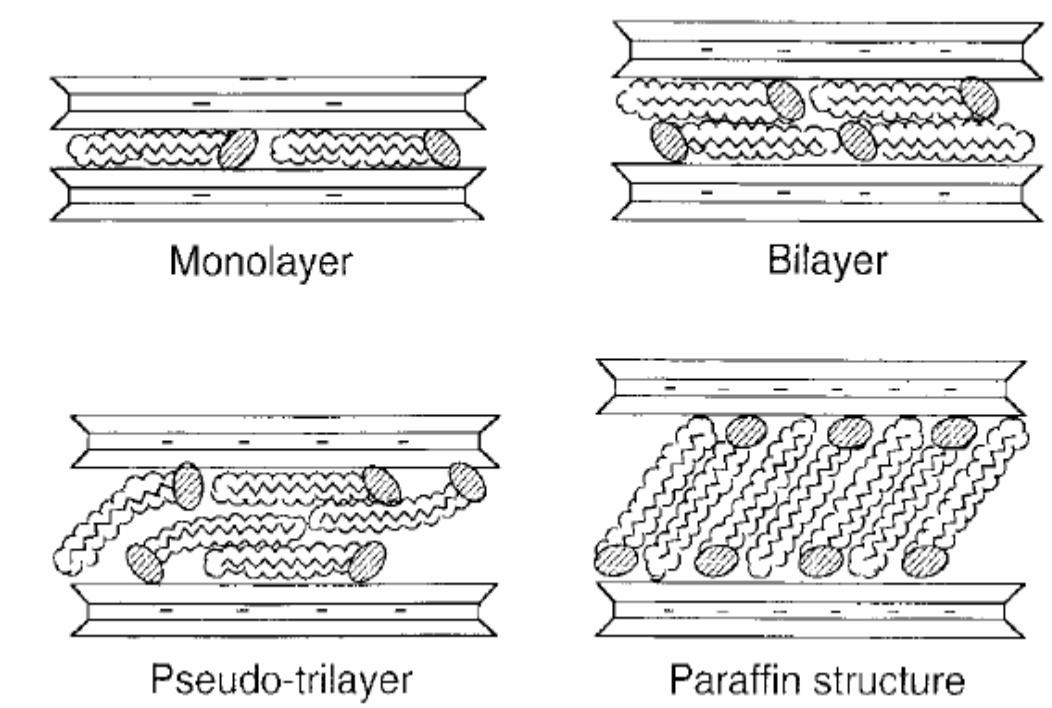

Figure 2.4 Schematic presentation of the orientation of alkylammonium ions in the galleries of layered silicates with different layer charge densities [7]

If the silicate layers are absolutely and homogenously dispersed in the polymer matrix, the morphology is known as exfoliated nanocomposites. It was proposed [13] that despite favourable compatibility between the polymer and the organically modified layered silicates, the final morphology of the nanocomposite evolves *via* four stages: disordered exfoliation, ordered exfoliation, dual morphologies of intercalation and exfoliation, and intercalation in sequence with the content of silicate. The formation of the ordered exfoliation state is attributed to the steric interaction between the anisotropic silicate plates. They claimed that the transition from exfoliation to intercalation provides a significant clue that the interaction between the layered silicates gets dominant when the distance between them is smaller than a certain value. It was found that the silicate layers need a layer spacing larger than 9 nm to avoid the attractive interaction between the adjacent silicate layers and to keep this nanocomposite system in the exfoliated state.

The existence of dual morphologies in the intercalated structure explained the effect of an attractive interaction between adjacent layers on the morphology evolution, as well as the range of the attractive interaction. A technique to determine the three-dimensional (3D) orientation of various organic and inorganic structures in polymer nanocomposite has been developed [14,15]. Solid-state NMR (1H and 13C) can also be used for the study of the morphology and surface chemistry of clay-polymer nanocomposites [16]. Depending on the strength of the interfacial interactions between the polymer matrix and layered silicate (modified or non-modified), three different types of composite morphology may be obtained. These types primarily depend on the method of preparation and the nature of the components used [17].

a. Phase separated composites: Layered silicates exist in their original aggregated state with no intercalation of the polymer matrix into the galleries. In this case, the particles act as microscale fillers. Their properties stay in the same range as seen in traditional microcomposites [6].

b. Intercalated composites: When the polymer resin penetrated the gallery between the adjacent layers, the spacing expands, and it is known as the intercalated state (Figure 2.5). In the intercalated state, the matrix polymer molecules are introduced between the ordered layers of the silicate, resulting in an increase in the interlayer spacing without disturbing the crystalline order. Intercalated nanocomposites are generally formed during melt blending or *in situ* polymerization [18].

c. Exfoliated composites: In exfoliated nanocomposites, the individual nanometre scale thick silicate layers are separated and dispersed in a continuous polymer matrix with the average distances between the layers depending on the silicate concentration. When the layers are fully separated, the silicate is considered to be exfoliated [5,8]. The exfoliation ability depends on the nature of the silicate, the blending process, and the agents used for curing. Exfoliated nanocomposites improve the specific properties better than intercalated ones.

Partially intercalated or exfoliated composite morphology may also be obtained. In this commonly occurring case, the exfoliated layers and intercalated clusters are randomly distributed in the matrix. The final structure of the silicate composite varies widely,

depending on the degree of intercalation and exfoliation. X-ray diffraction measurements are used to characterize the intercalated and exfoliated structures [19]. Reflections in the low angle region indicate an intercalated composite, but if the peaks are extremely broad or disappear completely, this indicates complete exfoliation. This is not generally true because other researchers found different results. Pozsgay et al. [20] claim that multiple peaks, appearing in their WAXS pattern of organophilized silicate, may have arisen from interference, but they may also have indicated the presence of several populations of layer distances. The water absorbed between the galleries of partially organophilized silicates led to the separation of the layers resulting in the appearance of new scattering peaks. Exfoliation occurs only above a critical gallery distance, which corresponds to the thickness of two aliphatic chains. Although exfoliation of the silicate is determined by its organophilization and gallery structure, composite properties are dominated by interfacial interaction. Béla Pukánszky and co-workers [21] studied the estimation of the reinforcing effect of layered silicates in polypropylene (PP) nanocomposites. Their results showed that complete exfoliation is rarely reached and the structure of PP nanocomposites was rather complicated. They further studied the structure and rheological properties of a large number of layered silicate poly(propylene) nanocomposites with widely varying compositions [22]. Morphology characterization at different length scales was achieved by SEM, TEM, and XRD. Rheological measurements supplied additional information about the structure. The results showed that these materials possess a very complex structural architecture. The introduction of functionalized polymer decreased the size of the original clay particles and improved their interaction with the polymer matrix. However, relatively large silicate particles were found also in composite samples yielding XRD traces without a silicate reflection. XRD supplies information of limited value if the amount of silicate is low, the gallery distance of the stacks is large or their regularity is limited. On the other hand, XRD indicates intercalation well. Although exfoliated individual layers can be detected by TEM, the method cannot be used to draw general conclusions about the structure of layered silicate nanocomposites because of statistical sampling and bias. A large number of individual layers, i.e. a large extent of exfoliation, led to the formation of a silicate network structure, which can be detected very sensitively by Cole-Cole plots of dynamic viscosity. They found that all four morphological entities (particles, intercalated stacks, individual layers, and networks) may be present simultaneously in the composites. The presence and relative amount must definitely influence the composite properties. However, currently used experimental protocols do not supply sufficient information even to estimate the relative influence as well as interplay among

different structural features quantitatively. They concluded that XRD and TEM alone are not sufficient for the characterization of nanocomposites with a complex structure.

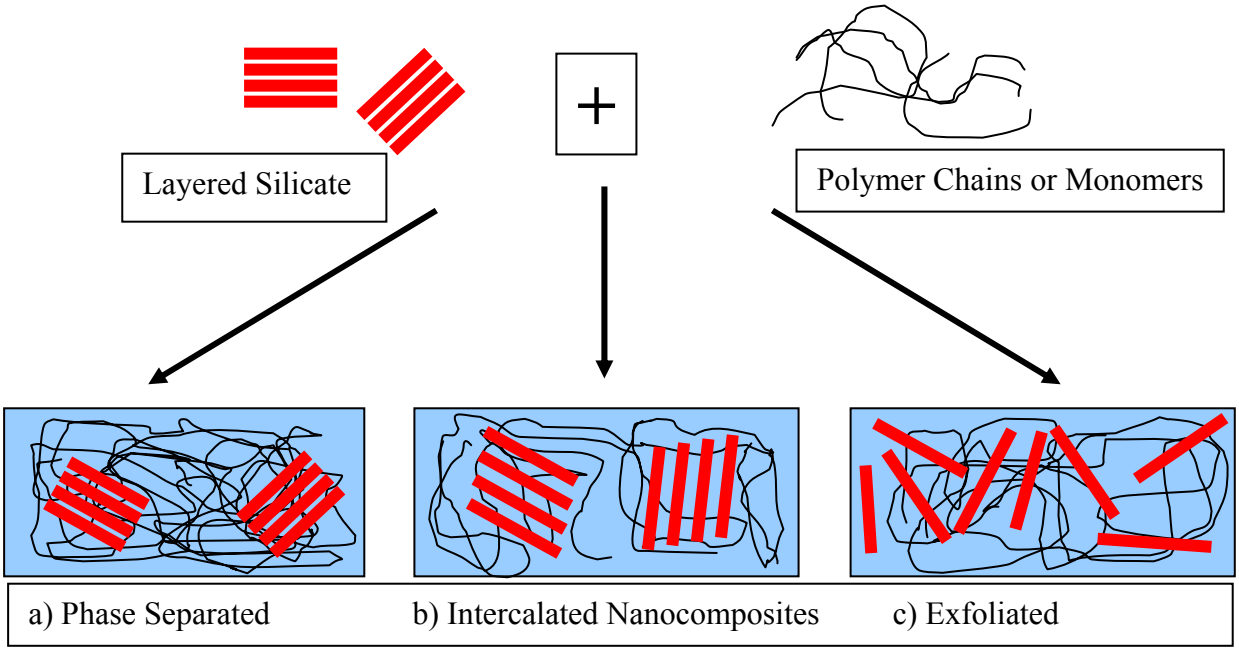

Figure 2.5 Different morphologies of layered silicate/polymer nanocomposites

They presented the XRD pattern of nanocomposites in which the silicate reflection was absent. The SEM micrograph of the same composite was taken and particles were clearly visible on the surface; that means exfoliation was obviously far from complete. It was concluded that XRD and TEM, do not reflect the differences in properties and do not give any reliable information about the extent of exfoliation either.

2.3 Clay containing polymer nanocomposites

Polymer-clay nanocomposites are formed through the union of two very different materials with organic and mineral pedigrees. This new class of materials emphasize their potential advantages in various applications [17] including high modulus, increased strength and heat resistance, decreased gas permeability and flammability [6,23]. One of their potential advantages is a high level of reinforcement at low silicate content leading to stronger and lighter parts [24-27]. The basic idea behind this expectation is the extremely large interface created by the exfoliation of the layered silicate, which is a precondition for improved properties [28]. Polymer-clay nanocomposites were first reported by Toyota's central research and development laboratories in the 1980's.They were successful in developing a nylon-

6/clay nanocomposite [29,30]. The clay used for these early nanocomposites was the smectite clay, montmorillonite.

Up to this date, almost all polymer matrices such as poly(ethylene oxide) [31], poly(vinyl alcohol) [32], polypropylene [33], polyethylene [34], polystyrene [35], poly(methyl methacrylate) [36], poly(ethylene terephthalate) [37], polylactide [38], poly[(butylene succinate)-co-adipate] [39], poly(ε-caprolactone) [40], and liquid crystal polymers [41], have been used for the preparation of nanocomposites with either pure or organically modified layered silicates. Different polymers are influenced by clay incorporation in different ways. Polymers that are usually synthesized from a diol and dicarboxylic acid through a condensation polymerization are considered to be the most promising biodegradable plastics, because of their low production costs and easy processibility in large-scale production. Difficulties are encountered, however, in their practical application because of their low melting temperature and poor thermal stability. If the properties of biodegradable aliphatic polyesters (BAPs) can be further improved by preparation of nanocomposite with organically modified layered silicates (OMLS), this polymer will become more suitable for a wide range of applications. Lim *et al.* [42] prepared BAP/MMT nanocomposites by a solvent casting method using chloroform as a co-solvent. XRD analyses and TEM observations established the intercalated structure of these nanocomposites. Recently, Lee et al. [43] reported the preparation of biodegradable polyester-OMLS nanocomposites using a melt intercalation method. Two kinds of OMLS, C30B and C10A, with different ammonium cations located in the silicate galleries, were chosen for the nanocomposite preparation. The WAXD patterns and TEM observations showed higher degrees of intercalation for C30B-based nanocomposites compared to those of the C10A-based nanocomposites. It was hypothesized that this behaviour may be due to the stronger hydrogen-bonding interaction between the polymer and the hydroxyl group in the galleries of the C30B nanocomposites, compared to that of the polyester/C10A nanocomposites. Sinha Ray *et al.* [6,38,39] used a melt intercalation technique for the preparation of intercalated polylactide (PLA)/layered silicate nanocomposites. Nanocomposites loaded with a very small amount of oligo-poly(ε-caprolactone) (o-PCL) as a compatibilizer, were also prepared in order to understand the effect of o-PCL on the morphology and properties of polylactide/clay nanocomposite (PLACNs). XRD patterns and TEM observations clearly established that the silicate layers of the clay were intercalated, and randomly distributed in the PLA matrix. Incorporation of a very small amount of o-PCL as a compatibilizer in the nanocomposites led to better parallel

stacking of the silicate layers, and also to much stronger flocculation due to the hydroxylated edge–edge interaction of the silicate layers. Owing to the interaction between the clay platelets and the PLA matrix in the presence of a very small amount of o-PCL, the strength of the disk–disk interaction plays an important role in determining the stability of the clay particles, and hence the enhancement of mechanical properties of such nanocomposites.

Poly(butylene succinate) (PBS) is a commercially available, aliphatic thermoplastic polyester with many interesting properties, including biodegradability, melt processability, and thermal and chemical resistance [44]. PBS has excellent processability, so it can be processed in the field of textiles into melt blow, multifilament, monofilament, nonwoven, flat, and split yarn products, and also in the field of plastics into injection-molded products [45]. It is therefore a promising polymer for various potential applications.

Sinha Ray *et al.* [46,47] reported the structure-property relationship of PBS nanocomposites. They used two different types of layered silicates: octadecyl ammonium modified montmorillonite (C18MMT) and quaternary hexadecyl tri-*n*butylphosphonium modified saponite (qC16SAP) for the preparation of nanocomposites with PBS. According to them the structure of the nanocomposites is directly related to the nature of the pristine layered silicates and also to the surfactant used for the modification of layered silicate, and hence this determines the final properties of nanocomposites. Mitsunaga *et al.* [48,49] prepared PBS/OMLS nanocomposites by a melt extrusion technique. They used maleic anhydride grafted PBS for the preparation of the nanocomposites. XRD patterns and TEM observations clearly indicate the formation of intercalated nanocomposites.

Poly(ethylene succinate)(PES), a condensate of succinic acid and ethylene glycol is an interesting thermoplastic polyester with properties comparable to many commodity plastics such as polypropylene and polyethylene [44]. Biodegradation is undoubtedly one of the most important properties of PES and a number of articles were published on the nature of PES degradation [50,51]. Unlike microbial polyesters such as poly(3-hydroxy butyrate) (PHB), that are susceptible to degradation in various environments [52], the degradation of PES was found to be strongly dependent on environmental factors [53]. A number of articles appeared on the crystallization behaviour and morphology of PES in the presence of other polymers and nucleating agents [54-59]. However, to the best of our knowledge, there is no report on the use of nano-dimensional clay particles as a means to increase the crystallinity and to

improve the thermal and mechanical properties of PES. Clay particles can be used as a strong nucleating agent for PES crystallization because they have large surface areas. MMT is one of the clay particles that can be used for PES because of its specific surface area (S_O) of about 700-800 m^2 g^{-1}, and the ability to be well dispersed in the polymer matrix [59].

2.4 Nanocomposite preparation

Intercalation of polymers into layered hosts, such as layered silicate, has proven to be a successful approach to synthesize polymer layered silicate nanocomposites. The processing methods are divided into three main groups according to the starting materials and processing techniques:

Exfoliation-adsorption: The layered silicate is exfoliated into single layers using a solvent in which the polymer (or a pre-polymer in the case of insoluble polymers such as polyimide) is soluble. It is well known that such layered silicates, owing to the weak forces that stack the layers together, can be easily dispersed in an adequate solvent. The polymer then adsorbs onto the delaminated sheets and when the solvent is evaporated (or the mixture precipitated), the sheets reassemble, sandwiching the polymer to form an ordered multilayer structure. This techniques also involves nanocomposites obtained through emulsion polymerization where the layered silicate is dispersed in the aqueous phase.

In situ *intercalative polymerization*: In this technique, the layered silicate is swollen within the liquid monomer (or a monomer solution) so that the polymer can form between the intercalated sheets. Polymerization can be initiated either by heat or radiation, by the diffusion of a suitable initiator, or by an organic initiator or catalyst fixed through cationic exchange inside the interlayer before swelling by the monomer.

Melt intercalation: The layered silicate is mixed with the polymer matrix in the molten state. Under these conditions, and if the layer surfaces are sufficiently compatible with the chosen polymer, the polymer can move slowly into the interlayer space and form either an intercalated or an exfoliated nanocomposite. In this technique, no solvent is required.

2.4.1 Exfoliation-adsorption

This technique has been widely used with water-soluble polymers to produce intercalated nanocomposites [60] based on poly(vinyl alcohol) (PVOH) [61,62], poly(ethylene oxide) (PEO) [62,63], poly(vinylpyrrolidone) (PVPyr) [41] or poly(acrylic acid) (PAA) [63]. When polymeric aqueous solutions are added to dispersions of fully delaminated sodium layered silicates, the strong interaction existing between the hydrosoluble macromolecules and the silicate layers often cause the re-aggregation of the layers, as was observed for PVPyr [64] or PEO [62]. In the presence of PVOH, the layers remained in colloidal distribution [62]. In the wet state or after mild drying (air drying), the silicate layers were distributed and embedded in the so-obtained PVOH gel. This state corresponds to a true nanocomposite hybrid material. However, more intense drying of the PVOH gel in vacuum causes part of the silicate layers to re-aggregate and an intercalated species are formed. Polymer intercalation using this technique can also be performed in organic solvents. PEO has been successfully intercalated in sodium montmorillonite and sodium hectorite by dispersion in acetonitrile [65], allowing the stochiometric incorporation of one or two polymer chains in between the silicate layers.

2.4.2 In situ intercalative polymerization

The Toyota research team studied the ability of Na-montmorillonite organically modified by protonated α,ω-aminoacid ($^{+}H_3N$-$(CH_2)_{n-1}$-COOH, with n = 2, 3, 4, 5, 6, 8, 11, 12, 18) to be swollen by the ω-caprolactam monomer (melting temperature = 70°C) at 100 °C and subsequently to initiate its ring opening polymerization to obtain nylon-6-based nanocomposites [66]. A clear difference occured in the swelling behaviour of the montmorillonite with relatively short (n<11) and those with longer alkyl chains.

A 12-aminolauric acid (n=12) modified montmorillonite was chosen to develop the intercalative ring opening polymerization of ε-caprolactam [66]. The intercalative polymerization of ε-caprolactam could also be realized without the necessity to render the montmorillonite surface organophilic [67]. This monomer was able to directly intercalate the Na-montmorillonite in water, in the presence of hydrochloric acid. This intercalation was proved by the increase in interlayer spacing observed on the isolated montmorillonite/ε-caprolactam product. At a high temperature (200 °C), in the presence of excess ε-caprolactam,

the modified clay can be swollen again, allowing for the ring opening polymerization to proceed at 260 °C when 6-aminocaproic acid is added as an accelerator. The resulting composite does not present any diffraction peak characteristic of an interlayer spacing in XRD, and TEM observations agree with a molecular dispersion of the silicate sheets. In attempts to carry out a one-pot synthesis [68], the system proved to be sensitive to the nature of the acid used to promote the intercalation of ε-caprolactam. These results show that only phosphoric acid allows for the preparation of a truly exfoliated nanocomposite, while the other acids tend to promote the formation of partially exfoliated-partially intercalated structures. It is not clear why only the phosphoric acid works. An intercalated structure was obtained, even if no acid was added, and the addition of 6-aminocaproic acid in each experiment as polymerization accelerator could have played the same role.

Another polyamide, nylon-12, formed nanocomposites using *in situ* intercalative polymerization. Reichert et al. [69] used 12-aminolauric acid (ALA) as both the layered silicate modifier and the monomer. They first studied, by XRD, the effect of ALA on the swelling behavior of a synthetic three-layer silicate. Increasing amounts of ALA dispersed in HCl (20 mmol/l) were poured into a water suspension of the silicate. The swelling process as function of ALA concentration was monitored and it can be separated in two regimes, as shown in Figure 2.6 and explained in Figure 2.7.

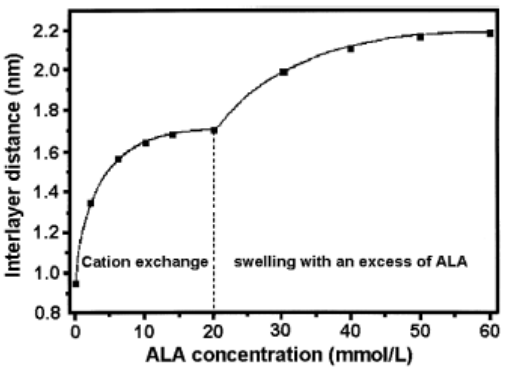

Figure 2.6 Interlayer distance of fluoro-modified talc (ME 100) as a function of an increasing amount of aminolauric acid used as the organic modifier [70]

The swelling was found to be independent of both the swelling temperature, the layered silicate concentration and the type of mineral acid used to protonate ALA (HCl, H_2SO_4, H_3PO_4). ALA was then polymerized at high a temperature (280 °C) and under a high pressure

(up to 20 bar) for 9.5 h with both types of swollen clay. The structures were confirmed to be partially exfoliated or intercalated nanocomposites.

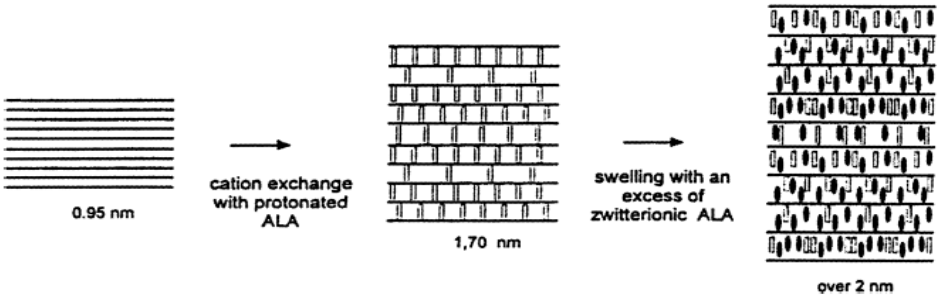

Figure 2.7 Schematic representation of the swelling behaviour of the fluoro-modified talc in the presence of aminolauric acid [66]

By using the method developed by Usuki et al. [66] for the polymerization of ε-caprolactam, Messersmith and Giannelis [70] modified a Na-montmorillonite by protonated aminolauric acid and dispersed this modified clay in liquid ε-caprolactone before polymerizing it at a high temperature. The poly(ε-caprolactone) (PCL) nanocomposites were prepared by mixing up to 30 wt.% of the modified clay with dried and freshly distilled ε-caprolactone at room temperature for a couple of hours, followed by ring opening polymerization under stirring at 170 °C for 48 h. XRD patterns of the modified clay after contact with ε-caprolactone at room temperature do not show any significant increase in the layered spacing. The authors assumed that the monomer intercalated into the gaps between the aminolauric acid chains so that no gallery expansion could be seen. This is in contrast with what is usually observed in the *in situ* intercalative polymerization where the insertion of the monomer within the silicate gallery induces an increase in the interlayer spacing. Another possibility is that the intercalation of the monomer occurred only during the heating of the solution. After polymerization, XRD patterns of the obtained composites did not show any diffraction peak indicating the presence of intercalated structures, and it is more likely that exfoliation occurred. This exfoliation induced some clear modifications in the onset temperature of polymer melting (T_m) of the obtained nanocomposites, which appeared at a lower temperature when the weight fraction of layered silicates increased (Figure. 2.8).

.

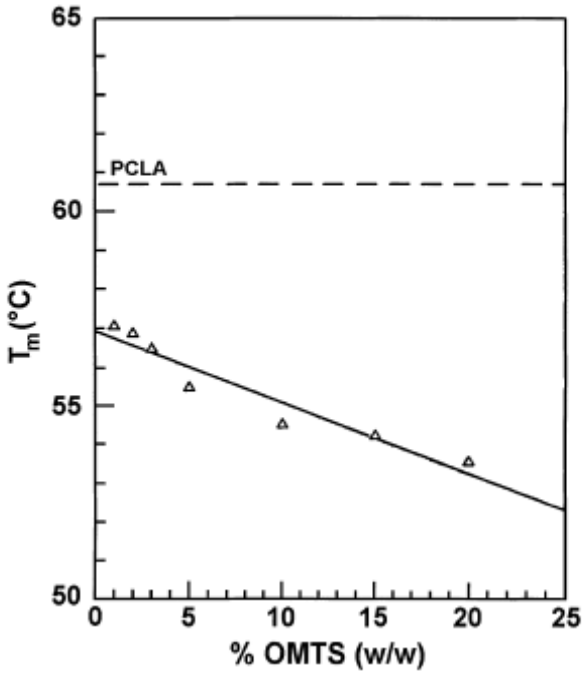

Figure 2.8 Polymer onset temperature of melting as a function of organomodified montmorillonite for poly(ε-caprolactone)(PCL)-based nanocomposites. PCLA corresponds to the melting temperature for unfilled PCL [71]

This phenomenon was attributed to the formation of smaller crystallites, probably due to the physical barrier effect of the dispersed layers that limited the extent of crystallization of the PCL chains. The authors proposed a polymerization mechanism where the carboxylic acid of the attached aminolauric acid undergoes a nucleophilic addition on the ε-caprolactone carbonyl function, creating by ring opening reaction a carboxylic anhydride bridge that links the first opened lactone monomer to the silicate surface. The ring opening reaction is then proposed to occur via an 'o-acryl' cleavage of the monomer with the formation of a hydroxyl end group that propagates the lactone polymerization. However, it is now commonly accepted [71] that carboxylic species are not reactive enough to promote the ring-opening polymerization of ε-caprolactone. At such a high temperature (170 °C), a mechanism known as the `active hydrogen polymerization' should rather take place where traces of water could initiate the ring opening polymerization of the lactone [72]. This mechanism ruled out the grafting of the growing polyester chains onto the silicate layers through the formation of a carboxylic anhydride link. If any links exist, they would rather be formed at a high temperature by a post-esterification reaction between the terminal hydroxyl group of some PCL chains with the carboxylic acid function of the fixed aminoacid surface agent. ε-caprolactone ring opening polymerization can also be initiated by the primary amino end-

groups of some aminolauric acids that did not react with the layered silicate surface. Rozenberg [73] claimed that ε-caprolactone polymerization initiated with amines in the presence of a protic acid at a high temperature (180 °C) can proceed through a zwitterionic mechanism. The resulting macromolecular zwitterions, i.e. α-H_3N^+, ω-CO_2^-PCL chains could then interact with the charged layered silicates, assuring some efficient surface grafting.

The above poly(ε-caprolactone)-based nanocomposite synthesis has been applied by Chen *et al.* [74] to produce novel segmented polyurethane-clay nanocomposites articulated on diphenylmethane diisocyanate, butanediol, and a preformed polycaprolactone diol. Even if the mechanism planned for the chemical link between the nanofiller surface and the polymer does not appear appropriate (ammonium salts are not known to induce ε-caprolactone ring-opening polymerization), they succeeded in producing a material where the nanofiller acts as a multifunctional chain extender inducing the formation of star-shaped segmented poly(urethane).

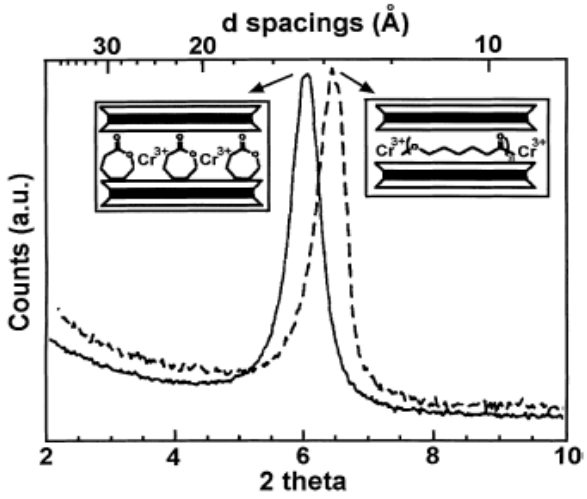

Figure 2.9 XRD patterns of ε-caprolactone intercalated in Cr^{3+} modified fluorohectorite (solid line) and the resulting poly(ε-caprolactone)-based nanocomposite (dashed line). Insets are schematic illustrations corresponding to the intercalated monomer (left) and intercalated polymer (right) [75]

Messersmith and Giannelis [75] also reported on the ε-caprolactone polymerization inside a Cr^{3+} exchanged fluorohectorite at 100 °C. The monomer intercalation was this time evidenced by an interlayer spacing increase upon the addition of the liquid monomer. After the polymerization reaction, an intercalated poly(ε-caprolactone) was obtained with an interlayer spacing of 13.7 Å, due to the dimensional change accompanying the polymerization of the

cyclic monomer (Figure. 2.9). The observed layer spacing of 13.7 Å correlates well with the sum of the thickness of the silicate layer (9.6 Å) and the known interchain distance (4.0 Å) of caprolactone.

In situ intercalative polymerization was also studied for the production of polystyrene (PS)-based nanocomposites. Akelah and Moet [76] modified the interlayer of Na-montmorillonite and Ca-montmorillonite by exchanging the inorganic cations with (vinylbenzyl)trimethyl ammonium chloride, increasing the interlayer spacing by 5.4 Å. These modified clays were then dispersed and swollen in various solvent and co-solvent mixtures such as acetonitrile, acetonitrile-toluene and acetonitrile/THF. Styrene polymerizations were carried out in the presence of N,N′-azobis(isobutyronitrile) (AIBN). Intercalated composites were produced with interlayer spacings varying between 17.2 and 24.5 Å depending on the nature of the solvent used. Even if the polymer is well intercalated, a drawback of this technique remains that the macromolecule produced is not pure PS, but rather a copolymer between styrene and (vinylbenzyl)trimethyl ammonium cations.

Do and Cho developed a technique by using more commonly modified montmorillonites [77]. The authors compared the ability of several tetraalkylammonium cations, incorporated into Na^+-montmorillonite through ion exchange, to promote the intercalation of PS through the free radical polymerization of styrene initiated by AIBN at 50 °C. Three tetraalkylammonium cations were tested, all based on the following formula: $(CH_3)_2N^+$(hydrogenated tallow alkyl)R, where the hydrogenated tallow alkyl corresponded to a mixture of mainly octadecyl chains together with small amounts of lower linear homologues, and R was either another hydrogenated tallow alkyl (Ta), 2- ethyl hexyl (Eh) or benzyl (Bz) group. These so-modified organo-montmorillonites were coded as Ta-MMT, Eh-MMT and Bz-MMT, respectively. The best intercalation occurred for Bz-MMT. This is probably due to a better affinity between the styrene and benzyl groups spread all along the layered montmorillonite surfaces, as further demonstrated by the perfect dispersibility of this organo-modified filler in styrene. If Eh-MMT did also intercalate some PS and the interlayer spacing for Ta-MMT did not change much, but TGA analysis indicated that intercalation also occurred in this composite. The authors concluded that intercalation within Ta-MMT should occur without an important increase in the interlayer spacing, because such hydrogenated tallow alkyl chains should be long enough (mainly C_{18} chains) to easily accommodate PS. Even though this technique allows an extensive intercalation of PS chains through an adequate choice of the

alkylammonium cation, neither exfoliation nor control over the molecular parameter of the PS produced were observed.

2.4.3 Melt intercalation

This method, an environmentally benign one, uses all types of polymers and is compatible with existing polymer industrial processes such as injection molding, and it is the most popular procedure to prepare nanocomposites for industrial applications. The thermodynamics that drives the intercalation of a polymer inside a modified layered silicate, while the polymer is in the molten state, was investigated through a lattice-based mean field theory [78]. It was found that the outcome of polymer intercalation is determined by the interplay of entropy and enthalpy factors. In fact, although the confinement of the polymer chains inside the silicate galleries results in a decrease in the overall entropy of the macromolecular chains, this entropic penalty may be rewarded by the increase in conformational freedom of the tethered alkyl surfactant chains as the inorganic layers separate, due to the less confined environment.

Balazs *et al.* [79,80] considered the self-consistent field theory (SFC) in order to investigate the factors promoting the penetration of polymers into layered silicates. They first varied properties related to the nature of the tethered surfactant chains. They found out that an increase in the surfactant length (approaching the length of the polymer chains) improves the layers' separation by the formation of a broad interface (or interphase) which allows the polymer to adopt more conformational degrees of freedom. Exfoliated or intercalated structures can therefore be formed, even for slightly unfavourable interactions between the polymer and the modified surfaces. However, an increase in the length of the polymer chains tends to render the interlayer mixture immiscible. These authors also showed that excessive density of the tethered alkyl chains can impede the formation of intercalated structures.

In order to model the macroscopic phase behavior of the polymer-clay mixture, Balazs et al. [80,81] developed a free energy expression for a mixture of a polymer and solid, thin disk-like particles. The free energy expression was adopted from the Onsager model for the equilibrium behaviour of rigid rods. This model allows one to calculate phase diagrams of the polymer/clay composites as a function of the Flory-Huggins interaction parameter. These diagrams can differentiate immiscible and miscible regions, further separated into isotropic or nematic (relatively ordered) arrangements. The blend miscibility was found to be strongly

negatively influenced by an increase in the length of the polymer chains. For very long polymer chains the particle-polymer mixture became immiscible, even for negative values of the interaction parameter. The phase diagram appears to be also strongly dependent upon the aspect ratio of the particle (Figure 2.10).

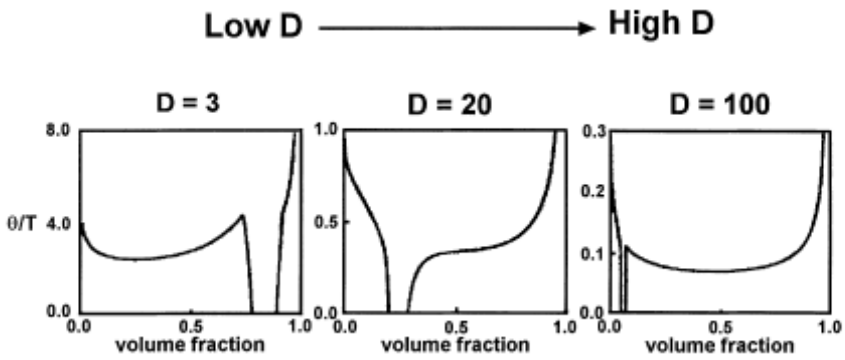

Figure 2.10 Phase diagrams of disks dispersed in a polymer matrix for different disk aspect ratios. The disk aspect ratios (D/L) were varied by changing the dimension of the diameter of the disks (D), and keeping their thickness constant (L=1) [81]

An increase in the particle diameter favours the apparition of a nematic phase at a low volume fraction, implying the formation of relatively ordered structures for low clay particle contents. Ginzburg and Balazs [82] developed an even more complex model, based on a perturbation-type density functional theory, to describe the complete (isotropic, nematic, smectic A) phase diagram of an incompressible polymer disk mixture. The phase diagram is strongly dependent upon the shape anisotropy of the filler particles, the polymer chain length, and the strength of the interparticle interaction. For instance, an increase in the interparticle interaction strength led to the complete disappearance of the nematic phase.

Melt intercalation of PS and derivatives has been widely studied and has served to experimentally describe the aforementioned thermodynamics as well as the kinetics and morphologies accordingly described. Vaia and Giannelis [83] studied PS as the matrix for dispersing different types of clays. Li-fluorohectorite (CEC=150 meq/100 g), saponite (100 meq/100 g), and sodium montmorillonite (80 meq/100 g) were modified using various ammonium cations: dioctadecyldimethylammonium, octadecyl trimethyl ammonium, and a series of primary alkylammonium cations with carbon chains of 6, 9-16 and 18 carbon atoms. The nanocomposites were synthesized by statically annealing (without any mixing or

shearing) a pelletized intimate mix of the modified silicate in PS under vacuum at 170°C, a temperature well above the PS glass transition [84]. Generally, for a given alkyl surfactant, increasing the cation exchange capacity from 80 to 120 meq/100 g allowed for PS intercalation to occur. At a low CEC and for a single alkyl chain built up cation, no intercalation was observed. Under these conditions, the aliphatic alkyl chain of the organic cation adopted a pseudo monolayer arrangement characterized by a low gallery height. However, excessive packing of the chains all along the layer surface led to the formation of a non-intercalated structure as predicted by the theory introduced by Vaia and Giannelis [78]. The authors also found out that polymer intercalation depended on the length of the exchange ammonium cation as well as on the annealing temperature. At annealing temperature equal to or lower than 160 °C and for chain lengths lower than 12 carbon atoms, no intercalation was detected, while for higher chain lengths PS readily intercalated. At 180 °C, intercalation occurred, whatever the ammonium chain length was. However, the width at half-maximum of the XRD diffraction peak, which is known to indicate the intercalation regularity, increased for chain lengths lower than or equal to 12 carbon atoms. Such a peak broadening attests for a more disordered and irregular structure and normally arises only for organomodified clays with a pseudo bilayer chain arrangement. The authors interpreted this behaviour as an extended propensity of the organoclays to separate under these conditions. This exfoliation is kinetically limited by the static conditions used to produce the nanocomposites, i.e. simple annealing without mixing or shearing. The effect of the PS molecular weight was also studied. Contrary to what was predicted by the theory, intercalation occurred for PS chains of all lengths. Only the period of time needed for the intercalation to proceed was different, going from 6 h for a M_w of 30,000 to 24 h for 90,000 and 48 h for 400,000 at 160 °C. Clearly, high molecular weight PS chains decrease the kinetics of intercalation by decreasing the diffusivity of the polymer in the interlayer. The authors also studied the influence of the nature of the polymer matrix. They prepared, under the same experimental conditions, different composites based on poly(vinylcyclohexane) (PVCH), poly(3-bromostyrene) (PS3Br) and poly(vinylpyridine) (PVP). All these polymers appeared to be immiscible with the dioctadecyldimethylammonium-modified fluorohectorite, but formed intercalated structures with montmorillonite (with a lower CEC) modified by the same ammonium cation with the exception for PVCH. These differences in intercalation behaviour indicate that the chemical nature of the polymer pendant group affects the formation of the hybrid composition. In the case of intercalated PVP, a broadening of the diffraction peak in the XRD pattern indicates a less regular arrangement of the intercalated structure, possibly due to some

tendency for exfoliation. For the dodecylammonium-modified fluorohectorite the broadening of the diffraction peak in the case of the PVP-based nanocomposite was even more pronounced. These results are totally in accordance with the proposed thermodynamic model that anticipated a better intercalation and even exfoliation when polar interactions between the layered silicates and the polymer chains are enhanced.

Vaia et al. [85] studied the kinetics of melt intercalation by following the time evolution of XRD diffraction patterns for statically annealed polystyrene-octadecylammoniumexchanged fluorohectorite. The change in intensity of the pristine and intercalated diffraction peaks with time was used as a reflection of the kinetics of the polymer intercalation process (Figure 2.11).

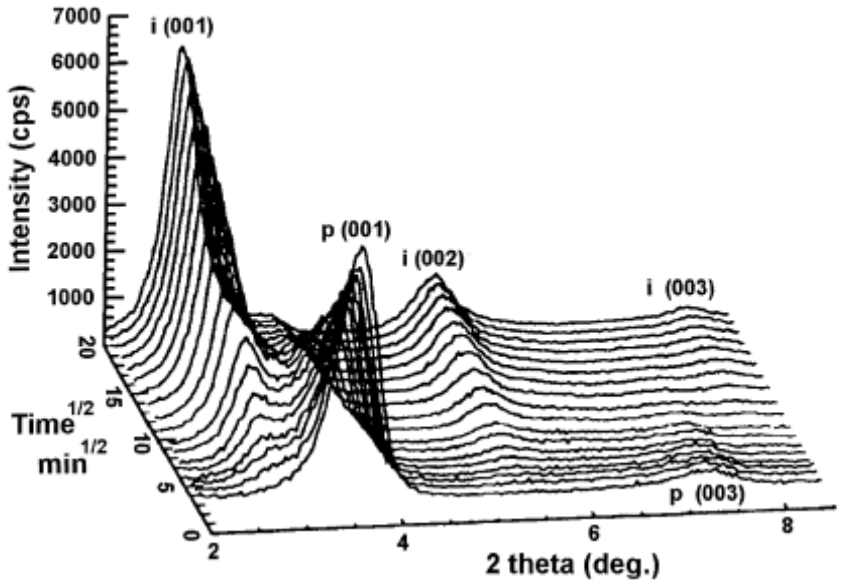

Figure 2.11 Temporal series of XRD patterns for organo-modified fluorohectorite/PS pellet annealed in situ at 160 °C in vacuum. *p*(001) and *p*(002) locate the basal reflections for the unintercalated fluorohectorite while *i*(001), i(002) and *i*(003) correspond to the basal reflections for the intercalated nanocomposite that is forming with time [85]

By integrating the intensity of both non-intercalated and intercalated peaks, the authors were able to estimate the fraction of intercalated silicates as a function of the annealing time. The influence of both annealing temperature and PS molecular weight was then determined. Higher annealing temperatures, as well as lower molecular weights, increased the rate of PS intercalation.

While the preparation of nanocomposites based on a nylon-6 matrix using an *in situ* intercalative polymerization has been widely described, less attention has been drawn to the nylon-6-based nanocomposites prepared by melt blending. Liu et al. [86] prepared nanocomposites based on a commercial nylon-6 melt blended with an octadecylammonium-exchanged montmorillonite (CEC=100 meq/100 g) in a twin screw extruder. They prepared composites with a filler content ranging from 1 to ~18 wt. %. An intercalated structure was observed for composites containing more than 10 wt. % of the organoclay, with the interlayer spacing increasing from 15.5 Å for the pristine organoclay to 36.8 Å for the intercalated species. At filler contents lower than 10 wt. %, no interlayer spacing could be detected through XRD, and the TEM micrographs showed an exfoliated structure, indicating that exfoliation in this case is highly dependent upon the filler content. XRD and DSC data also showed that exfoliated structures strongly influenced the nature of the nylon-6 crystallization, favoring the formation of γ-crystals in addition to the crystals of the α-form observed in the native nylon-6 matrix. The exfoliated layered silicates also increased the crystallization rate, having a strong heterophase nucleation effect.

Polypropylene (PP) nanocomposites were also investigated. No direct intercalation of PP in simple organically modified layered silicates has been observed so far, because PP is too much apolar to properly interact with the modified layers. Kato *et al.* [87] described the melt intercalation of PP chains modified with either maleic anhydride (PP-MA) or hydroxyl groups (PP-OH) in octadecylammonium-exchanged montmorillonite (CEC: 119 meq/100 g). When PP-MA or PP-OH was melt blended under shearing with the same amount of modified montmorillonite, intercalated nanocomposites were formed. However, a PP-MA matrix with a lower maleic anhydride content did not intercalate under the same conditions, showing that a small functionalization of the PP chains was needed for intercalation to proceed. The authors also examined the effect of polymer to clay ratio on the intercalation extent and showed that intercalation increased when the PP-MA fraction was increased. Intercalation of PP-MA in modified clay was used to prepare PP-based nanocomposites [88,89]. In both studies, the three components (PP, PP-MA and modified clay) were melt blended in a twin-screw extruder at 210°C in order to obtain composites filled with 5 wt. % clay. Formation of an exfoliated structure was observed for: (1) relatively high PP-MA content (typically 22 wt. %), and (2) sufficient polar functionalization of PP-MA chains (acid value = 26 mg KOH/g for M_w = 40,000). However, the relative maleic anhydride content cannot exceed a given value in order

to keep some miscibility between PP-MA and PP chains. When too many carboxyl groups are spread along the polyolefin chains (e.g. acid value = 52 mg KOH/g), no further increase in the interlayer spacing was obtained in clay/PP/PP-MA blends, leading rather to the dispersion of the PP-MA intercalated clay in the PP matrix.

Based on studies by Kato et al. [87–89], Reichert and Mülhaupt [90,91] mentioned the possibility of chemical reactions between MAPP and the octadecylamine used for the organophilization of the silicate. However, they assumed that strong hydrogen bonds are induced between the polypropylene grafted with N-ocatecyl-succinimide formed in the reaction and the silanol groups at the silicate surface. They also claimed that the octadecyl group, attached to the modified PP, promoted hydrophobic interaction with the surfactant remaining on the surface of the silicate. This latter explanation is contradicted by the experience that the strength of interaction between $CaCO_3$ and PP or PE decreases when the filler is covered by stearic acid, although both are very hydrophobic in nature [92–95]. Nevertheless, the occurrence of chemical reactions cannot be excluded between the very reactive MAPP and the amine used for treatment, in spite of the fact that it has been mentioned only as a possibility up to now [90,91,96]. For example, the formation of amide and imide groups was proved to take place in PA6/PP blends containing a MAPP coupling agent [97-100].

Taking into consideration the uncertainty related to the effect of MAPP, Pukánszky et al. [101] studied the possible interactions acting among the components in layered silicate PP nanocomposites. The results proved that maleinated polypropylene (MAPP) can react chemically with the surfactant applied for the organophilization of the filler, if this latter contains active hydrogen groups. The reaction of hexadecylamine (HDA) and MAPP was detected by MALDI-TOF spectroscopy, DSC measurements and FTIR spectroscopy. Anhydride groups are consumed and mainly amide groups form in the reaction. The formation of cyclic imides could not be proved by the techniques used. MAPP also reacted with the surfactant adsorbed on the surface of the silicate in ionic form. On the other hand, N-cetylpyridinium chloride (CPCl) not containing active hydrogen atoms did not react with maleinated PP. Intercalated or exfoliated composites could be prepared from the silicate organophilized with HDA, while microcomposites formed from the filler treated with CPCl. Chemical reactions remove the surfactant from the surface of MMT and hydrogenated silicate sites are left behind. The high energy surface interacts either with the anhydride or the amide

groups by dipole–dipole interactions. Even the unmodified polypropylene chains may be attached much stronger to the surface by London dispersion forces than to the silicate covered with aliphatic chains. Although the effect of competitive adsorption (MAPP, HDA) and mutual solubility of the components (PP, MAPP, surfactant, reaction products) cannot be neglected, chemical reactions play a crucial role in structure formation in PP nanocomposites containing a functionalized polymer. Direct interaction of the silicate surface and the functionalized polymer as well as the formation of hydrogen bridges seem to play a lesser role, but the relative influence of processes may change with the type of surfactant, functionalized polymer, surface coverage and processing conditions.

A symmetric (styrene-butadiene-styrene) (SBS) block copolymer was the first thermoplastic elastomer matrix investigated in the preparation of nanocomposites. Laus *et al.* [102] melt blended a commercial SBS with a dimethyldioctadecylammonium-exchanged montmorillonite in a Brabender mixer at 120 °C for 10 min. Composites with 10, 20 and 30 wt. % of filler were compounded. A comparative set of composites with the corresponding native Na-montmorillonite was also prepared. All the samples were further annealed at 120°C under nitrogen for periods ranging from 16 to 73 h in order to study the effect of the thermal treatment on their structural characteristics. The authors made sure that no chemical modification or degradation occurred during the compounding and thermal treatments by checking the molecular parameters of the SBS copolymers. SBS, recovered by complete extraction in $CHCl_3$ of these composites, displayed unmodified molecular parameters compared to the starting materials. While no change in XRD patterns appeared for the composites prepared with Na-montmorillonite, a substantial change in the XRD patterns could be observed for the composites based on the organo-montmorillonite. These composites showed both a small increase in the interlayer spacing and a broadening of the diffraction peak that increased with annealing time. This information indicated the formation of intercalated nanocomposites that was far from being complete during the blending time. Analysis of the dynamic mechanical properties showed an increase in the glass transition temperature (T_g) of the polystyrene outer blocks with increasing filler content, while the T_g corresponding to the polybutadiene block remained unchanged (Figure 2.12).

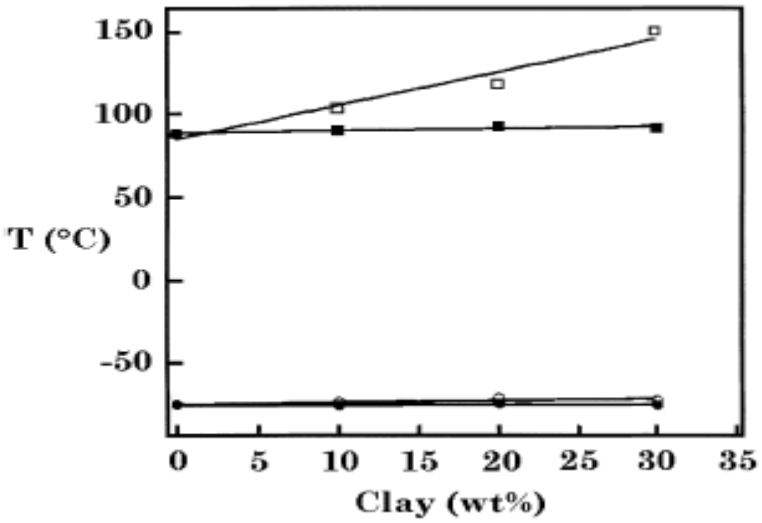

Figure 2.12 Trends of the glass transition temperatures of the polystyrene (squares) and polybutadiene (circles) blocks domains for symmetric (styrene-butadiene-styrene) block copolymer-based nanocomposites (open symbols) and microcomposites (full symbols) as a function of the filler content [102]

Under similar conditions the presence of pristine Na-montmorillonite did not have any effect on both the PS and PBD blocks. This T_g increase for the PS blocks (which was also enhanced for longer annealing times) can be interpreted by a selective intercalation of the styrene blocks into the silicate galleries, which was more important at higher nanofiller content and longer annealing times.

2.5 Characterization techniques

Various techniques are generally used to study polymer nanocomposites (Table 2.1). The structure of polymer nanocomposites is normally characterized by x-ray diffraction (XRD) and transmission electron microscopy (TEM). XRD, and in particular wide angle XRD, is the most commonly used technique for examining the structure and occasionally for studying the process kinetics of polymer nanocomposites. Either intercalated or exfoliated nanostructures can be studied by monitoring the position, shape, and intensity of the basal reflections of the XRD patterns of the materials. For instance, the broad layer separation in an exfoliated nanocomposite is seen in the disappearance of any coherent XRD peak. The finite layer expansion in an intercalated nanocomposite is associated with the appearance of a new basal reflection corresponding to the larger gallery height. XRD offers a convenient method to determine the interlayer spacing of original layered clays and intercalated nanocomposites.

Table 2.1 Common techniques for the characterization of clay-based polymer nanocomposites

Techniques	Characteristics and properties
XRD/WAXRD	Degree of swelling and interlayer distance of clays Dispersion degree of clay platelets Morphology (conventional, intercalated, exfoliated or mixed) Kinetics of intercalation process
SEM	Surface roughness and morphology Dispersion degree of clay particles
TEM/HRTEM	Morphology and its development Microstructure (intercalated vs. exfoliated) Spatial distribution of clay platelets Structural heterogeneities Defect structure and atomic arrangement
AFM	Crystallization behaviour of polymers Surface roughness Particle size and distribution Morphology and microstructure (intercalated vs. exfoliated)
FTIR	Component identification and analysis Interfacial interactions Crystallization and orientation of polymers
NMR	Local dynamics of polymer chains Morphology and dispersion of clay particles Surface chemistry
SAXS	Dispersion of nanoscale clay platelets Morphology (conventional, intercalated, exfoliated or mixed) and its development Lamellar texture and thickness
TGA	Thermal stability/ Weight change
DSC	Melting and crystallization behaviour Glass transition temperature Local dynamics of polymer chains
DMA	Response of a material to oscillatory deformation as a function of temperature, giving storage modulus
Rheometry	Nanorheology
Mechanical testing	Young's modulus, tensile strength and elongation at break Viscoelastic properties

Unfortunately, this technique cannot provide information about the spatial distribution of the clay layers or structural non-homogeneities in the nanocomposites. It is also difficult to properly study systems that show broad peaks and weak intensities. From this point of view, information from XRD patterns is not sufficient to reveal the formation mechanism and ultimate structure of nanocomposites. One should be cautious about data from XRD when the layer spacing in intercalated nanocomposites exceeds 6–7 nm or when the layers become relatively disordered in exfoliated nanocomposites. In this case, the simultaneous use of small angle X-ray scattering (SAXS) with wide angle XRD can yield quantitative characterization of the structure in polymer nanocomposites. TEM can, however, provide direct qualitative information of structure, morphology and spatial distribution of the various components as well as the defect structure. Nuclear magnetic resonance (NMR) spectroscopy is another important tool for probing the surface chemistry and coordination in exfoliated polymer nanocomposites, which may help quantify the level of clay exfoliation. Fourier transforms infrared (FTIR) and Raman spectroscopy can be used to understand the structural formation of polymer nanocomposites. Atomic force microscopy (AFM) is another technique to characterize nanocomposites [103]. AFM can provide information about the mechanical properties of a surface at a length scale that is limited by the dimensions of the AFM tip.

2.6 Properties

Polymer nanocomposites generally show enhanced properties and better performance compared to both their conventional polymer composites and pure polymers. Such improvements are obtained without an increase in the polymer density or a loss in its optical properties and recyclability. For example, polymer nanocomposites containing 2–8% of clay show an observable improvement in mechanical (tensile, stress, strain) properties together with thermal (dimensional) stability. They also reduce the gas and liquid permeability and flame retardancy of the polymer, while retaining the optical clarity of the polymer. They also show interesting conductivity properties and improved biodegradability when conductive polymers and biodegradable polymer are involved.

2.6.1 Mechanical properties

The enhancement in mechanical properties of polymer nanocomposites can be attributed to the high rigidity and aspect ratio of the filler, together with the good affinity between polymer

and the organoclay. For instance, stronger interfacial interactions significantly reduce the stress concentration point upon repeated distortion, which easily occurs in conventional composites reinforced by glass fibers and thus lead to weak fatigue strength. The unprecedented mechanical properties of nylon 6-clay nanocomposites synthesized by *in-situ* polymerization were first demonstrated by researchers at the Toyota Central Research Laboratories [104]. These nanocomposites exhibited significant improvement in strength and modulus, namely, 40% in tensile strength, 60% in flexural strength, 68% in tensile modulus, and 126% in flexural modulus. The RTP Company also reported equivalent property enhancement of nylon 6-clay nanocomposites synthesized by direct melt intercalation [105]. The increase in modulus is believed to be directly related to the high aspect ratio of the clay layers, as well as the ultimate nanostructure.

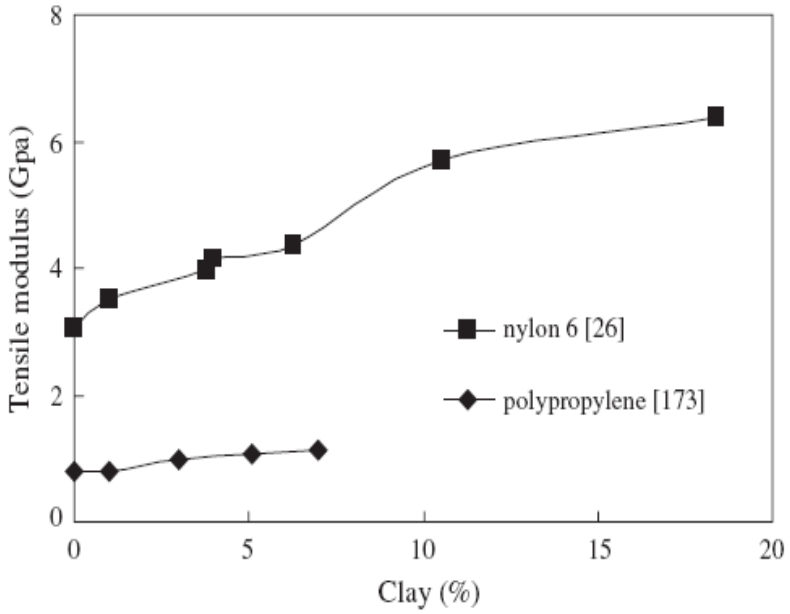

Figure 2.13 Effect of clay loading on tensile modulus for different clay-based polymer nanocomposites [104]

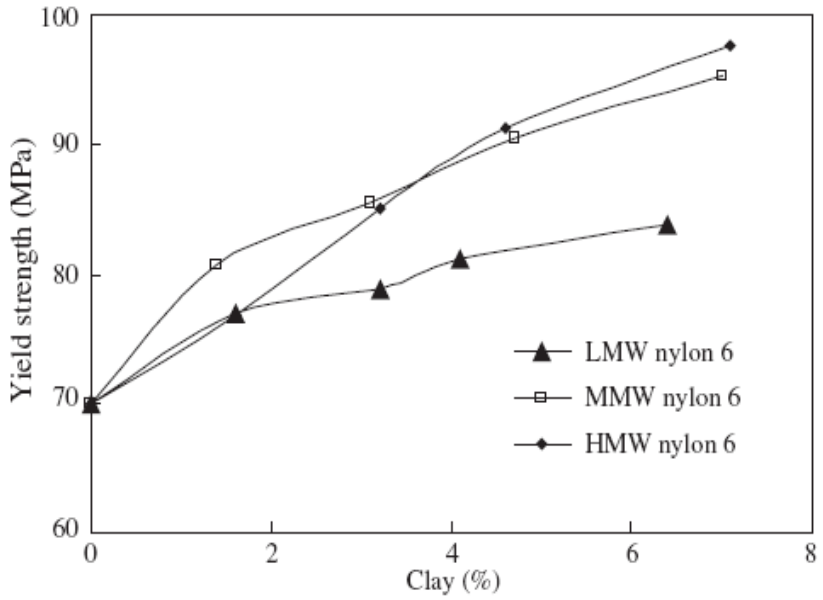

Figure 2.14 Effect of clay loading on yield strength for different clay-based nylon 6 nanocomposites [109]

A dramatic increase in the toughness balance was observed in exfoliated nanostructures such as MMT-based thermoset amine-cured epoxy and magadiite-based elastomeric epoxy nanocomposites [106,107]. Figures 2.13 and 2.14 show the effect of clay loading on the tensile modulus [104,107,108] and yield strength [109] of some polymer nanocomposites. In contrast, a relatively small improvement was reported for intercalated nanocomposites such as those from clay and poly(methylmethacrylate) (PMMA) [110] and PS [111]. The interaction strength at the interface would greatly affect the mechanical properties of polymer nanocomposites. For example, polar PMMA and ionic nylon 6 interacts with clay layers, which may explain the stress increase for the intercalated PMMA and the exfoliated nylon 6 nanocomposites. The impact properties measured for the nylon 6 nanocomposites showed that it was not affected much by the exfoliation process [112]. In the case of PP nanocomposites [113], the slight enhancement in tensile stress was attributed partially to the lack of interfacial adhesion between apolar PP and polar clays, which may be improved by adding maleic anhydride grafted PP to the matrix. The tensile stress was even more reduced in PS intercalated nanocomposites due to the weak interaction between PS and clay [66].

2.6.2 Thermal properties

The thermal stability of polymer composites is generally estimated from the weight loss upon heating which is the result of the formation of volatile products. The improved thermal stability in polymer nanocomposites is due to the clay platelets that hinder the diffusion of volatiles and assist the formation of char after thermal decomposition. Blumstein [114] first reported the thermal stability improvement in PMMA nanocomposites, and showed that intercalated PMMA containing 10% clay started degrading at about 40-50 °C higher than unfilled PMMA. There has been a number of reports on the improved thermal stability of nanocomposites made with various organoclays and polymer matrices [110,115,116]. For example, an improvement in thermal stability was reported for cross-linked poly(dimethylsiloxane) exfoliated with 10% of montmorillonite [117], and intercalated nanocomposites made from the polymerization of methyl methacrylate [110], styrene [111,118] and epoxy precursors [119].

Another type of thermal behaviour is the heat resistance upon external loading, which can be measured from the heat distortion temperature (HDT). The HDT of nylon 6 nanocomposites reported by Toyota researchers increased from 65 °C of pristine nylon to 145 °C. The increase in HDT was also observed in clay-based nanocomposites for other polymer systems such as PP [120] and polylactide (PLA) [121]. Such an increase in HDT is very difficult to achieve in conventional polymer composites reinforced by micro-particles. Finally, flame retardancy and mechanical properties are both improved in clay-based polymer nanocomposites, while the mechanical properties are always degraded in polymer composites with conventional flame retardants. Such fire resistance of polymer nanocomposites is attributed to the carbonaceous char layers formed during burning and the structure of the clay minerals. The multilayered clay structure acts as an excellent insulator and mass transport barrier. Char formation and clay structure impede the escape of the decomposed volatiles from the interior of a polymer matrix [122]. The flame retardancy of polymer nanocomposites was reviewed by Gilman [115]. The flame retardancy is normally evaluated by the reduction of the peak of the heat release rate (HRR).

2.6.3 Rheological properties

Aside from the understanding of the fabrication, characterization, and improved mechanical and other properties, the measurement of rheological properties of polymer-clay nanocomposites in the molten state is crucial to gain a fundamental understanding of the processability of these materials [123]. The dispersion state of the clays and the polymer-clay interaction are significant for the design of tailored polymer systems with enhanced properties. It was shown that these factors play a crucial role in controlling the final physical and chemical properties of the nanocomposites. It is well known that the clay nanostructure and polymer-clay interaction can strongly influence the linear and nonlinear rheological responses of polymer-clay nanocomposites. Because of the widespread use of fillers in polymeric products, the influence of the filler particles on the viscoelastic properties of polymer-based composite materials has been of significant technological interest. At the same time, the rheological properties are essential to determine the structure-property relationships of these materials [124].

Krisnamoorti and Giannelis [125] reported on the rheological properties of *in situ* polymerized nanocomposites with end-tethered polymer chains. They observed that the flow of poly(ε-caprolactone) (PCL) and nylon-6-based nanocomposites differed significantly from that of the corresponding neat matrices. The linear dynamic mechanical properties of polymer-clay nanocomposites were also intensively studied for a wide range of polymer matrices, including nylon-6 with various matrix molecular weights [107], (low-density polyethylene)/(ethylene vinyl acetate copolymers) blends [126], polystyrene-polyisoprene (PS-PI) block copolymers [127,128], poly(butylene succinate) [46], and other systems [6,17].

Clay sheets are highly anisotropic inorganic nanoparticles, which can be oriented under a shear field. Shear field-induced orientation of the polymer-clay nanocomposites has attracted considerable interest. Krishnamoorti *et al.* [129] reported on the shear-induced orientation-disorientation of clays in P-PI/intercalated-clay nanocomposites, while Schmidt *et al.* [130] reported on the shear-induced structural change in PEO/intercalated-clay solutions using a small-angle neutron scattering (SANS) technique. Both papers concluded that a strong flow field could enhance and maintain a continuous increase in the clay orientation of the polymer-clay system.

2.6.4 Crystallization behaviour

The mechanical properties and degradation rates of biodegradable aliphatic polyesters depend strongly on their crystal structures, morphology and crystallinity, as well as their chemical structures, which in turn are determined directly by the thermal treatment imposed on the polymers during the solidification process. It is therefore important to investigate the crystallization kinetics and morphology of these polymers, to understand the relationship between structural features and crystallization conditions under isothermal and non-isothermal conditions.

Sinha Ray et al. [46,47] reported the structure-property relationship of PBS nanocomposites. They used two different types of layered silicates: octadecyl ammonium modified montmorillonite (C18MMT) and quaternary hexadecyl tri-n-butylphosphonium modified saponite (qC16SAP). According to them, the structure of the nanocomposites is directly related to the nature of the pristine layered silicates and also to the surfactant used for the modification of the layered silicate. The effect of silicate layers on the crystallite structure, kinetics, and morphology of neat PLA upon nanocomposite formation with OMSL has been studied by Pluta et al. [131]. They first studied the crystallization behaviour and morphology of neat PLA and PLA/OMSL nanocomposites. Figure 2.15 represents the polarised optical microscopy (POM) photos of neat PLA and its composites taken at ambient temperature for samples crystallized at 120 °C. They found that clay particles act as nucleating agents for the crystallization of the PLA matrix, but they did not report the linear growth rate and overall crystallization rate of PLA before and after composite preparation.

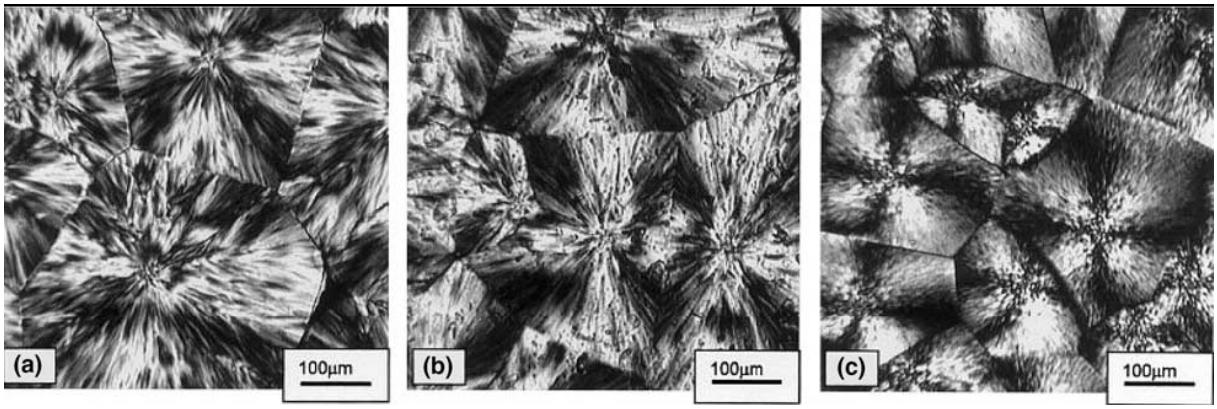

Figure 2.15 Polarized light micrographs taken at ambient temperature for samples crystallized at 120 °C from the molten state: (a) pure PLA, (b) PLA-based microcomposite, and (c) PLA-based nanocomposites [131]

Ren et al. [127] examined the bulk crystallization kinetics of PBS/A under isothermal and non-isothermal conditions. The morphology development and the spherulitic growth rate in PBS/A thin films as function of temperature were investigated. The spherulitic growth rates of PBS/A measured in isothermal conditions compared well with those measured by non-isothermal procedures. The kinetic data were analysed using the Hoffman-Lauritzen nucleation theory. The observed spherulites of PBS/A had different shapes and textures that depended upon the crystallization temperatures.

2.6.5 Other properties

Polymer nanocomposites also show significant improvements in most other polymer properties. For example, they have a transparency similar to the pristine polymers, because the clay platelets are about one nanometer in thickness. Thus, such clay platelets with sizes less than the wavelength of visible light do not hinder the light's passage. Scratch resistance is also enhanced by the incorporation of layered silicates [132]. The polymer nanocomposites can be used in highly technical areas to improve the ablative properties in aeronautics [133]. Silicate minerals exhibit unique electrical properties, which is mainly attributed to their ionic conductivity. Although the silicate layers can be regarded as insulators, the hydrated interlayer cations and their mobility ensure a significant ionic conductivity of the system [134]. The intercalation of the silicate particles also affects the hydration shells of interlayer cations, and therefore modifies the ion mobility, electrical conductivity and other electrical parameters.

2.7 References

1. C. Roco. Nanoparticles and nanotechnology research. Journal of Nanoparticles Research 1999; 1**:**1-6.
2. P. Holister, J-W. Weener, C. Romàn, T. Harper. Cientifica, Nanoparticles-Technology. White papers 2003; Nr.3:1-11.
3. Polymer Sciences Learning Center. http://www.pslc.
4. M. Zanetti, S. Lomakina, G. Camino. Polymer layered silicate nanocomposites. Macromolecular Materials and Engineering 2000; 279:1–9 (DOI: 10.1002/1439-2054(20000601)).

5. J. Luo, I.M. Daniel. Characterization and modeling of mechanical behavior of polymer/clay nanocomposites. Composites Science and Technology 2003; 63:1607-1616 (DOI:10.1016/S0266-3538(03)00060-5).
6. S. Sinha Ray, M. Okamoto. Polymer/layered silicate nanocomposites: A review from preparation to processing. Progress in Polymer Science 2003; 28:1539-1641 (doi:10.1016/j.progpolymsci.2003.08.002).
7. S. Qutubuddin, X. Fu. Polymer-clay nanocomposites: Synthesis and properties, In: Nano-Surface Chemistry. M. Rosoff. Eds.; Marcel Dekker: New York. 2002; M:653-673.
8. E.T. Thostenson, C. Li, T. Chou. Review: Nanocomposites in context. Composites Science and Technology 2005; 65:491-516 (DOI:10.1016/j.compscitech. 2004.11.003).
9. F. Gao. Clay/polymer composites: The story. Materials Today. 2004; 7:50-55 (DOI:10.1016/S1369-7021(04)00509-7).
10. H. Fischer. Polymer nanocomposites: from fundamental research to specific applications. Materials Science and Engineering C 2003; 23:763-772 (doi:10.1016/ j.msec.2003.09.148).
11. T.B. Tolle, D.P. Anderson. Morphology development in layered silicate thermoset nanocomposites. Composites Science and Technology 2002; 62:1033-1041 (PII: S0266-3538(02)00039-8).
12. P.M. Ajayan, L.S. Schadler, P.V. Braun. Nanocomposite Science and Technology. Wiley VCH: Verlag GmbH & Co. KGaA, Weinheim (2003).
13. C.M. Koo, H.T. Ham, S.O. Kim, K.H. Wang, I.J. Chung. Morphology evolution and anisotropic phase formulation of the maleated polyethylene-layered silicate nanocomposites. Macromolecules 2002; 35:5116-5122 (DOI: 10.1021/ma011770d).
14. A. Bafna, G. Beaucage, F. Mirabella, S. Mehta. 3D hierarchical orientation in polymer-clay nanocomposite films. Polymer 2003; 44:1103–1115 (PII: S0 03 2 -3 86 1 (0 2) 00 8 33 -9).
15. D.L. Van der Hart, A. Asano. NMR measurements related to clay-dispersion quality and organic-modifier stability in nylon-6/clay nanocomposites. Macromolecules 2001; 34:3819-3822 (DOI: 10.1021/ma002089z).
16. A. Tidjani, C.A. Wilkie. Photo-oxidation of polymeric-inorganic nanocomposites: Chemical, thermal stability and fire retardancy investigations. Polymer Degradation and Stability 2001; 74:33-37 (PII: S0141-3910(01)00061-1).

17. E.P. Giannelis. Review: Polymer-layered silicate nanocomposites: synthesis, properties and applications. Applied Organometallic Chemistry 1998; 12:675–680 (DOI: 10.1002/(SICI)1099-0739(199810/11)12:10/11<675).
18. J. Jordan, K.I. Jacob, R. Tannenbaum, M.A. Sharaf, I. Jasiuk. Experimental trends in polymer nanocomposites – a review. Materials Science and Engineering A 2005; 393:1-11 (DOI:10.1016/j.msea.2004.09.044).
19. J.W. Gilman. Flammability and thermal stability studies of polymer layered silicate clay-nanocomposites. Applied Clay Science 1999; 15:31-49 (DOI:10.1016/S0169-1317(99)00019-8).
20. A. Pozsgay, T. Fráter, L. Százdi, P. Müller, I. Sajó, B. Pukánszky. Gallery structure and exfoliation of organophilized montmorillonite: effect on composite properties. European Polymer Journal 2004; 40:27-36 (DOI: 10.1016/j.eurpolymj.2003.09.010).
21. L. Százdi, B. Pukánszky Jr, J.G. Vancso, B. Pukánszky. Quantitative estimation of the reinforcing effect of layered silicates in PP nanocomposites. Polymer 2006; 47:4638-4648 (DOI: 10.1016/j.polymer.2006.04.053).
22. L. Szazdi, A. Abranyi, B. Pukánszky, J.G. Vancso, B. Pukánszky. Morphology characterization of PP/clay nanocomposites across the length scales of the structural architecture. Macromolecular Materials and Engineering 2006; 291:858-868 (DOI: 10.1002/mame.200600026).
23. M. Alexandre, P. Dubois. Polymer-layered silicate nanocomposites: preparation, properties and uses of a new class of materials. Materials Science and Engineering 2000; 28:1-63 (DOI:10.1016/S0927-796X(00)00012-7).
24. D. Schmidt, D. Shah, E.P. Giannelis. New advances in polymer/layered silicate nanocomposites. Current Opinion in Solid State & Materials Science 2002; 6:205-212 (DOI: 10.1016/S1359-0286(02)00049-9).
25. J.J. Luo, I.M. Daniel. Characterization and modeling of mechanical behavior of polymer-clay nanocomposites. Composites Science and Technology 2003; 63:1607-1616 (DOI:10.1016/S0266-3538(03)00060-5).
26. E. Reynaud, T. Jouen, C. Gauthier, G. Vigier, J. Varlet. Nanofillers in polymeric matrix: A study on silica reinforced PA6. Polymer 2001; 42:8759-8768 (DOI:10.1016/S0032-3861(01)00446-3).
27. K. Varlot, E. Reynaud, M.H. Kloppfer, G. Vigier, J. Varlet. Clay-reinforced polyamide: Preferential orientation of the montmorillonite sheets and the polyamide crystalline

lamellae. Journal of Polymer Science Part B: Polymer Physics 2001; B39:1360-1370 (DOI: 10.1002/polb.1108).

28. R.A. Vaia. Structural characterization of polymer-layered silicate nanocomposites. In: T. J. Pinnavaia, G.W. Beall, (Ed). Polymer–clay nanocomposites. Wiley: New York (2001) p.229-266.
29. K. Yano, A. Usuki, T. Kurauchi, O. Kamigaito. Synthesis and properties of polyimide-clay hybrid. Journal of Polymer Science Part A: Polymer Chemistry 1993; 31:2493-2498 (DOI: 10.1002/pola.1993.080311009).
30. H. Fong, R.A. Vaia, J.H. Sanders, D. Lincoln, P.J. John, A.J. Vreugdenhil, J. Bultman, C.A. Cerbus, H.G. Jeon. Formation of self generating inorganic passivation layer on Nylon 6-layered silicate nanocomposite. Chemistry of Materials 2001; 13:4123-4129 (DOI: 10.1021/cm010150o).
31. P. Aranda, E. Ruiz-Hitzky. Poly(ethylene oxide)-silicate intercalation materials. Chemistry of Materials 1992; 4:1395-1403 (DOI: 10.1021/cm00024a048).
32. N. Ogata, S. Kawakage, T. Ogihara. Poly(vinyl alcohol)-clay and poly(ethylene oxide)-clay blends prepared using water as solvent. Journal of Applied Polymer Science 1997; 66:573-581 (CCC: 0021-8995/97/030573-09).
33. E. Manias, A. Touny, L. Wu, K. Strawhecker, B. Lu, T.C. Chung. Polypropylene/ montmorillonite nanocomposite: review of the synthetic routes and material properties. Chemistry of Materials 2001; 13:3516-3523 (DOI: 10.1021/cm0110627).
34. J. Rong, J. Jing, H. Li, M. Sheng. A polyethylene nanocomposite prepared via in-situ polymerization. Macromolecular Rapid Communications 2001; 22:329-334 (DOI: 10.1002/1521-3927(20010301)22:5<329).
35. J. Zhao, A.B. Morgan, J.D. Harris. Rheological characterization of polystyrene-clay nanocomposites to compare the degree of exfoliation and dispersion. Polymer 2005; 46:8641-8660 (DOI:10.1016/j.polymer.2005.04.038).
36. K.R. Ratinac, R.G. Gilbert, L. Ye, A.S. Jones, S.P. Ringer. The effects of processing and organoclay properties on the structure of poly(methyl methacrylate) clay nanocomposites. Polymer 2006; 47:6337-6361 (DOI:10.1016/j.polymer. 2006.07.005).
37. J. Bandyopadhyay, S. Sinha Ray, M. Bousmina. Thermal and thermo-mechanical properties of poly(ethylene terephthalate) nanocomposites. Journal of Industrial and Engineering Chemistry 2007; 13:614-623.

38. S. Sinha Ray, P. Maiti, M. Okamoto, K. Yamada, K. Ueda. New polylactide-layered silicate nanocomposites. 1. Preparation, characterization and properties. Macromolecules 2002; 35:3104-3110 (DOI: 10.1021/ma011613e).
39. S. Sinha Ray, M. Bousmina, K. Okamoto. Structure and properties of nanocomposites based on poly(butylene succinate-co adipate) and organically modified montmorillonite. Macromolecular Materials and Engineering 2005; 290:759-768 (DOI: 10.1002/mame.200500203).
40. B. Lepoittevin, M. Devalckenaere, N. Pantoustier, M. Alexandre, D. Kubies, C. Calberg, R. Jerome, P. Dubois. Poly(ε-caprolactone) clay nanocomposites prepared by melt intercalation: mechanical, thermal and rheological properties. Polymer 2002; 43:4017-4023 (DOI:10.1016/S0032-3861(02)00229-X).
41. J. Bandyopadhyay, S. Sinha Ray, M. Bousmina. Effect of organoclay on the orientation and thermal properties of liquid-crystalline polymers. Macromolecular Chemistry and Physics 2007; 208:1979-1991 (DOI: 10.1002/macp.200700350).
42. S.T. Lim, Y.H. Hyun, H.J. Choi, M.S. Jhon. Synthetic biodegradable aliphatic polyester-montmorillonite nanocomposites. Chemistry of Materials 2002; 14:1839-44 (DOI: 10.1021/cm010377j).
43. S.R. Lee, H.M. Park, H.L. Lim, T. Kang, X. Li, W.J. Cho, et al. Microstructure, tensile properties, and biodegradability of aliphatic polyester-clay nanocomposites. Polymer 2002; 43:2495–2500 (doi:10.1016/S0032-3861(02)00012-5).
44. T. Fujimaki. Processability and properties of aliphatic polyesters, 'BIONOLLE', synthesized by polycondensation reaction. Polymer Degradation and Stability 1998; 59:209-214 (DOI: 10.1016/S0141-3910(97)00220-6).
45. D.R. Ishioka, E. Kitakuni, Y. Ichikawa. Aliphatic polyesters: Bionolle, in: biopolymers, polyesters III. Application and commercial products. Y. Doi, A. Steinbuchel (Eds), Wiley-VCH, Weinheim (2002) 4:275.
46. S. Sinha Ray, K. Okamoto, M. Okamoto. Structure-property relationship in biodegradable poly(butylene succinate)/layered silicate nanocomposites. Macromolecules 2003; 36:2355-2367 (DOI: 10.1021/ma021728y).
47. K. Okamoto, S. Sinha Ray, M. Okamoto. New poly(butylene succinate)/layered silicate nanocomposites. II. Effect of organically modified layered silicates on structure, properties melt rheology, and biodegradability. Journal of Polymer Science: Part B: Polymer Physics 2003; 41:3160-3172 (DOI: 10.1002/polb.10708).

48. T. Mitsunaga, K. Okada, Y. Nagase. Properties of biodegradable resin/clay nanocomposites. PPS Asia/Australia Meeting. Taipei, Taiwan, 2002; Paper No. 139.
49. T. Mitsunaga, K. Okada, Y. Nagase. Properties of biodegradable resin/natural fiber composites containing nano-scale particles. PPS Asia/Australia Meeting, Taipei, Taiwan, 2002; Paper No. 140.
50. M.L. Tansengco, Y. Tokiwa. Thermophilic microbial degradation of polyethylene succinate. World Journal of Microbiology and Biotechnology 1997; 14:133-138 (DOI: 10.1023/A:1008897121993).
51. J. Mergaert, A. Webb, C. Anderson, A. Wouters, J. Swings. Microbial degradation of poly(3-hydroxybutyrate) and poly(3-hydroxybutyrate-co-3-hydroxyvalerate) in soils. Applied and Environmental Microbiology 1993; 59:3233-3238 (0099-2240/93/103233-06$02.00/0).
52. K. Kasuya, K. Takagi, S. Ishiwatari, Y. Yoshida, Y. Doi. Biodegradabilities of various aliphatic polyesters in natural waters. Polymer Degradation and Stability 1998; 59:327-332 (DOI: 10.1016/S0141-3910(97)00155-9).
53. Y. Tokiwa, T. Suzuki. Purification and some properties of polyethylene adipate degrading enzyme produced by Penicillium sp. strain 14-3. Agricultural and Biological Chemistry 1977; 41:265-274.
54. Z. Gan, H. Abe, Y. Doi. Biodegradable poly(ethylene succinate) (PES). 1. Crystal growth kinetics and morphology. Biomacromolecules 2000; 1:704-712 (DOI: 10.1021/bm0000541).
55. I.A. Al-Raheli, M.A. Qudah Ali. On the triple melting behaviour of poly(ethylene succinate). Polymer International 1995; 37:249-254 (DOI: 10.1002/pi.1995. 210370402).
56. Y. Ichikawa, H. Kondo, Y. Igarashi, K. Noguchi, K. Okuyama, J. Washiyama. Crystal structures of α and β forms of poly(tetramethylene succinate). Polymer 2000; 41:4719-4727 (DOI:10.1016/S0032-3861(99)00659-X).
57. H.A. Al-Salah. Crystallization and morphology of poly(ethylene succinate) and poly(β-hydroxybutyrate) blends. Polymer Bulletin 1998; 41:593-600 (DOI: 10.1007/ s002890050406).
58. H.L. Chen, S.F. Wang. Crystallization induced microstructure of polymer blends consisting of two crystalline constituents. Polymer 2000; 41:5157-5164 (DOI:10.1016/S0032-3861(99)00745-4).

59. Z.B. Qiu, T. Ikehara, T. Nishi. Unique morphology of poly(ethylene succinate)/poly(ethylene oxide) blends. Macromolecules 2002; 35:8251-8254 (DOI: 10.1021/ma025599x).
60. G. Lagaly. Introduction: from clay mineral–polymer interactions to clay mineral–polymer nanocomposites. Applied Clay Science 1999; 15:1–9 (PII: S0169-1317_99.00009-5).
61. D.J. Greenland. Adsorption of polyvinyl alcohols by montmorillonite. Journal of Colloid Science 1963; 18:647-664 (DOI:10.1016/0095-8522(63)90058-8).
62. N. Ogata, S. Kawakage, T. Ogihara. Poly(vinyl alcohol)-clay and poly(ethylene oxide)-clay blends prepared using water as solvent. Journal of Applied Polymer Science 1997; 66:573-581 (CCC: 0021-8995/97/030573-09).
63. I. Billingham, C. Breen, J. Yarwoord. Adsorption of polyamine, polyacrylic acid and polyethylene glycol on montmorillonite: An in situ study using ATR-FTIR. Vibrational Spectroscopy 1997; 14:19-34.
64. R. Levy, C.W. Francis. Interlayer adsorption of polyvinylpyrrolidone on montmorillonite. Journal of Colloid and Interface Science 1975; 50:442-450 (DOI:10.1016/0021-9797(75)90167-8).
65. I. Wu, M.M. Lerner. Structural, thermal, and electrical characterization of layered nanocomposites derived from Na-Montmorillonite and polyethers. Chemistry of Materials 1993; 5:835-838 (DOI: 10.1021/cm00030a019).
66. A. Usuki, M. Kawasumi, Y. Kojima, A. Okada, T. Krauchi, O. Kamigaito. Synthesis of nylon-6 clay hybrid. Journal of Materials Research 1993; 8:1179-1184 (DOI: 10.1557/JMR.1993.1179).
67. Y. Kojima, A. Usuki, M. Kawasumi, A. Okada, T. Kurauchi, O. Kamigaito. Synthesis of nylon-6-clay hybrid by montmorillonite intercalated with ε-caprolactam. Journal of Polymer Science Part A: Polymer Chemistry 1993; 31:983-986 (DOI: 10.1002/pola.1993.080310418).
68. Y. Kojima, A. Usuki, M. Kawasumi, A. Okada, T. Kurauchi, O. Kamigaito. One-pot synthesis of nylon-6 clay hybrid. Journal of Polymer Science Part A: Polymer Chemistry 1993; 31:1755-1758 (DOI:10.1002/pola.1993.080310714).
69. P. Reichert, J. Kressler, R. Thomann, R. Müllhaupt, G.S. Stöppelmann. Nanocomposites based on a synthetic layer silicate and polyamide-12. Acta Polymerica 1998; 49:116-123 (0323-7648/98/0203-0116$17.50+.50/0).

70. P.B. Messersmith, E.P. Giannelis. Synthesis and barrier properties of poly(ε-caprolactone)-layered silicate nanocomposites. Journal of Polymer Science Part A: Polymer Chemistry 1995; 33:1047-1057 (DOI: 10.1002/pola.1995.080330701).
71. D. Mecerreyes, R. Jerome, P. Dubois. Novel macromolecular architectures based on aliphatic polyesters:relevance of the "coordination-insertion" ring-opening polymerization. Advances in Polymer Science 1999; 147:1-59.
72. A. LÖfgren, A-C. Albertsson, P. Dubois, R. Jerome. Recent advances in ring-opening polymerization of lactones and related compounds. Journal of Macromolecular Science - Reviews in Macromolecular Chemistry & Physics 1995; C35:379-418 (DOI: 10.1080/15321799508014594).
73. B.A. Rozenberg. Kinetics and mechanism of ε-caprolactone anionic polymerization under the influence of amines. Pure and Applied Chemistry 1981; 53:1715-1727 (0033—4545/81/091715—13$02.OO/O).
74. T.K. Chen, Y.I. Tien, K.H. Wei. Synthesis and characterization of novel segmented polyurethane/clay nanocomposite via poly(ε-caprolactone)/clay. Journal of Polymer Science Part A: Polymer Chemistry 1999; 37:2225-2233 (DOI: 10.1002/(SICI)1099-0518(19990701)37:13<2225).
75. P.B. Messersmith, E.P. Giannelis. Polymer-layered silicate nanocomposites: in situ intercalative polymerization of epsilon-caprolactone in layered silicates. Chemistry of Materials 1993; 5:1064-1066 (DOI: 10.1021/cm00032a005).
76. A. Akelah, A. Moet. Polymer-clay nanocomposites: free-radical grafting of polystyrene on to organophilic montmorillonite interlayers. Journal of Materials Science 1996; 31:3589-3596 (DOI:10.1007/BF00360767).
77. J.G. Doh, I. Cho. Synthesis and properties of polystyrene-organo ammonium montmorillonite hybrid. Polymer Bulletin 1998; 41:511-517.
78. R.A. Vaia, E.P. Giannelis. Lattice of polymer melt intercalation in organically-modified layered silicates. Macromolecules 1997; 30:7990-7999 (DOI: 10.1021/ma9514333).
79. A.C. Balazs, C. Singh, E. Zhulina. Modeling the interactions between polymers and clay surfaces through self consistent field theory. Macromolecules 1998; 31:8370-8381 (DOI: 10.1021/ma980727w).
80. A.C. Balazs, C. Singh, E. Zhulina, Y. Lyatskaya. Modeling the phase behavior of polymer/clay nanocomposites. Accounts of Chemical Research 1999; 8:651-657 (DOI: 10.1021/ar970336m).

81. Y. Lyatskaya, A.C. Balazs. Modeling the phase behavior of polymer-clay composites. Macromolecules 1998; 31:6676-6680 (DOI: 10.1021/ma980687w).
82. V.V. Ginzburg, A.C. Balazs. Calculating phase diagram of polymer-platelet mixtures using density functional theory: implication for polymer-clay composites. Macromolecules 1999; 32:5681-5688 (DOI: 10.1021/ma990135t).
83. R.A. Vaia, E.P. Giannelis. Polymer melts intercalation in organically-modified layered silicates: model predictions and experiment. Macromolecules 1997; 30:8000-8009 (DOI: 10.1021/ma9603488).
84. R.A. Vaia, H. Ishii, E.P. Giannelis. Synthesis and properties of two-dimensional nanostructures by direct intercalation of polymer melts in layered silicates. Chemistry of Materials 1993; 5:1694-1696 (DOI: 10.1021/cm00036a004).
85. R.A. Vaia, K.D. Jandt, E.J. Kramer, E.P. Giannelis. Kinetics of polymer melt intercalation. Macromolecules 1995; 28:8080-8085 (DOI: 10.1021/ma00128a016).
86. L.M. Liu, Z.N. Qi, X.G. Zhu. Studies on nylon-6 clay nanocomposites by melt-intercalation process. Journal of Applied Polymer Science 1999; 71:1133-1138 (CCC 0021-8995/99/071133-06).
87. M. Kato, A. Usuki, A. Okada. Synthesis of polypropylene oligomer-clay intercalation compounds. Journal of Applied Polymer Science 1997; 66:1781-1785 (CCC 0021-8995/97/091781-05).
88. M. Kawasumi, N. Hasegawa, M. Kato, A. Usuki, A. Okada. Preparation and mechanical properties of polypropylene-clay hybrids. Macromolecules 1997; 30:6333-6338 (DOI: 10.1021/ma961786h).
89. N. Hasegawa, M. Kawasumi, M. Kato, A. Usuki, A. Okada. Preparation and mechanical properties of polypropylene-clay hybrids using a maleic anhydride-modified polypropylene oligomer. Journal of Applied Polymer Science 1998; 67:87-92 (DOI: 10.1002/(SICI)1097-4628(19980103)67:1<87)
90. P. Walter, D. Mader, P. Reichert, R. Mülhaupt. Novel polypropylene materials. Journal of Macromolecular Science: Part A 1999; 36:1613–1639 (DOI: 10.1081/ MA-100101617).
91. P. Reichert, H. Nitz, S. Klinke, R. Brandsch, R. Thomann, R. Mülhaupt. Poly(propylene)/organoclay nanocomposite formation: Influence of compatibilizer functionality and organoclay modification. Macromolecular Materials and Engineering 2000; 275:8–17 (DOI: 10.1002/(SICI)1439-2054(20000201)275:1<8).

92. B. Pukánszky, E. Fekete, F. Tüdős. Surface tension and mechanical properties in polyolefin composites. Makromolekulare Chemie: Macromolecular Symposia 1989; 28:165–186.
93. B. Pukánszky, E. Fekete. Adhesion and surface modification. Advances in Polymer Science 1999;139:109-153.
94. E. Fekete, J. Móczó, B. Pukánszky. Determination of the surface characteristics of particulate fillers by inverse gas chromatography at infinite dilution: A critical approach. Journal of Colloid and Interface Science 2004; 269:143–152 (DOI:10.1016/S0021-9797(03)00719-7).
95. J. Móczó, E. Fekete, B. Pukánszky. Adsorption of surfactants on CaCO3 and its effect on surface free energy. Progress in Colloid and Polymer Science 2004; 125:134-141 (DOI: 10.1007/b13435).
96. D. García-López, O. Picazo, J.C. Merino, J.M. Pastor. Polypropylene–clay nanocomposites: Effect of compatibilizing agents on clay dispersion. European Polymer Journal 2003; 39:945–950 (DOI:10.1016/S0014-3057(02)00333-6).
97. W.S. Chow, Z.A.M. Ishak, J. Karger-Kocsis, A.A. Apostolov, U.S. Ishiaku. Compatibilizing effect of maleated polypropylene on the mechanical properties and morphology of injection molded polyamide 6/polypropylene/organoclay nanocomposites. Polymer 2003; 44:7427–7440 (DOI:10.1016/j.polymer. 2003.09.006).
98. F. Ide, A. Hasegawa. Studies on polymer blend of nylon 6 and polypropylene or nylon 6 and polystyrene using the reaction of polymer. Journal of Applied Polymer Science 1974; 18:963–974 (DOI: 10.1002/app.1974.070180402).
99. S.N. Sathe, S. Devi, G.S.S. Rao, K.V. Rao. Relationship between morphology and mechanical properties of binary and compatibilized ternary blends of polypropylene and nylon. Journal of Applied Polymer Science 1996; 61:97–107 (DOI: 10.1002/(SICI)1097-4628(19960705)61:1<97).
100. Y. Seo, B. Kim, S. Kwak, K.U. Kim, J. Kim. Morphology and properties of compatibilized ternary blends (nylon 6/a thermotropic liquid crystalline polymer/a functionalized polypropylene) processed under different conditions. Polymer 1999; 40:4441–4450 (PII: S0032-3861(98)00685-5).
101. L. Százdi, B. Pukánszky Jr, E. Földes, B. Pukánszky. Possible mechanism of interaction among the components in MAPP modified layered silicate PP nanocomposites. Polymer 2005; 46:8001-8010 (DOI: 10.1016/j.polymer. 2005.06.108).

102. M. Laus, O. Francescangeli, F. Sandrolini. New hybrid nanocomposites based on an organophilic clay and poly(styrene-b-butadiene) copolymers. Journal of Materials Research 1997; 12:3134-3139 (DOI: 10.1557/JMR.1997.0409).
103. M. Greene, C. Kinser, D. Kramer, L. Pingree, M. Hersam. Application of scanning probe microscopy to the characterization and fabrication of hybrid nanomaterials. Microscopy Research and Technique 2004; 64:415-434 (DOI: 10.1002/jemt.20100).
104. Y. Kojima, A. Usuki, M. Kawasumi, A. Okada, Y. Fukushima, T. Kurauchi, O. Kamigaito. Mechanical properties of nylon 6-clay hybrid. Journal of Materials Research 1993; 8:1185-1189 (DOI: 10.1557/JMR.1993.1185).
105. L. Sherman. Clay-filled 'nanocomposites' offer extraordinary properties. Plastic Technology 1999; 45:52-55.
106. C. Zilg, R. Mulhaupt, J. Finter. Morphology and toughness/stiffness balance of nanocomposites based upon anhydride-cured epoxy resins and layered silicates. Macromolecular Chemistry and Physics 1999; 200:661-670 (DOI: 10.1002/(SICI) 1521-3935(19990301)200:3<661).
107. Z. Wang, T.J. Pinnavaia. Hybrid organic-inorganic nanocomposites: Exfoliation of magadiite nanolayers in an elastomeric epoxy polymer. Chemistry of Materials 1998; 10:1820-1826 (DOI: 10.1021/cm970784o).
108. X.H. Liu, Q.J. Wu. PP/clay nanocomposites prepared by grafting-melt intercalation. Polymer 2001; 42:10013-10019 (PII:S0032-3861(01)00561-4).
109. T.D. Fornes, P.J. Yoon, H. Keskkula, D.R. Paul. Nylon 6 nanocomposites: the effect of matrix molecular weight. Polymer 2001; 42:9929-9940 (PII:S0032-3861(01) 00552-3).
110. D.C. Lee, L.W. Jang. Preparation and characterization of PMMA-clay hybrid composite by emulsion polymerization. Journal of Applied Polymer Science 1996; 61:1117-1122 (DOI: 10.1002/(SICI)1097-4628(19960815)61:7<1117).
111. M.W. Noh, D.C. Lee. Synthesis and characterization of PS-clay nanocomposite by emulsion polymerization. Polymer Bulletin 1999; 42:619-626.
112. A. Okada, A. Usuki. The chemistry of polymer-clay hybrids. Materials Science and Engineering 1995; C3:109-115 (SSDI: 0928-4931(95)00110-7).
113. N. Hasegawa, M. Kawasumi, M. Kato, A. Usuki, A. Okada. Preparation and mechanical properties of polypropylene-clay hybrids using a maleic anhydride-modified polypropylene oligomer, Journal of Applied Polymer Science 1998; 67:87-92 (DOI: 10.1002/(SICI)1097-4628(19980103)67:1<87).

114. A. Blumstein. Polymerization of adsorbed monolayers. II. Thermal degradation of the inserted polymer. Journal of Polymer Science Part A: General Papers 1965; 3:2665-2672 (DOI: 10.1002/pol.1965.100030721).
115. J.W. Gilman. Flammability and thermal stability studies of polymer layered-silicate clay-nanocomposites. Applied Clay Science 1999; 15:31-49 (PII: S0169-1317-99.00019-8).
116. M. Zanetti, G. Camino, R. Thomann, R. Mullhaupt. Synthesis and thermal behaviour of layered silicate-EVA nanocomposites. Polymer 2001; 42:4501-4507 (PII: S0032-3861(00)00775-8).
117. S.D. Burnside, E.P. Giannelis. Synthesis and properties of new poly(dimethylsiloxane) nanocomposites. Chemistry of Materials 1995; 7:1597-1600 (DOI: 10.1021/cm00057a001).
118. J.G. Doh, I. Cho. Synthesis and properties of polystyrene-organo ammonium montmorillonite hybrid. Polymer Bulletin 1998; 41, 511-518.
119. A.C. Lee, L.W. Jang. Characterization of epoxy-clay hybrid composite prepared by emulsion polymerization. Journal of Applied Polymer Science 1998; 68:1997-2005 (DOI: 10.1002/(SICI)1097-4628(19980620)68:12<1997).
120. P.H. Nam, P. Maiti, M. Okamoto, M. Kotaka, M. Ohshima, N. Hasegawa, A. Usuki. Foam processing and cellular structure of polypropylene/clay nanocomposites, In: The First World Congress of Nanocomposites. Chicago, USA, 2001.
121. S. Sinha Ray, K. Yamada, M. Okamoto, K. Ueda. New polylactide-layered silicate nanocomposites. 2. Concurrent improvements of material properties, biodegradability and melt rheology. Polymer 2003; 44:857-866 (PII: S0032-3861(0 2) 00818-2).
122. J.W. Gilman, T. Kashiwagi, J.E.T. Brown, S. Lomakin, E.P Giannelis, E. Manias. Flammability studies of polymer layered silicate nanocomposites. International SAMPE Symposium and Exhibition, 1998; 43:1053-1066.
123. S. Sinha Ray. Rheology of polymer-layered silicate nanocomposites. Journal of Industrial and Engineering Chemistry 2006; 12:811-842.
124. X. Wang, Y. Gao, K. Mao, G. Xue, T. Chen, J. Zhu, B. Li, P. Sun, Q. Jin, D. Ding. Unusual rheological behavior of liquid polybutadiene rubber-clay nanocomposite gels: the role of polymer-clay interaction, clay exfoliation, and clay orientation and disorientation. Macromolecules 2006; 39:6653-6660 (DOI: 10.1021/ma0605494).
125. R. Krishnamoorti, E.P Giannelis. Rheology of end-tethered polymer layered silicate nanocomposites. Macromolecules 1997; 30:4097-4102 (DOI: 10.1021/ma960550a).

126. H. Yang, Q.J. Zheng. Structure stability of organic montmorillonite used for preparing polyethylene/montmorillonite nanocomposite. Journal of Materials Science Letters 2003; 22:1431-1433.
127. J. Ren, A.S. Silva, R. Krishnamoorti. Linear viscoelasticity of disordered polystyrene-polyisoprene block copolymer based layered-silicate nanocomposites. Macromolecules 2000; 33:3739-3746 (DOI: 10.1021/ma992091u).
128. C.A. Mitchell, R. Krishnamoorti. Rheological properties of diblock copolymer/layered-silicate nanocomposites. Journal of Polymer Science Part B: Polymer Physics 2002; 40:1434-1443 (DOI: 10.1002/polb.10209).
129. R. Krishnamoorti, J. Ren, A.S. Silva. Shear response of layered silicate nanocomposites. Journal of Chemical Physics 2001; 114:4968-4973 (DOI:10.1063/ 1.1345908).
130. G. Schmidt, A.I. Nakatani, P.D. Butler, C.C. Han. Small-Angle neutron scattering from viscoelastic polymer-clay solutions. Macromolecules 2002; 35:4725-4732 (DOI: 10.1021/ma0115141).
131. M. Pluta, A. Galeski, M. Alexandre, M-A. Paul, P. Duois. Polylactide/montmorillonite nanocomposites and microcomposites prepared by melt blending: structure and some physical properties. Journal of Applied Polymer Science 2002; 86:1497-1506 (10.1002/app.11309).
132. R.A. Vaia, G. Price, P.N. Ruth, H.T. Nguyen, J. Lichtenhan. Polymer layered silicate nanocomposites as high performance ablative materials. Applied Clay Science 1999; 15:67-92 (PII: S0169-1317_99.00013-7).
133. M. Kawasumi, N. Hasegawa, A. Usuki, A. Okada. Nematic liquid crystal-clay mineral composites. Materials Science and Engineering 1998; C6:135-143 (PII: S0928-4931(98)00045-9).
134. H. Wong, B. Sen, V. Filip, M.C. Poon. Material properties of interfacial silicate layer and its influence on the electrical characteristics of MOS davices using hafnia as the gate dielectric. Thin Solid Films 2006; 504:192-196 (DOI:10.1016/ j.tsf.2005.09.123).

CHAPTER 3

EXPERIMENTAL

3.1 Materials

3.1.1 Polyethylene succinate (PES)

Polyethylene succinate (PES), a condensate of succinic acid and ethylene glycol, is an interesting thermoplastic polyester with properties comparable to many commodity plastics such as polypropylene and polyethylene [1]. PES used in this study is a commercial product from Nippon Shokubai (Japan), which according to the supplier, has a weight-average molecular weight, M_w = 181 kg mol^{-1}. PES was dried under vacuum at 50 °C for 36 h prior to use. Its molecular structure is presented in Figure 3.1.

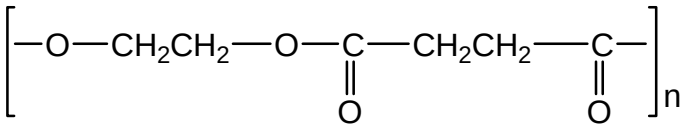

Figure 3. 1 Molecular structure of PES

3.1.2 Organically modified montmorillonite (OMMT)

Clay particles have a huge surface area (MMT has a specific surface area (S_O) of about 700-800 m^2 g^{-1} and are able to be well dispersed in the polymer matrix [2]. They can also act as strong nucleating agents for PES crystallization. OMMT used in this study was Cloisite®30B (C30B), purchased from Southern Clay Products, USA. According to the supplier, the original MMT clay is modified with 30 wt.% of methyl tallow bis(2-hydroxylethyl) quaternary ammonium salt. The reason for choosing C30B as an OMMT in this study is that it has the closest value of solubility parameter of the surfactant with that of the PES matrix [3].

3.1.3 Polybutylene succinate (PBS)

Poly(butylene succinate) (PBS) is a commercially available, aliphatic thermoplastic polyester with many interesting properties, including biodegradability, melt processability, and thermal and chemical resistance [1]. PBS (Bionolle#1020) used in this study is a commercial product of Showa Denko, Japan. High molecular weight PBS used in this research was prepared by a coupling reaction of relatively low molecular weight PBS in the presence of hexamethylene diisocyanate (OCN-C_6H_{12}-NCO) as a chain extender (Figure 3.2) [4]. PBS was dried under vacuum at 70 °C for 36 h prior to use.

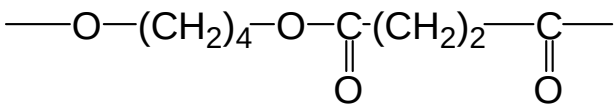

Figure 3.2 Molecular structure of PBS

3.1.4 Organically modified synthetic fluorine mica (OMSFM)

The organically modified synthetic fluorine mica (OMSFM) used in this study was supplied by CO-OP Chemicals Ltd., Japan, and was synthesized by replacing Na^+ in synthetic fluorine mica (SFM) (original thickness of ~1 nm and average length of 200-300 nm) with a cation exchange capacity (CEC) of 120 mequiv/100 g with N-(coco alkyl)-N,N-[bis(2-hydroxyethyl)]-N-methylammonium cation (Figure 3.3) by an ion exchange reaction.

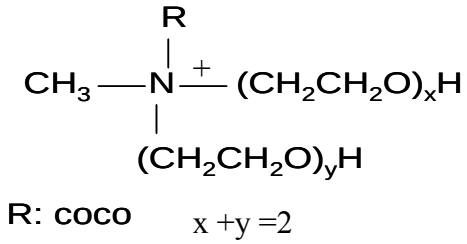

Figure 3.3 Molecular structure of surfactant used for the modification of synthetic fluorine mica

Synthetic fluorine mica (trade name SOMASIF) used in this study was synthesized by heating a mixture of talc and Na_2SiF_6 for several hours in an electric furnace. Like montmorillonite (MMT), synthetic fluorine mica also belongs to the same general family of 2:1 layered or phyllosilicates. The only difference between MMT and SFM is that SFM [$NaMg_{2.5}(Si_4O_{10})F_2$] contains 'F' groups on its surface (Figure 3.4) [5]. The reason for choosing N-(coco alkyl)-N,N-[bis(2-hydroxyethyl)]-N-methylammonium modified synthetic fluorine mica as an OMLS in this study was due to the closest value of solubility parameter of the surfactant with that of PBS. The solubility parameter (δ) for PBS and the organic modifier, N-(coco alkyl)-N,N-[bis(2-hydroxyethyl)]- N-methylammonium was roughly calculated from the group contribution methods of Fedors [6] The values of δ for PBS and surfactant are 21.7 and 22.5 $J^{1/2}\,cm^{-3/2}$, respectively.

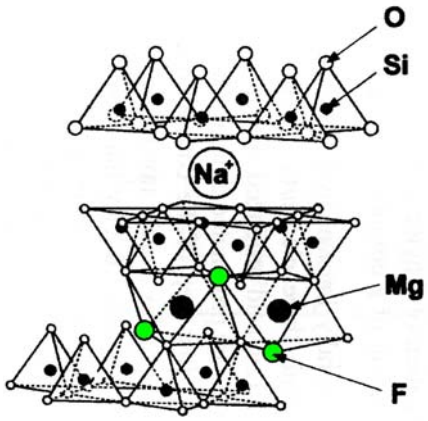

Figure 3.4 Crystal structure of synthetic fluorine mica

3.2 Methods

3.2.1 PES-OMMT nanocomposite preparation

The PES nanocomposite containing 5 wt. % C30B was prepared by using the solution-intercalation film casting technique. 5 g of PES was dissolved in 20 ml of chloroform ($CHCl_3$) at room temperature (24 ºC). A C30B dispersion $CHCl_3$ was obtained by suspension of well-dried C30B in another conical flask. Both the PES solution and the C30B suspension were sonicated separately for 30 min and subsequently mixed. The final mixture was further sonicated for 30 min at room temperature. The mixture was then cast on a glass surface and dried in a vacuum oven for 12 h. The solvent-cast nanocomposite film was compression moulded into sheets of 0.6 mm thickness, using a Carver Laboratory press at 135 ºC for 10

min. These compression moulded sheets were then used for various characterizations. For comparison purposes, a PES sheet without OMMT was prepared using the same processing techniques.

3.2.2 PBS-OSFM nanocomposite preparation

The nanocomposites were prepared through melt-mixing using a twin rotor thermohaake-mixer (Polylab system) operated at 140 °C (set point) and a rotor speed of 60 rpm for 8 min. The OMSFM powder was slowly added after one and half minutes of melting of PBS inside the mixer, which was considered as time zero.

The PBS nanocomposites (PBSCNs), prepared with three different amounts of OMSFM of 3, 6, and 9 wt. % were correspondingly abbreviated as PBSCN3, PBSCN6 and PBSCN9. The nanocomposite strands were then dried under vacuum at 70 °C for 7 h prior to molding the samples for various characterizations.

3.3 Characterization techniques

3.3.1 Characterization of the PES-OMMT nanocomposite

3.3.1.1 Small- and wide- angle x-ray scattering (SWAXS)

To check the degree of dispersion of silicate layers in the PES matrix, SWAXS experiments of pure C30B powder and annealed (at 50 ºC for 5 h) compression-moulded sheets of pure PES and the nanocomposites were performed with the SAXSess system from Anton Paar GmbH, operated at 40 kV and 40 mA. The radiation used was a Ni filtered CuK_{α} radiation source of wavelength of 0.154 nm (PAN analytical). The two-dimensional (2-D) detector was a curved imaging plate covering the scattering vector (q) range of 0.13-28 nm^{-1}. The read-out angles were calculated from the pixel size and the exactly known sample-to-detector distance of 264.5 mm. The obtained q scale was cross-checked by measuring silver behenate whose equidistant peak positions are known. To investigate the effect of crystal growth during non-isothermal crystallization, both pure PES and nanocomposite (annealed and compression moulded) samples were heated in a paste-cell from 30 to 50 ºC at a heating rate of 10 ºC min^{-1} and then cooled down to 40 ºC at a cooling rate of 10 ºC min^{-1} using a TCU50 (Anton-Paar)

temperature control unit, attached to the SAXSess instrument. SAXS data were collected at different temperatures during both heating and cooling. The samples were kept at each temperature for 5 min including 1 min exposure time under x-ray.

3.3.1.2 Transmission electron microscopy (TEM)

The degree of dispersion of silicate layers in the PES matrix was investigated by means of TEM (JEOL JEM 2100), operated at an accelerating voltage of 200kV. A thin film was cut using a cryo-ultramicrotome (-140 ºC) and collected onto 300 mesh carbon coated copper grids and was observed without further treatment.

3.3.1.3 Differential scanning calorimetry (DSC)

The melting and crystallization behaviour of compression-moulded pure PES and nanocomposite samples were investigated with DSC (TA-Instruments model Q2000 series), under a constant nitrogen flow of 50 mL min^{-1}. The samples weights were maintained at low levels (6-9 mg) for all measurements in order to minimize any possible thermal lag during the scans. The instrument was calibrated by using the temperature and heat-of-fusion of an indium standard, and the baseline was checked according to the TA Instruments protocols. To study the non-isothermal crystallization behaviour, samples were first heated to 120 °C at a heating rate of 20°C min^{-1}, kept at that temperature for 5 min to destroy any previous thermal history, and cooled to -60 °C at constant cooling rates of 2, 5, 10, 15 and 20 °C min^{-1}. To study the effect of crystallization on the melting behaviour, samples were heated from -60 °C to 120 °C at a heating rate of 20°C min^{-1} as soon as the cooling was finished. Each reported result is an average of three different measurements.

To separate the heat capacity and kinetic related components during heating of pure PES and the nanocomposite samples, temperature-modulated DSC (TMDSC) experiments were carried out using the same DSC instrument with a constant nitrogen flow of 50 ml min^{-1}. TMDSC generally applies a sinusoidal temperature oscillation on a conventional heating DSC and allows the total heat flow (as obtained from conventional DSC) to be separated into heat capacity related (reversible) and kinetic (non-reversible) components. The heating rate was 2

ºC min^{-1}, with an amplitude of ± 0.796 ºC, and a period of 60 s. The TMDSC was started as soon as cooling from the melt was finished.

3.3.1.4 Polarized optical microscopy (POM)

The spherulite structure of both pure PES and the nanocomposite samples during non-isothermal crystallization was studied with a Carl-Zeiss Imager Z1M polarized optical microscope (POM) equipped with a Linkam hot stage (Linkam Scientific Instruments Ltd, UK). Compression-moulded thin films were placed in between two covering glasses and placed on a Linkam hot stage, mounted on an optical microscope. Samples were melted at 120 °C at a heating rate of 20 °C min^{-1}, held at that temperature for 5 min and then cooled down to 40 °C at a precisely controlled cooling rate of 10 °C min^{-1}.

3.3.1.5 Thermogravimetric analysis (TGA)

The thermogravimetric analyses of pure PES and the nanocomposite samples were conducted on a TGA (TA Q500 Instrument) at a heating rate of 10 °C min^{-1} under pyrolytic conditions, from room temperature to 800 °C. Typically three consecutive runs were conducted for each sample and the averages are reported with an uncertainty of ±1.7 ºC.

3.3.2 Characterization of PBS-OMSFM nanocomposites

3.3.2.1 Gel Permeation Chromatography (GPC)

The weight-average (M_w) and number-average (M_n) molecular weights of the PBS matrix before and after nanocomposites preparation with three different amounts of OMSFM were determined from GPC (LC-VP, Shimadzu Co.), which was calibrated using polystyrene standards and chloroform ($CHCl_3$) as a carrier solvent at 40 °C with flow rate of 0.5 mL min^{-1}.

3.3.2.2 X-ray diffraction (XRD) analysis

XRD analyses were performed for the OMSFM powder and compression moulded sheets of three different types of PBSCNs using a MXlabo diffractometer (MAC Science Co.), which

has an x-ray generator of 3 kW, a graphite monochromator, CuK_α radiation (wavelength, λ 0.154 nm) and operated at 40 kV/20 mA. The samples (annealed in the case of PBSCNs) were scanned in fixed time (FT) mode with a counting time of 2 s over diffraction angle 2θ range of 1–10°.

3.3.2.3 Transmission electron microscopy (TEM)

Dispersability of the intercalated silicate particles in the PBS matrix was evaluated by means of transmission electron microscopy (TEM, JEOL model JEM-1230 instrument), operated at an accelerating voltage of 80 kV. The TEM specimens were about 50–70 nm thick. They were prepared by ultramicrotoming the PBSCNs encapsulated in epoxy with a diamond knife.

3.3.2.4 Differential scanning calorimetry (DSC)

The melting and non-isothermal crystallization behavior of the pure PBS and the nanocomposite samples were studied by using DSC (TA Instruments model Q2000 series) under constant nitrogen flow. The DSC samples were weighed such that all the samples had identical PBS content. The sample weight was maintained at low levels (7-10 mg) for all measurements in order to minimize any possible thermal lag during the scans. Each reported result is an average of four separate measurements. Temperature and heat of fusion were calibrated with an indium standard, and the base line was checked according to the TA Instruments protocols. The thermal histories of all the samples were the same.

To separate the heat capacity and kinetic related components during heating of neat PBS and the nanocomposite samples, temperature modulated DSC (TMDSC) of the compression moulded samples was carried out using the same DSC instrument with a constant nitrogen flow. TMDSC generally applies a sinusoidal temperature oscillation (modulation) on a conventional heating DSC and allows the total heat flow (as obtained from conventional DSC) to be separated into the heat capacity related (reversible) and kinetic (non-reversible) components. The heat capacity was calibrated with a sapphire sample. The heating rate was 2 °C min^{-1}, with an amplitude of ± 0.318 °C, and a period of 60 s.

3.3.2.5 Thermomechanical properties

The thermomechanical properties of the neat PBS and the nanocomposite samples were measured by using a Paar Physics MCR501 rheometer in the tension-torsion mode. The temperature dependence of the storage modulus (G'), loss modulus (G''), and tan δ of neat PBS and the nanocomposites were measured at a constant frequency of 6.28 rad s^{-1} with a strain amplitude of 0.02% (selected after a series of strain sweep tests at different temperatures because we are interested in the linear region) and in the temperature range of -60 to 110 °C at a heating rate of 5 °C min^{-1}.

3.3.2.6 Tensile testing

Tensile testing is normally used to determine the initial (or Young's) modulus, as well as the tensile strengths, and sample elongations, at yield and break. In a typical tensile test, a sample of known dimensions is firmly tightened between two grips. The tensile tester pulls the sample from both ends, and measures the force required to pull the specimen apart, as well as the elongation of the sample. This data is then used to construct a stress-strain curve, from which the required tensile values are determined [7].

A Hounsfield H5KS universal testing machine was used for the tensile analysis of the samples. Test specimens for the tensile measurements were prepared from 1.5 mm thick plates according to ASTM D 638. The dumbbell samples were stretch at a speed of 50 mm min^{-1} under a cell load of 250.0 N and at room temperature (27 ºC and 37% humidity). About eight test samples were cut using a dumbbell cutter and they were all tested with a maximum error of 9%. The dimensions of the dumbbell shaped sample were as follows:

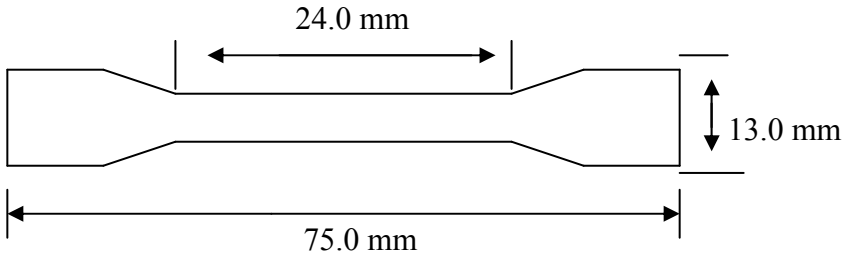

The instrument settings for the analyses were as follows:

Load range	250.0 N
Extension range	300.0 mm
Gauge length	24.0 mm
Speed	50.0 mm min^{-1}
Approach speed	0.02 mm min^{-1}

3.3.2.7 Thermogravimetric analysis (TGA)

The thermogravimetric analyses were conducted on a TGA Q500 instrument (TA Instruments) at a heating rate of 10 °C min^{-1} under both pyrolytic and thermo-oxidation conditions, from room temperature to 700 °C. Typically three consecutive runs were conducted for each sample and averages are reported with an uncertainty of ±1.7 °C.

3.4 References

1. J.E. Mark. Some novel polymeric nanocomposites. Accounts of Chemical Research 2006; 39:881-888 (DOI: 10.1021/ar040062k).
2. T. Fujimaki. Processability and properties of aliphatic polyesters, "BIONOLLE", synthesized by polycondensation reaction. Polymer Degradation and Stability 1998; 59:209-224 (PII: S0141-3910(97)00220-6).
3. Z. Gan, H. Abe, Y. Doi. Biodegradable poly(ethylene succinate) (PES). 1. Crystal growth kinetics and morphology. Biomacromolecules 2000; 1:704-712 (DOI: 10.1021/bm0000541).
4. T. Yasuda, E. Takiyama. Polyester injection-moulded articles. US Patent: 5391 644 (1995).
5. Z.B. Qiu, T. Ikehara, T. Nishi. Unique morphology of poly(ethylene succinate)/poly(ethylene oxide) blends. Macromolecules 2002; 35:8251-8254 (DOI: 10.1021/ma025599x).
6. D.W.V. Krevelen. Properties of Polymers. Elsevier: Amsterdam (1990).
7. F. Khan, J. Koo, D. Monk, E. Eisbrenner. Characterization of shear deformation and strain recovery behavior in shape memory polymers. Polymer Testing 2008; 27:498-503 (DOI: 10.1016/j.polymertesting.2008.02.006).

CHAPTER 4

THERMAL PROPERTIES OF POLY(ETHYLENE SUCCINATE) NANOCOMPOSITE

4.1 Overview

This chapter describes the thermal properties of clay-containing poly(ethylene succinate) (PES) nanocomposites. The nanocomposites of PES with organically modified montmorillonite (o-mmt) were prepared by a solution-intercalation-film-casting technique. Small-angle x-ray scattering patterns and transmission electron microscopy observations show the homogeneous dispersion of the silicate layers in the PES matrix. The crystallization and melting behaviour of the PES matrix in the presence of dispersed silicate layers were studied by differential scanning calorimetry, polarized optical microscopy, and wide-angle x-ray scattering. Results show that the incorporation of o-mmt stops the super-cooling effect and significantly accelerates the nucleation and crystal growth of the PES matrix. The incorporation of o-mmt also dramatically improves the thermal stability of neat PES.

4.2 Nanocomposite structure

The structure and morphology of the clay-containing polymer nanocomposites are generally probed by x-ray scattering and TEM observations. X-ray scattering offers a convenient method to determine the interlayer spacing of the silicate layers in the original clay and in the intercalated polymer/clay nanocomposites, while TEM allows a qualitative understanding of the internal structure through direct visualization. The SAXS patterns of the pure Cloisite 30B (C30B) powder and the normalized background (PES was taken as background) subtracted SAXS pattern of the nanocomposite are shown in Figure 4.1. The mean interlayer spacing of the (001) plane ($d_{(001)}$) for the C30B powder obtained by SAXS measurement is 1.85 nm (q = 3.4 nm^{-1}, as determined by using equation $d_{spacing} = 2\pi/q$ nm). In the SAXS pattern of the nanocomposite, a small peak appears at $q = 0.68$ nm^{-1}, which corresponds to a *d*-spacing of 9.2 nm. This is due to the crystalline structure of the PES chains in the very small angle region (see inset in Figure 4.1). However, it is very interesting to note that this crystalline

arrangement of the PES matrix remains almost unaltered after nanocomposite formation with C30B.

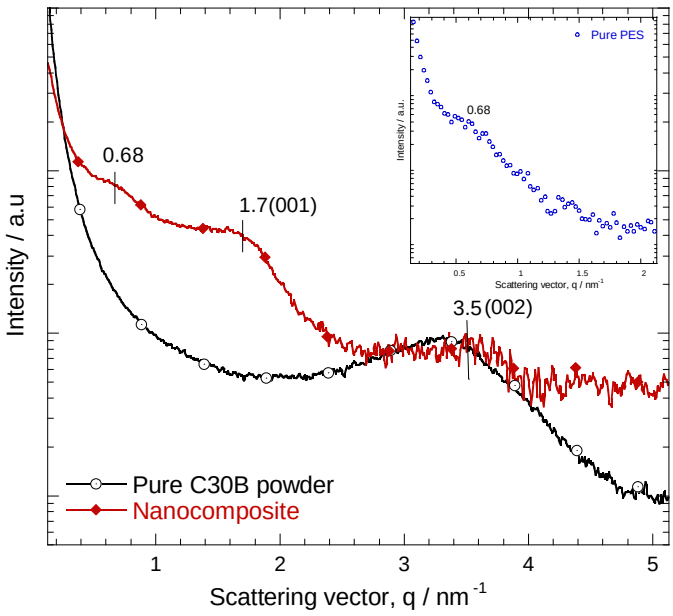

Figure 4.1 The normalized small-angle x-ray scattering (SAXS) pattern of pure C30B powder and normalized background (polymer was considered as background) subtracted SAXS pattern of nanocomposite. The small peak at $q = 0.68$ nm^{-1} is due to the crystalline structure of the polymer (see inset SAXS pattern of the pure polymer)

The intensity of the characteristic peak [(001) plane] of C30B is significantly reduced, and a broad peak is observed at $q = 1.7$ nm^{-1} [$d_{(001)} = 3.7$ nm]. Such an observation indicates that most of the silicate layers lost their initial stacking and are highly dispersed in the PES matrix. This may be due to the favourable interfacial interactions between the 'CO' groups on the PES backbone with the hydroxyl groups on the C30B surface. In the SAXS pattern of the nanocomposite another broad peak is observed at $q = 3.5$ nm^{-1}. After calculation, it is confirmed that this peak is from the (002) plane of the silicate layers dispersed in the PES matrix [1].

To support the observed SAXS pattern of the nanocomposite, the degree of dispersion of the silicate layers in the PES matrix was studied by TEM. Figure 4.2 shows the TEM bright field images of the nanocomposite containing 5 wt% C30B. The figures show a lower magnification, illustrating the dispersion of the silicate layers in the PES matrix, and a higher magnification, permitting the observation of the discrete silicate layers. The TEM images for

the nanocomposite reveal that there are some intercalated and disordered and/or exfoliated silicate layers coexisting in the nanocomposite. This is more discernible in the high magnification TEM image (marked by the arrow in the TEM images in Figure 4.2b). The stacked intercalated silicate layers are responsible for the very weak and broad scattering peak observed in the SAXS pattern (Figure 4.1) for the nanocomposite, whereas the disordered and exfoliated silicate layers have no periodic stacking and thus remain x-ray silent. This kind of mixed intercalated and/or exfoliated structure originates from the chemical and size inhomogeneities of the silicate layers. Typically the larger in-lateral sized silicate layers create stacked intercalated structures, whereas the smaller layers tend to exfoliate [2,3].

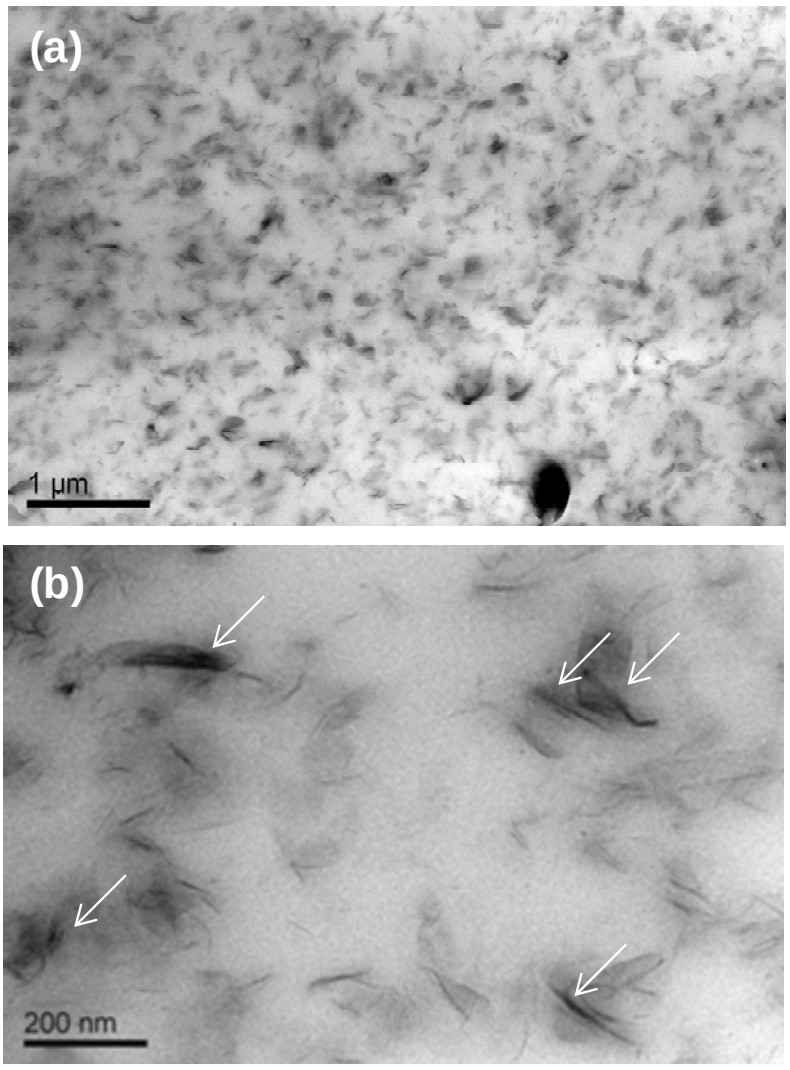

Figure 4.2 Bright field transmission electron microscopy images of the nanocomposite containing 5 wt% C30B at two different magnifications, where black entities are the dispersed silicate layers

The form factors obtained from the SAXS analyses and TEM observations, i.e. average length (L_{clay}) and thickness (d_{clay}) of the dispersed silicate layers and the correlation length (ξ_{clay}) between them, are summarized in Table 1. The average thickness of the dispersed clay particles calculated from the SAXS patterns of the nanocomposite matches with the value obtained from the TEM image. This indicates that a disordered intercalated structure is probably formed in the case of a PES/C30B nanocomposite.

Table 4.1 Comparison of the form factors of the nanocomposite obtained from the SAXS pattern and the TEM observations

	SAXS	**TEM[a]**
Average length of dispersed clay particles, L_{clay}/nm	–	171 ± 29
Average thickness of dispersed clay particles, d_{clay}/nm	7.12[b]	6.9 ± 1.5
Aspect ratio, L_{clay}/d_{clay}	–	~24.9
Average correlation length between dispersed clay particles, ξ_{clay}		150 ± 98
The mean interlayer spacing of (001) plane, $d_{(001)}$/nm	3.7[c]	–

[a] Calculated on the basis of 6 TEM images.

[b] Calculated using the Scherrer equation, $D = k\lambda/\beta\ Cos\theta$, where k is a constant (the value generally = 0.9), λ is the X-ray wavelength (λ = 0.154 nm), β is the width of the SAXS peak (in radians) and is measured by the full width at half-maximum, and θ is the SAXS peak position.

[c] Calculated from the (001) peak of the clay particles in the SAXS pattern.

4.3 Crystallization behaviour and morphology

To understand the effect of C30B incorporation on the crystallization behaviour of the PES matrix, DSC experiments of pure PES and the nanocomposite samples were carried out according to the method described in Chapter 3. The crystallization exotherms of neat PES and its nanocomposite during non-isothermal crystallization from their melts at five different cooling rates are shown in Figure 4.3. The results show that it is very difficult for the pure polymer sample to crystallize when the cooling rate was more than 5 °C min^{-1}. However, in

the case of the nanocomposite sample, the dispersed silicate layers stop the super-cooling effect and accelerate the mechanism of crystal growth of the polymer matrix. In the case of pure PES, when the sample was cooled at a cooling rate of 2 °C min^{-1} from the melt, a small and broad peak appears at 47.5 °C. With an increase in the cooling rate to 5 °C min^{-1}, this peak moves to a lower temperature. With a further increase in the cooling rate, a very broad peak is observed, which indicates an incomplete crystallization process. This indicates that when the cooling rate from melt was higher than 5 °C min^{-1}, it is very difficult for the PES matrix to crystallize and the sample stays in a super-cooled state. On the other hand, for the nanocomposite sample, a sharp crystallization peak is observed at 60 °C when the sample was cooled at 2 °C min^{-1} from the melt. As the cooling rate increases, this exothermic curve becomes wider and is shifted to lower temperatures. This observation is normal because, at a higher cooling rate, the sample passes through the crystallization process so quickly that there is not enough time for the molten sample to fully crystallize. Another interesting observation is that, when the nanocomposite sample cooled at 15 °C min^{-1} from melt, a small shoulder peak appears at -9.6 °C. This peak moves to 14.2 °C when the sample is cooled at 20 °C min^{-1}. This may be due to the growth of two different types of crystal at the higher cooling rate. On the basis of the above observations, one can conclude that the delaminated silicate layers have an active nucleating role causing the PES crystals to grow faster at higher cooling rates.

During non-isothermal crystallization, the true link between the DSC exotherms and the nucleation behaviour of the clay particles can further be examined by polarized optical microscopy (POM). The POM experiments were done at a cooling rate of 10 °C min^{-1} because during injection moulding the cooling rate is very fast and we are interested to see the effect of the incorporation of the C30B particles on the crystal growth behaviour at a higher cooling rate. The POM images of pure PES and the nanocomposite samples taken at three different temperatures during non-isothermal crystallization from their melts at a cooling rate of 10 °C min^{-1} are presented in Figure 4.4. It is clear from the images that it is very difficult for the pure PES crystals to grow at a cooling rate of 10 °C min^{-1}, while PES spherulites grew faster in the presence of the highly dispersed silicate particles. This observation confirms that the delaminated silicate layers actively nucleate the PES crystallization and because of this the PES matrix achieves a higher degree of spherulite formation.

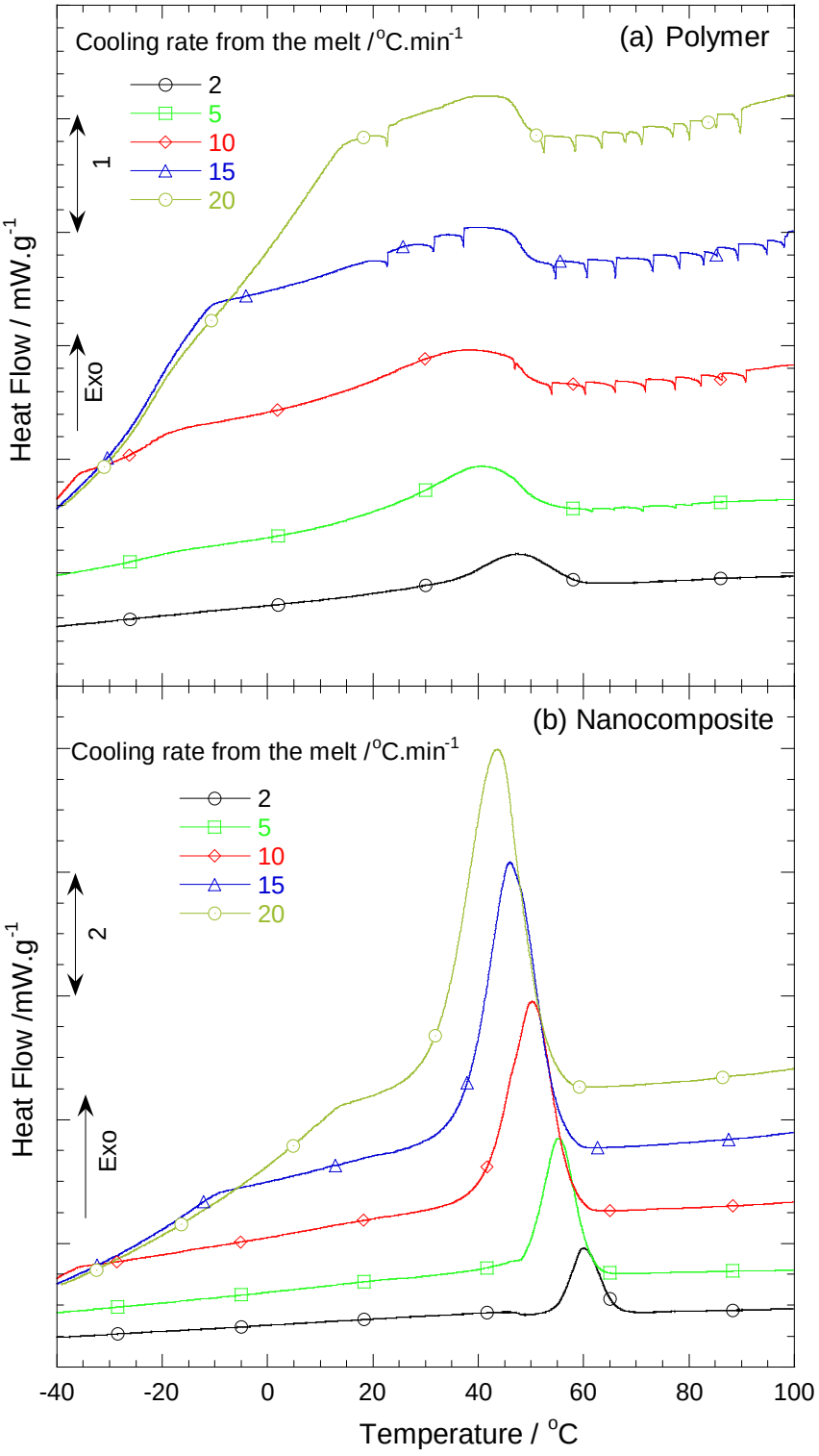

Figure 4.3 The DSC cooling curves of (a) the neat polymer and (b) the nanocomposite for the non-isothermal crystallization from the melt at five different cooling rates ranging from 2 to 20 °C min-1

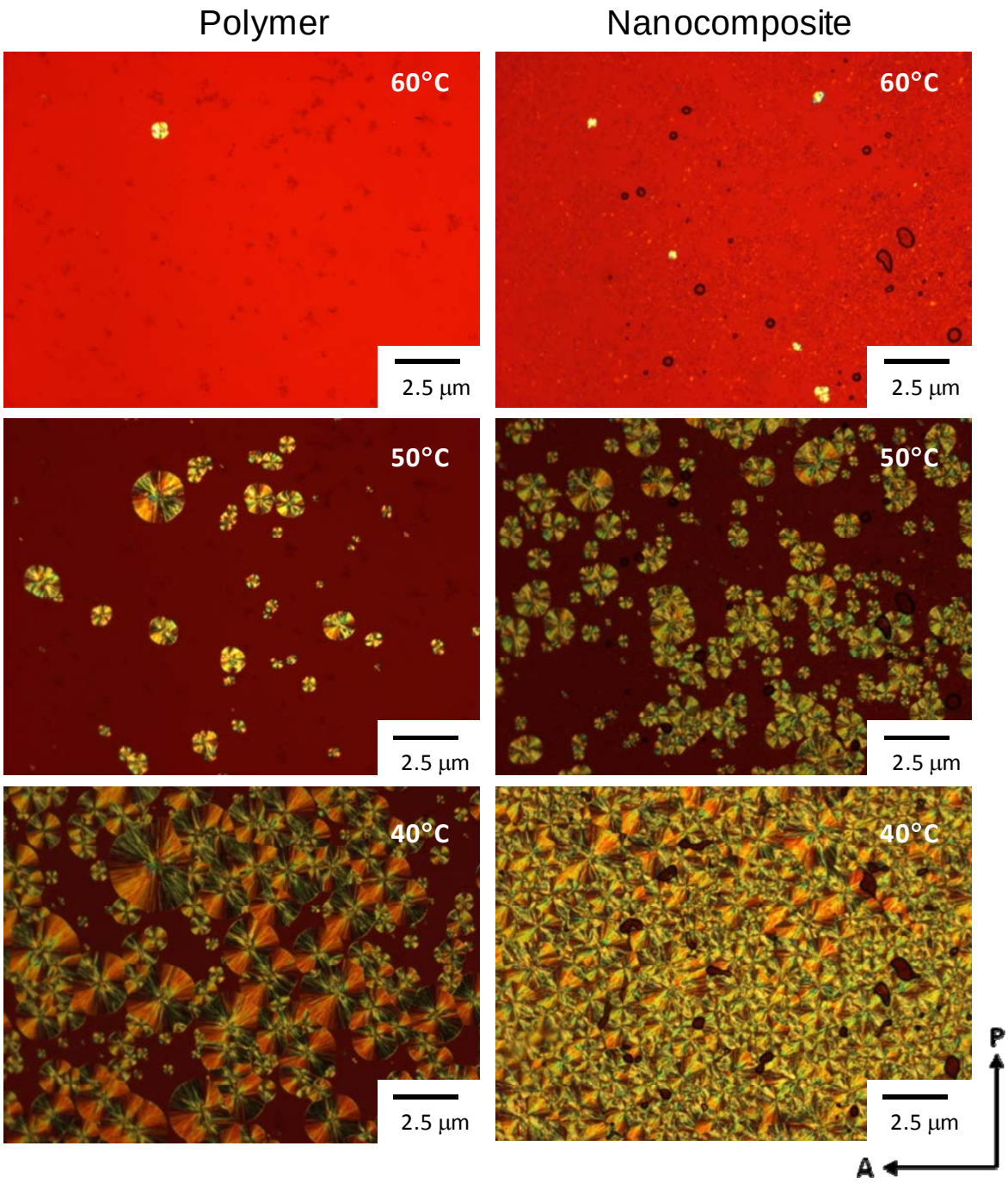

Figure 4.4 The polarized optical microscopy (POM) images of the pure polymer and its nanocomposite containing 5 wt% C30B at temperatures of 60, 50 and 40 °C during the non-isothermal crystallization from the melt at a cooling rate of 10 °C/min

4.4 Effect of the non-isothermal crystallization rate on the melting behaviour

To study the influence of non-isothermal crystallization on the melting behaviour, both PES and the nanocomposite samples were heated at a heating rate of 20 °C min^{-1} directly from −60 °C as soon as the cooling was finished. Figure 4.5 shows these curves, and the results are summarized in Table 4.2. It is clear from the figure that both samples, after cooling at a rate of 2 °C min^{-1} show three melting peaks for PES, labelled I, II, and III from low to high temperatures, and two re-crystallization peaks in between. However, with an increase in the cooling rate to 5 °C min^{-1}, in the case of pure PES, peak I disappears and a broad cold crystallization peak appears at 35.5 °C. With a further increase in the cooling rate, the cold crystallization phenomenon becomes more important. With an increase in the cooling rate, it is difficult for the PES polymer chains to crystallize during cooling and therefore more PES chains crystallize during heating. The melting temperature of peak II systematically moves to lower temperatures, while the different cooling rates did not affect peak III. This suggests that the crystals associated with the peak III melting are more perfect than the crystals associated with II-melting. Another interesting observation is that both the re-crystallization peaks moved towards low temperatures with an increase in the cooling rate during non-isothermal crystallization. The intensity of the re-crystallization peak between peaks II and III decreased with an increase in cooling rate during non-isothermal crystallization. This is also true for the nanocomposite. Finally, a small relaxation peak appears around −17.5 °C in the DSC curve of the pure PES sample. This is due to the disentanglement of the PES chains just before cold crystallization. With an increase in cooling rate, the cold crystallization phenomenon becomes more important and therefore this relaxation becoming more prominent with an increase in cooling rate.

In the case of the nanocomposite, the cold crystallization phenomenon does not appear. This indicates that the crystallization was complete after the non-isothermal crystallization at all the cooling rates. Like the pure PES, the peak II melting temperature systematically moves to lower temperatures with an increase in cooling rate; however, the positions of peak I and peak III remain unaffected by the cooling rate. This suggests that the crystals associated with the I- and III-melting are more perfect than the crystals associated with the II-melting. It is interesting to note that in the case of the nanocomposite, all the melting peaks appear at higher temperatures than that for pure PES. This is due to the higher crystallinity of the PES matrix in the presence of the dispersed silicate layers (see Table 4.2) [4].

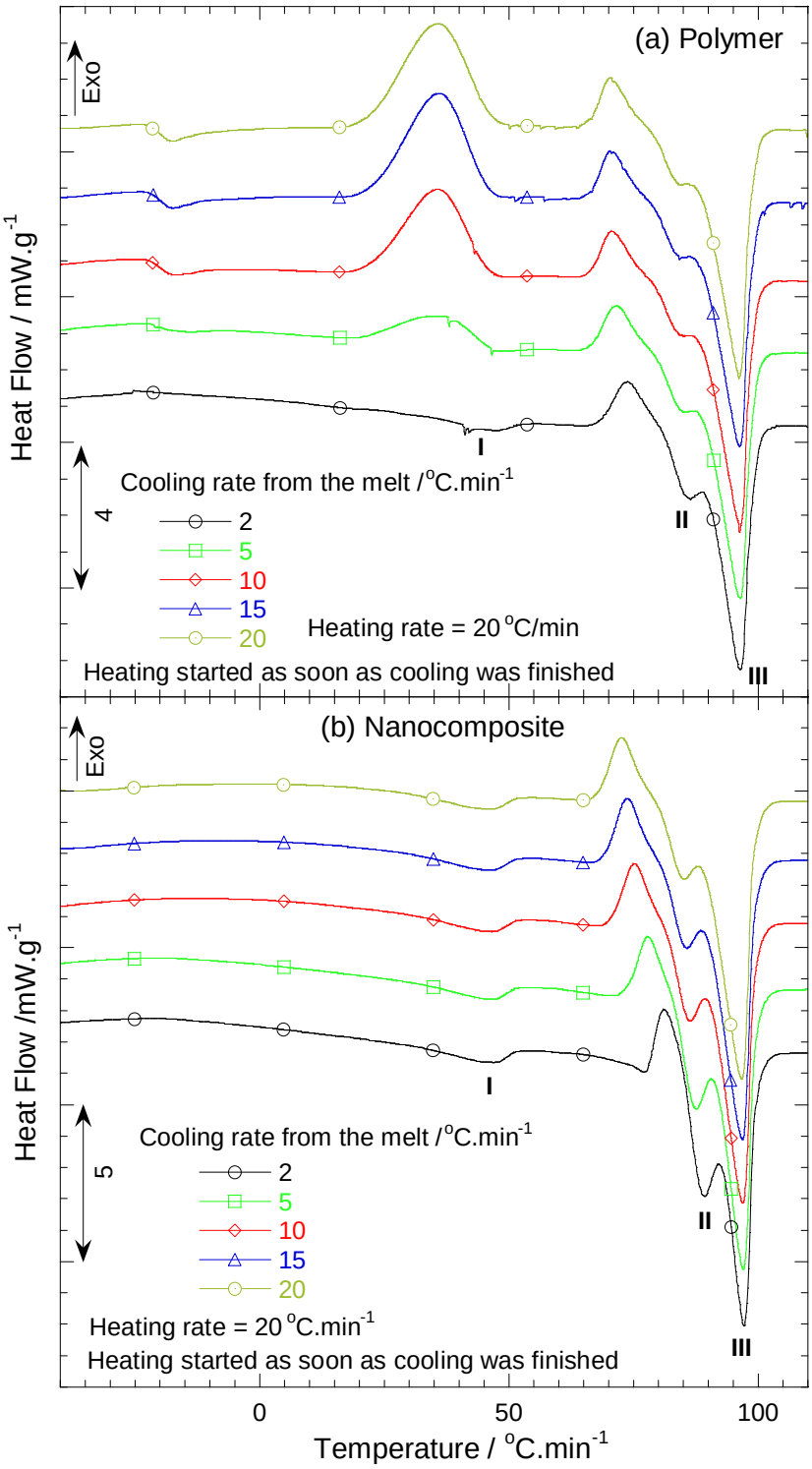

Figure 4.5 Melting behaviour of (a) the pure polymer and (b) the nanocomposite samples after non-isothermal crystallization at cooling rates of 2, 5, 10, 15, and 20 °C min^{-1}. The samples were heated at rate of 20 °C min^{-1} as soon as cooling was finished

Table 4.2 Rough estimation of the degree of crystallinity of PES from the II- and III-melting endotherms

Sample	Cooling rate	Melting enthalpy/J g^{-1}[a]	Crystallinity/%[b]
Polymer	2	34.1	18.9
	5	35.2	19.6
	10	35.0	19.4
	15	35.5	19.7
	20	35.3	19.6
Nanocomposite	2	44.9	26.9
	5	47.4	26.3
	10	49.1	27.2
	15	48.8	27.1
	20	49.3	27.4

[a] The total heat of fusion of the two melting peaks (II & III) of PES evaluated by integration of the area under the edothermic peaks from the heating scans after non-isothermal-crystallization

[b] Calculated using the 100% crystallinity value of PES, 180 J g^{-1} [4].

The multiple melting behaviour have already been reported for various types of semicrystalline polymers such as poly(ethylene terephthalate) [5], poly(butylene terephthalate) [6], polypropylene [7], poly(butylene succinate) [8], and poly[(butylene succinate)-co-adipate] [9,10]. There are several models to explain the multiple melting behaviour of semicrystalline polymers, of which the two most important ones are (a) the presence of melting, re-crystallization, and re-melting phenomena, and (b) the crystal structure modification during the heating scan [11,12]. According to the first model, the first

step is the melting and re-crystallization of the low melting crystallites with lower thermal stability, and then the melting of the crystallites with higher thermal stability formed through the re-crystallization of the crystallites molten at the lower temperatures.

Temperature modulated DSC (TMDSC) was used to verify the presence of the melting, re-crystallization, and re-melting phenomena of PES. TMDSC generally applies a sinusoidal temperature oscillation (modulation) on a heating conventional DSC and separates the total heat flow (as obtained from conventional DSC) into heat capacity related (reversible) and kinetic (non-reversible) components. This allows us to see whether a re-crystallization process occurs as soon as the PES begins to melt. Figure 4.6 shows the TMDSC curves of neat the PES and nanocomposite samples heated at a heating rate of 2 °C min^{-1} from -60 °C as soon as the cooling was finished (cooling rate from their melt was 2 °C min^{-1}). For both samples the total heat flow (middle curve) is separated into a well-defined, non-reversible heat flow (top curve) and a reversible heat flow (bottom curve).

In the case of the pure PES sample the following behaviour was observed: (1) A well distinguished melting endotherm appears at 74 °C in the reversible curve; (2) The intensities of the two re-crystallization peaks in the non-reversible curve are higher than those observed in the reversible and total heat flow curves; (3) Melting is also observed in the non-reversible heat flow curve along with the total and reversible heat flow curves. All these observations indicate that the multiple melting behaviour of the PES originates from the melting and re-crystallization of the low melting crystallites with lower thermal stability. The higher melting endotherm corresponds to the melting of the crystallites with higher thermal stability formed through the re-crystallization of the crystallites formed after the first melting.

The nanocomposite sample shows almost the same behaviour, but all the melting and re-crystallization peaks moved to higher temperatures. This is due to the very strong nucleation effect of the dispersed silicate layers in the PES matrix [13-15].

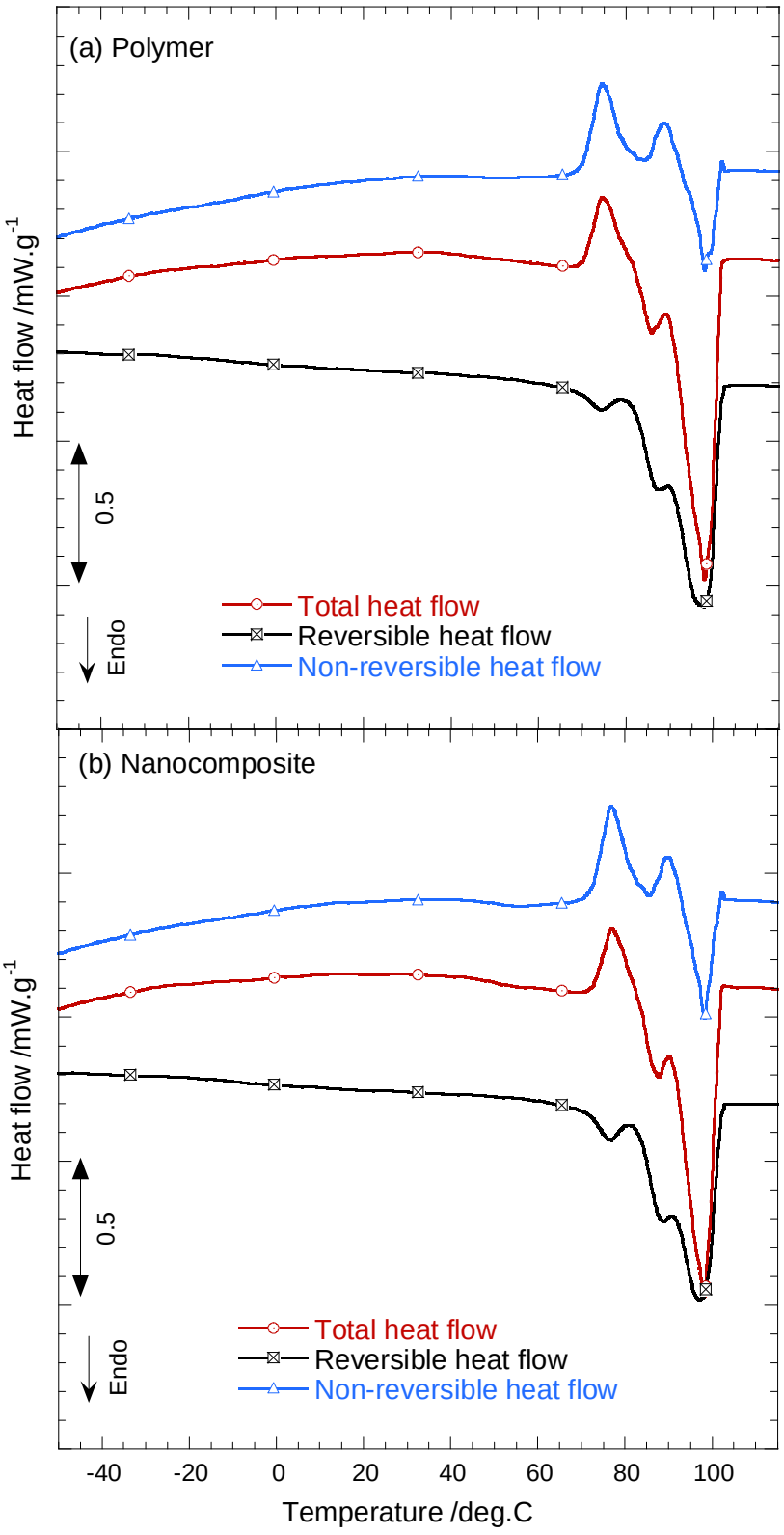

Figure 4.6 MTDSC curves of (a) the pure polymer and (b) the nanocomposite samples during the second heating

4.5 Wide-angle x-ray scattering (WAXS)

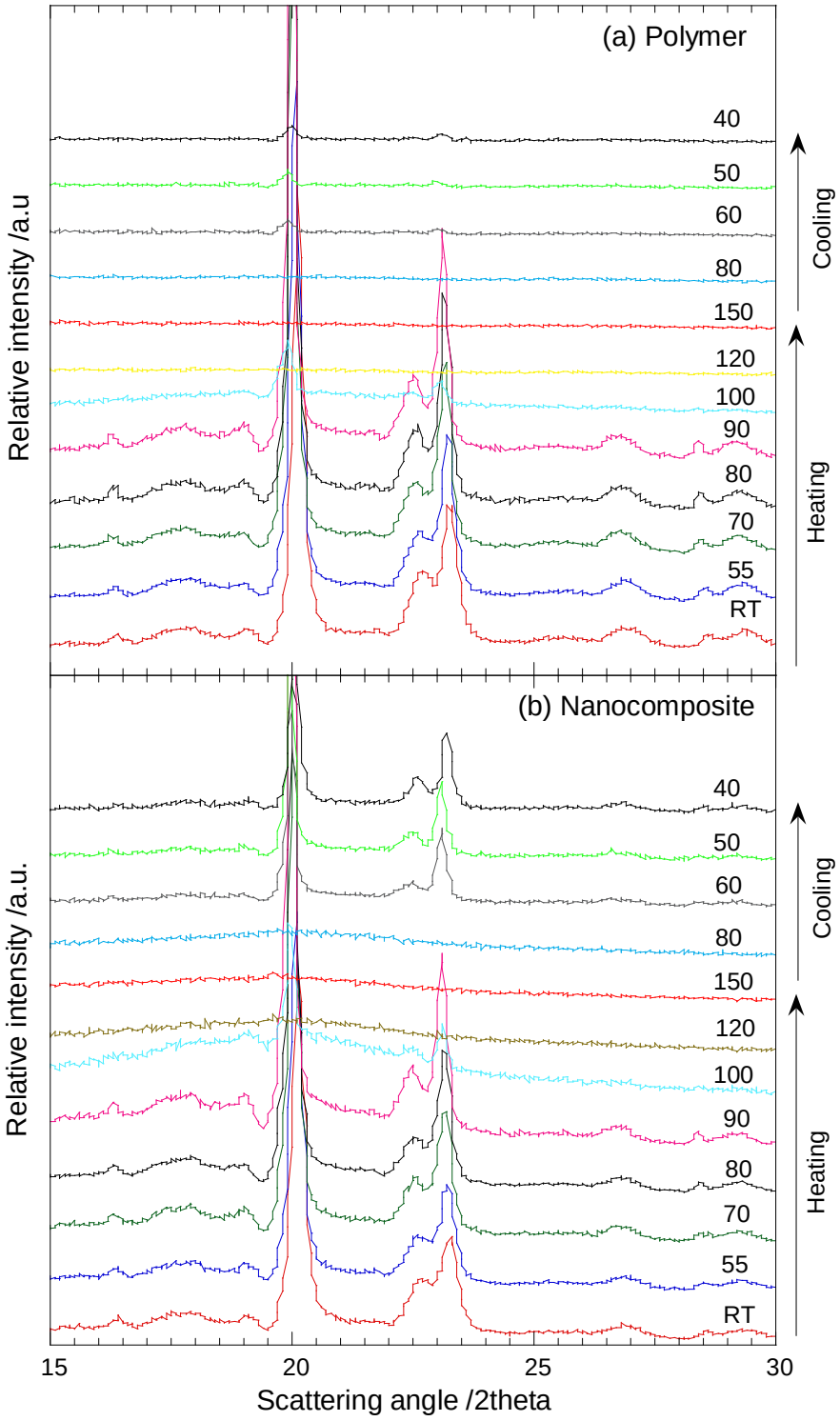

Figure 4.7 Temperature dependence wide-angle x-ray scattering patterns of (a) the pure polymer and (b) the nanocomposite sample during both heating and cooling cycles. For clarity, data were vertically offset.

To determine the crystal structure modification of the PES matrix during heating, which may be responsible for the multiple melting behaviour, WAXS experiments of pure PES and nanocomposite sample were carried out at above and below the temperature of each endotherm during both heating and cooling. The samples were kept at each temperature for 5 min including a 1 min x-ray exposure time. Figure 4.7 represents the one-dimensional WAXS patterns of pure PES and the nanocomposite samples. It is clear from the figure that, for both pure PES and the nanocomposite samples, the crystals are becoming more perfect with an increase in temperature; however, there is no indication of the formation of new crystals or the modification of any crystals. This supports the observation that the presence of melting, re-crystallization, and re-melting phenomena are responsible for the triple-melting behaviour of the PES matrix.

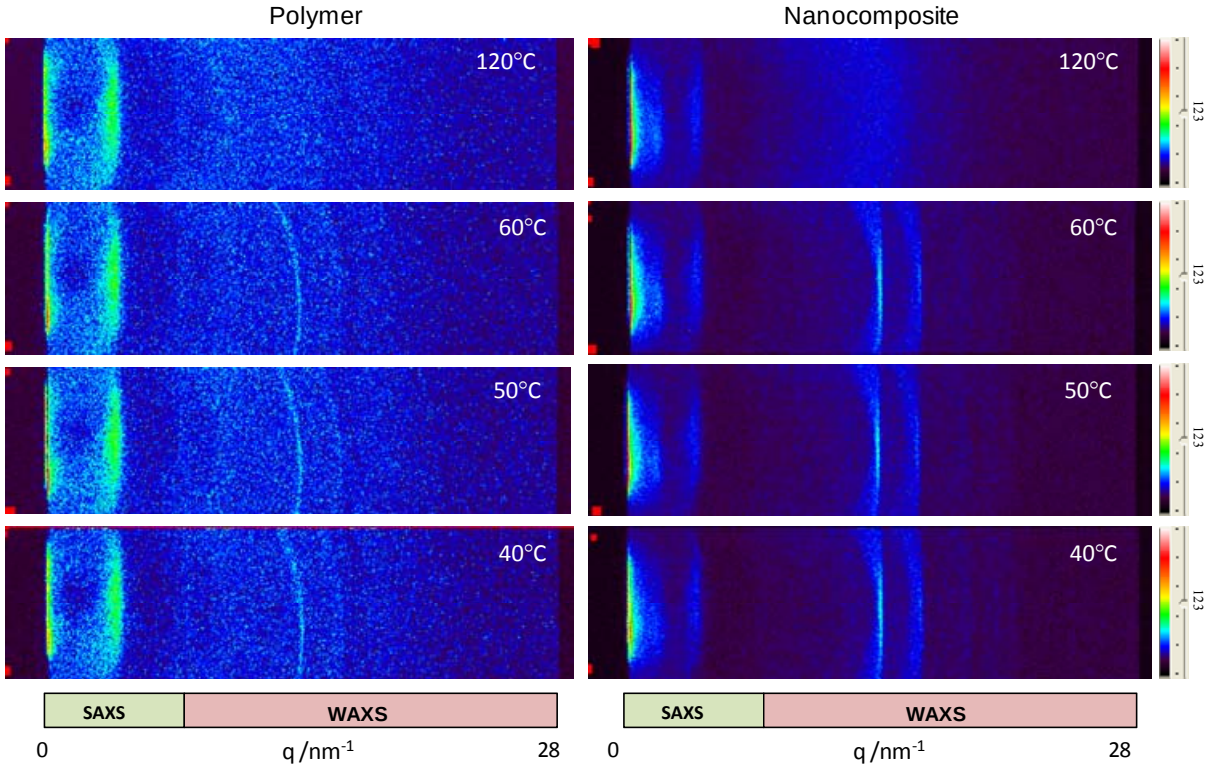

Figure 4.8 2-D small and wide angle x-ray scattering profiles of pure PES and the nanocomposite sample during cooling at a rate of 10°C min^{-1} from their melt

The most interesting behaviour was observed when both samples were cooled from their melt (Figure 4.8). The results show that it was very difficult for the pure PES sample to crystallize during cooling from its melt at a cooling rate of 10 °C/min – the sample remained in its super-cooled state. However, because of the active nucleation effect of the dispersed silicate layers, perfect PES crystals were formed during cooling of the nanocomposite from its melt at the same cooling rate. The WAXS results therefore support the conclusions made from the DSC and POM results.

4.6 Thermogravimetric analysis

The TGA curves of the pure PES and nanocomposite samples in a nitrogen environment are shown in Figure 4.9. The data available from the TGA scan include: $T_{0.05}$, the temperature at 5% mass loss, $T_{0.5}$, the temperature at 50% mass loss, which is another measure of thermal stability; and finally, the non-volatile fraction at 650 °C, denoted as char formation. These values are summarized in Table 4.3.

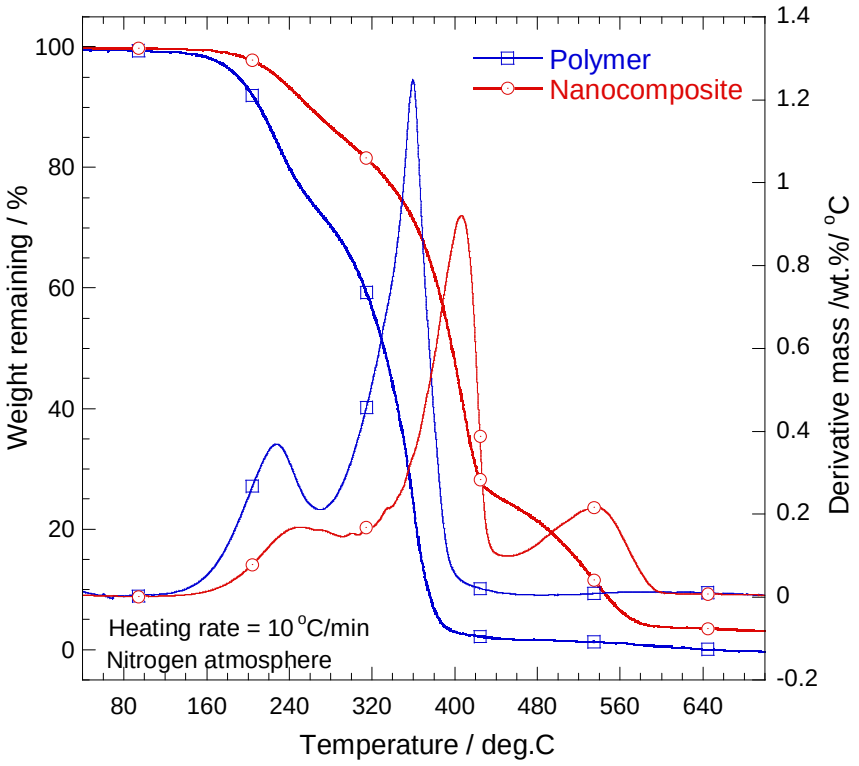

Figure 4.9 TGA curves of the pure polymer and nanocomposite samples obtained under nitrogen at a heating rate of 10 °C min^{-1}

Table 4.3 Data summarized from the TGA curves. The values are averages of three consecutive runs with an uncertainty of ± 1.7 °C.

Sample	$T_{0.05}$/°C	$T_{0.5}$/°C	Char at 650 °C/%
Pure PES	192.5	331.6	0
Nanocomposite	231.5	395.8	3.6

It is clear from Figure 4.9 and Table 4.3 that the thermal stability of PES improved after nanocomposite formation with the incorporation of 5 wt% C30B. This improvement in thermal stability of nanocomposite is due to the homogeneous dispersion of the highly delaminated silicate layers in the PES matrix, and the silicate layers have a natural higher thermal stability [16]. Another reason may be due to the increase in crystallinity of the PES phase in the nanocomposite sample, since the thermal stability of a crystalline phase is normally higher than that of the amorphous phase.

The first derivative TGA (dTGA) curves of both samples are shown in Figure 4.9. The dTGA curves are presented because they more clearly show the difference in thermal stability. The pure PES sample shows a two-step decomposition process: the first degradation step is mainly due to the scission of shorter chains, and the second step is related to that of the longer polymer chains. Chrissafis *et al.* [17] studied the thermal degradation mechanism of PES and PBS in a comparative study. They found that the first degradation step at low temperatures in Figure 4.9 is related to a much smaller mass loss, while the second is auto-catalysis. They also found that the activation energy and reaction order related to the first step were lower than those related to the second degradation step.

The nanocomposite sample shows an extra peak at 520 °C, and we believe that this peak is due to char formation. In the case of the nanocomposite sample, the first two dTGA peaks move to a higher temperature and the intensities of these peaks decrease significantly in comparison to those of the pure polymer sample. This indicates that the thermal stability of

PES improves significantly after the formation of a nanocomposite with C30B, which is important for products made from PES like packaging that can be exposed to different temperatures.

4.7 Conclusions

The effect of the incorporation of C30B on the non-isothermal crystallization and melting behaviour and thermal stability of PES was investigated. Structural and morphological analyses reveal the formation of a disordered intercalated nanocomposite where the intercalated and/or exfoliated silicate layers are homogeneously dispersed in the polymer matrix. This is due to the favourable interaction between the poly(ethylene succinate) matrix and the surfactant used to modify the pristine clay. The highly dispersed silicate particles accelerate the mechanism of nucleation and crystal growth of PES by offering a large surface area and also by stopping the super-cooling phenomenon of the PES matrix during non-isothermal crystallization. The significant improvement in the thermal stability of the PES after nanocomposite formation is due to the homogeneous dispersion of the silicate layers in the PES matrix. Another reason may be the higher crystallinity of the polymer matrix in the nanocomposite. These improved properties are very important to obtain fully crystallized poly(ethylene succinate) nanocomposite based products or parts in an injection moulding cycle.

4.8 References

1. S. Sinha Ray, P. Maiti, M. Okamoto, K. Yamada, K. Ueda. New polylactide-layered silicate nanocomposites. 1. Preparation, characterization and properties. Macromolecules 2002; 35:3104-3110 (DOI: 10.1021/ma011613e).
2. S. Sinha Ray, K. Yamada, M. Okamoto, A. Ogami, K. Ueda. New polylactide-layered silicate nanocomposites. 3. High performance biodegradable materials. Chemistry of Materials 2003; 15:1456-1465 (DOI: 10.1021/cm020953r).
3. S. Sinha Ray, K. Yamada, M. Okamoto, A. Ogami, K. Ueda. New polylactide/layered silicate nanocomposites. 2. Nanoscale control over multiple properties. Macromolecular Rapid Communications 2002; 23:943-947 (DOI: 10.1002/1521-3927(200211) 23:16-943).

4. G.Z. Papageorgiou, D.N. Bikiaris. Crystallization and melting behaviour of three biodegradable poly(alkylene succinates). A comparative study. Polymer 2005; 46:12081-12092 (DOI:10.1016/j.polymer.2005.10.073).
5. G. Qiu, Z. Tang, N. Huang, L. Gerking. Dual melting endotherms in the thermal analysis of poly(ethylene terephthalate). Journal of Applied Polymer Science 1998; 69:729-742 (DOI: 10.1002/(SICI)1097-4628(19980725)69:4<729).
6. H.G. Kim, R.E. Robertson. Multiple melting endotherms in isothermally melt-crystallized poly(butylene terephthalate. Journal of Polymer Science: Part B Polymer Physics 1998; 36:1757-1767 (CCC: 0887-6266/98/101757-11).
7. C. Passingham, P.J. Hendra, M.E.A. Cudby, Z. Zichy, M. Weller. The re-evaluation of multiple peaks in the DSC melting endotherm of isotactic polypropylene. European Polymer Journal 1990; 26:631-638 (DOI:10.1016/0014-3057(90)90219-T).
8. M. Yasuniwa, S. Tsubakihara, T. Satou, K. Iura. Multiple melting behavior of poly(butylene succinate). II. Thermal analysis of isothermal crystallization and melting process. Journal of Polymer Science: Part B Polymer Physics 2005; 43:2039-2047 (DOI: 10.1002/polb.20499).
9. Y. Wang, M. Bhattacharyay, J.F. Mano. Thermal analysis of the multiple melting behavior of poly(butylene succinate-co-adipate). Journal of Polymer Science: Part B Polymer Physics 2005; 43:3077-3082 (DOI: 10.1002/polb.20589).
10. S. Sinha Ray, J. Bandyopadhyay, M. Bousmina. Thermal and thermomechanical properties of poly[(butylene succinate)-co-adipate] nanocomposite. Polymer Degradation and Stability 2007; 92:802-812 (DOI: 10.1016/j.polymdegradstab.2007.02.002).
11. Y. Kong, J.N. Hay. Multiple melting behaviour of poly(ethylene terephthalate). Polymer 2003; 44:623-633 (DOI: 10.1016/S0032-3861(02)00814-5).
12. F.J. Medellin-Rodriguez, P.J. Phillips, J.S. Lin, R. Campos. The triple melting behavior of poly(ethylene terephthalate): molecular weight effect. Journal of Polymer Science: Part B Polymer Physics 1997; 35:1757-1774 (CCC: 0887-6266/97/111757-18).
13. S. Sinha Ray, M. Bousmina. Crystallization behaviour of poly[(butylenes succinate)-co-adipate nanocomposite]. Macromolecular Chemistry and Physics 2006; 207:1207-1219 (DOI: 10.1002/macp.200600163).
14. S. Sinha Ray, J. Bandyopadhyay, M. Bousmina. Influence of degree of intercalation on the crystal growth kinetics of poly[(butylene succinate)-co-adipate] nanocomposites.

European Polymer Journal 2008; 44:3133-3145 (DOI:10.1016/j.eurpolymj. 2008.07.035).

15. J. Bandyopadhyay, S. Sinha Ray, M. Bousmina. Nonisothermal crystallization kinetics of poly(ethylene terephthalate) nanocomposites. Journal of Nanoscience and Nanotechnology 2008; 8:1812-1822 (DOI: 10.1166/jnn.2008.022).
16. S. Sinha Ray, J. Bandyopadhyay, M. Bousmina. Effect of organoclay on the morphology and properties of poly(propylene)/poly[(butylene succinate)-co-adipate] blends. Macromolecular Materials and Engineering 2007; 292:729-747 (DOI: 10.1002/ mame.200700029).
17. K. Chrissafis, K.M. Paraskevopoulos, D.N. Bikiaris. Thermal degradation mechanism of poly(ethylene succinate) and poly(butylene succinate): Comparative study. Thermochimica Acta 2005; 435:142–150 (DOI:10.1016/j.tca.2005.05.011).

CHAPTER 5

CRYSTALLIZATION KINETICS AND MELTING BEHAVIOUR OF A POLY(BUTYLENE SUCCINATE)/CLAY NANOCOMPOSITE

5.1 Overview

This chapter reports on the effect of the incorporation of organoclay on the non-isothermal crystallization kinetics of poly(butylene succinate) (PBS). The non-isothermal crystallization behaviour of PBS and its nanocomposite were studied by differential scanning calorimetry (DSC). The effect of the change of variables like temperature, time, as well as heating rates on the crystallization behaviour was studied. It was observed that the double melting behaviour of the PBS matrix is a function of these variables. Various models, namely the Avrami method, the Ozawa method, and the combined Avrami-Ozawa method, were applied to describe the kinetics of the pure PBS and its nanocomposite during non-isothermal crystallization. The Ozawa equation did not provide an adequate description of the non-isothermal crystallization kinetics of PBS and its nanocomposite, but the Avrami analysis modified by Jeziorny and the method developed by Liu *et al.* were successful in describing the non-isothermal crystallization kinetics of pure PBS and its nanocomposite. The results show that the crystal growth kinetics of the PBS matrix retard in the presence of the dispersed intercalated organoclay.

5.2 Theoretical background

During the non-isothermal crystallization process, the heat flow (dH / dT) was recorded as a function of time. The relative degree of crystallization, X_T, as a function of temperature, is defined as:

$$X_T = \frac{\int_{Ton}^{T} (dH / dT) dT}{\int_{Ton}^{T\infty} (dH / dT) dT} \qquad (1)$$

where T_{on} and T_{∞} are the onset and final temperature of crystallization, and where the relation between crystallization time (t), rate (ϕ) and temperature (T) is given by:

$$t = \frac{T_{on} - T}{\phi} \tag{2}$$

According to Eq. (2), one can define the relative degree of crystallinity, X_t, as a function of time:

$$X_t = \frac{\int_{ton}^{t} (dH/dT)dT}{\int_{ton}^{t\infty} (dH/dT)dT} \tag{3}$$

The kinetics of the non-isothermal crystallization of polymers is generally analyzed using the Ozawa-equation [1]. The equation is a modification of the Avrami equation [2], which considers the effect of the cooling rate on crystallization from the melt, and replaces the crystallization temperature under isothermal conditions with the cooling rate (ϕ) as follows:

$$1 - X_T = \exp[-K(T)/\phi^m] \tag{4}$$

where *K(T)* represents the cooling function of the process and *m* represents the Ozawa exponent depending on the dimension of crystal growth. If the relative crystallinities at different cooling rates and a given temperature are chosen, the following plot should give a series of parallel lines:

$$\ln[-\ln(1 - X_T)] \text{ vs. } \ln\phi \tag{5}$$

K(T) and *m* are respectively determined from the y-intercept and slope. The adopted model by Avrami expressed the equivalent time-dependent crystallinity as:

$$X_T = 1 - \exp(-Z_t t^n) \tag{6}$$

Jeziorny [3] suggested the parameter Z_t should be modified when the Avrami analysis is applied to explain the non-isothermal crystallization kinetics. Assuming a constant or almost constant cooling rate, the final form of this parameter as suggested by Jeziorny [3] is

$$\ln(Z_t) = \phi \times \ln(Z_c) \tag{7}$$

where Z_t is a composite rate constant involving both nucleation and growth rate parameters, and the Avrami exponent (*n)* is a constant depending on the type of nucleation and the growth process. Taking a double logarithm on both sides of Eq. 6,

$$\ln[-\ln(1 - X_t)] = \ln Z_t + n \ln t \tag{8}$$

Eq. 8 should give a straight line if this model is valid, and Z_t and *n* can be determined from the antilogarithmic values of the y-intercept and slope, respectively. It must be taken into account that the temperature changes constantly, hence the values of Z_t and *n* do not have the same physical significance as in isothermal crystallization. They are just parameters to be

fitted to the data and help to analyze the crystallization kinetics because of the temperature effects on the rates of both nuclei formation and spherulite growth.

Liu [4] proposed the use of combined Avrami and Ozawa models to describe the non-isothermal crystallization kinetics by the following equation:

$$\ln Z_{t+} n\ln t = \ln K(T) - m \ln \phi \quad (9)$$

By rearranging Eq. 9 the final form becomes

$$\ln \phi = \ln F(T) - a \ln t \quad (10)$$

where $F(T) = [K(T)/Z_t]^{1/m}$ refers to a cooling rate to reach a defined degree of crystallinity and a is the ratio of the Avrami exponent to the Ozawa exponent i.e. a = *n/m.*

5.3 Melting behaviour of PBS and the nanocomposite

To understand the initial melting behaviour and re-crystallization response of neat PBS and the nanocomposite sample, DSC analyses of the compression molded samples were conducted at a heating rate of 10 ºC min^{-1} and the relative first scans are shown in Figure 5.1. The samples were heated as fast as possible inside the DSC to different equilibration temperatures from 60 to 90 ºC, kept at this temperature for 30 min, and cooled as fast as possible to -60 ºC, and then they were heated to 150 ^{o}C at a rate 10 ^{o}C min^{-1}. The samples were also weighed such that all the samples had identical PBS content. Both samples show three endothermic melting peaks for PBS, labelled as I, II, and III from the low to high temperature and one re-crystallization peak in between the last two melting peaks. Endotherm I, in both PBS and the nanocomposite, was influenced by the value of the equilibration temperature. They shifted to higher temperatures with an increase in equilibration temperature. A possible explanation for the shift is that the lamellar thickness increased as the equilibration temperature increased. The intensity of endotherm II decreases as the equilibration temperature increases, and this suggest that there are smaller or shorter chains in the polymer that rearrange at very low temperatures. In the case of the nanocomposite endotherm II reduces to be almost nonexistent. This is an indication that the C30B incorporation has restricted the short chains' mobility in the polymer. The shape and position of the re-crystallization peak are not changed by the equilibration temperature in both the polymer and the nanocomposite. Only the intensity has changed in the nanocomposite, and this may also be because of the mobility restriction of the rearrangement of the chains by the

clay. Endotherm III is associated with the most perfect crystals after reorganization during the heating process in the DSC measurements.

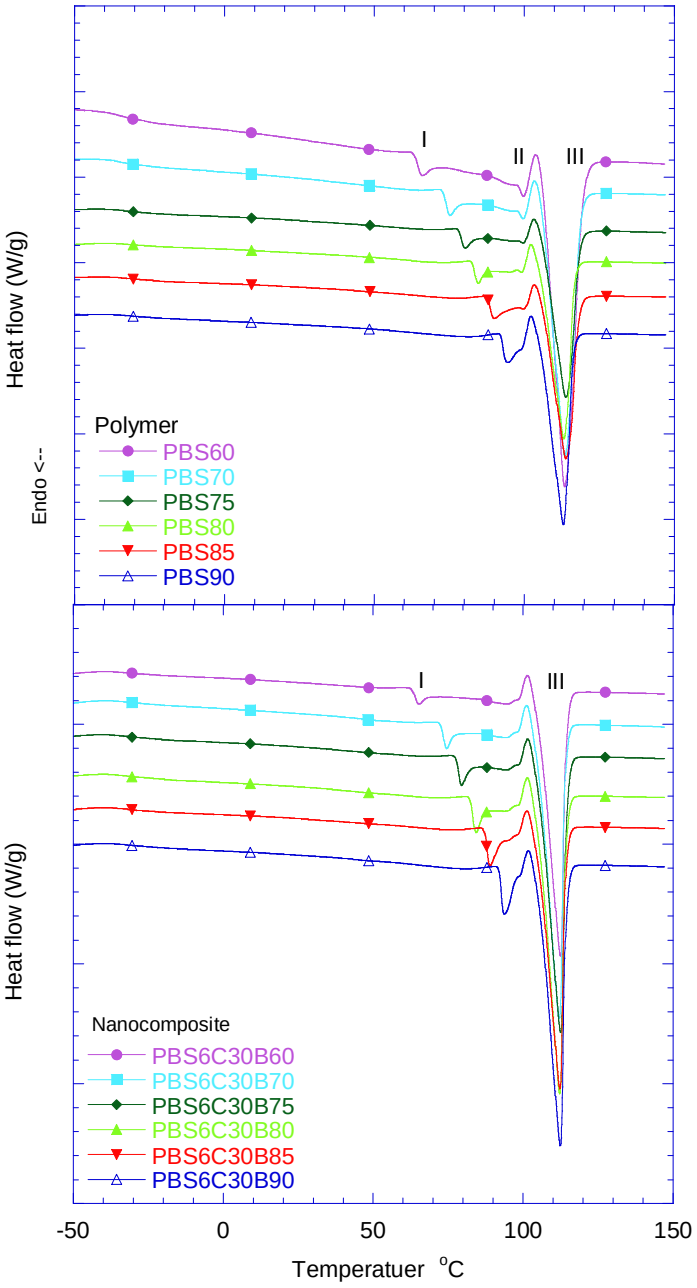

Figure 5.1 DSC curves of the samples equilibrated at different temperatures

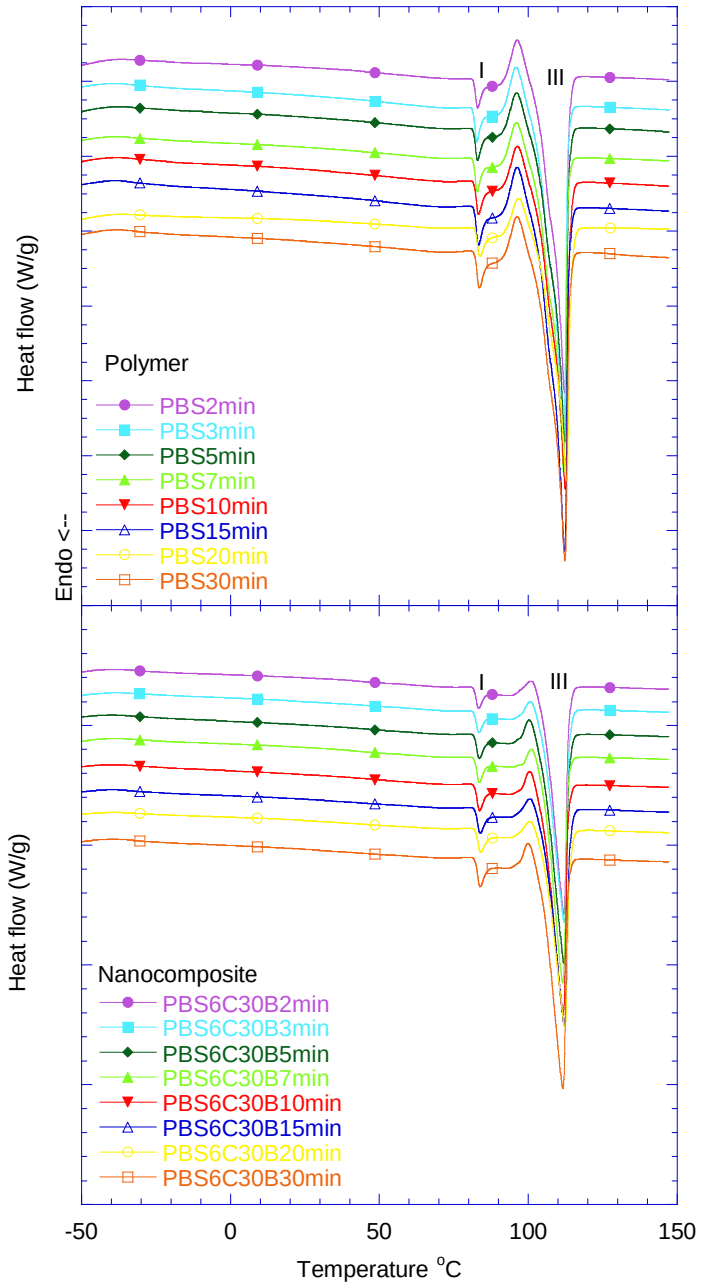

Figure 5.2 Effect of crystallization time on the melting behaviour of the samples equilibrated at 80 °C

Kong et al. [5] reported the multiple melting behaviour of PET. There are several models that explain the multiple melting behaviour of thermoplastic semi-crystalline polymers, of which the most important one is the presence of melting, re-crystallization, and re-melting phenomena [5-7]. According to this model, the first step is the melting and re-crystallization of the lower melting crystallites with lower thermal stability, and then the melting of the

crystallites with higher thermal stability formed during the re-crystallization of the crystallites that melted at lower temperatures.

All the samples were heated as fast as possible inside the DSC to 80 ºC (equilibration temperature), kept at this temperature for different times from 2 to 30 min, cooled as fast as possible to -60 ºC, and then they were heated to 150 °C at a rate 10 °C min^{-1}. The DSC curves in Figure 5.2 are similar to those in Figure 5.1, except that endotherm I is observed at the same melting temperature for the different equilibration times at the same temperature. It therefore seems that after equilibration at 80 °C, where only the smaller crystallites melted, the equilibration time did not change the re-crystallization behaviour of these crystallites. The crystallites that melted at 80 °C were probably small enough to melt within the first two minutes at this temperature, and no further melting occurred when the samples were left for longer times at this temperature. Crystallites with the same morphology then re-formed during rapid cooling, and therefore the melting behaviour on re-heating did not change.

In this case the endotherm I in Figure 5.2 is independent of different times the samples were kept at, as it does not shift to higher and lower temperatures like in Figure 5.1 where the shortest chains will melt at lower temperatures. The possible explanation is that the shorter chains in the polymer that melt at 80 ºC, are melting so quickly that even when they are kept at this temperature for a longer time they still show one peak melting at the same temperature.

To verify the presence of melting, re-crystallization, and re-melting phenomena, both the pure polymer and the nanocomposite were scanned at different heating rates of 1, 2, 5, 7, 10, 15, 20 and 25 °C min^{-1}. The results are presented in Figure 5.3. In the case of the polymer sample, the endotherm III is shifted slightly towards a lower temperature with increasing the heating rate, while the endotherm I became more prominent. Another interesting feature is that the re-crystallization process became more important with increasing heating rate. This observation indicates that the melting and re-crystallization processes occur at the same time in the temperature range of the higher endotherm. At a very slow heating rate, the sample passes through the re-crystallization process slowly, so there is enough time for the molten sample to reorganize into new crystals. For this reason only endotherm III is well defined at very slow heating rates. At higher heating rates (more than 5°C min^{-1}) the sample passes through the re-crystallization region so fast that there is not enough time for the disordered

polymer chains to reorganize into new crystals. For this reason, the reorganization process is largely inhibited as the heating rate increases and at the same time the number of perfect crystals decreases, which finally contributes to the decrease in the peak temperature of endotherm III. These observations indicate that the presence of melting, re-crystallization and melting phenomena are actually responsible for the multiple melting behaviour of the PBS sample. The nanocomposite sample also shows the same type of melting behaviour. However, the melting endotherm II appears only with a decreased intensity in the curves obtained at the two highest rates (20 and 25 °C min^{-1}). This may be because there is probably a moderate interaction between the CO groups in PBS structure and the hydroxyl groups in the C30B surfactant, the silicate layers act as obstacles for the mobility and flexibility of the polymer chains to fold and join the re-crystallization growth.

To study the influence of cooling rate during non-isothermal crystallization on the melting behaviour of PBS, all samples were heated at a rate of 10°C min^{-1} directly from -60°C as soon as the cooling has finished. Figure 5.4 represents the melting behaviour of PBS and the PBS6C30B nanocomposite that were non-isothermally crystallized from the melt (150°C) at cooling rates of 1, 2, 5, 10, 15 and 20°C min^{-1}. The melting endotherm I, which was observed in the previous results (Figure 5.3), is not observed in these results. This indicates that the crystals, associated with the endotherm I, did not form during the non-isothermal crystallization at all cooling rates. Endotherms II and III are observed, and one small re-crystallization exotherm appears when the samples were crystallized non-isothermally from the melt at a cooling rate of 10°C min^{-1}. However, endotherm II decreased with increasing the cooling rate. In the case of neat PBS, with decreasing the cooling rate, endotherm II shifted slightly towards a higher temperature, whereas the endotherm III moved in the opposite direction. As the cooling rate decreased, endotherm II moved closer to endotherm III and at the very slow cooling rate of 1°C min^{-1}, the endotherms merged into a broad melting endotherm. This observation indicates that with decreasing the cooling rate, the crystal growth associated with both the melting endotherms become equally important and controls the total melting behaviour.

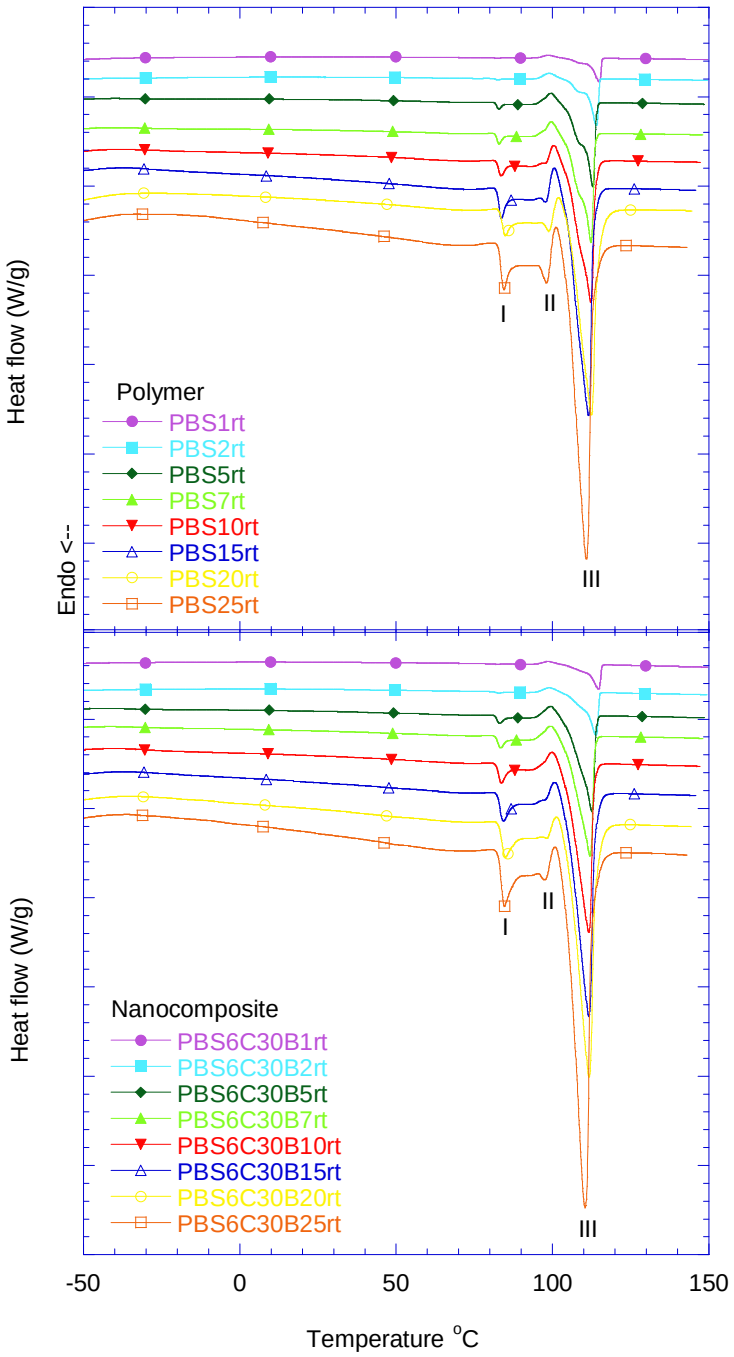

Figure 5.3 Heating rate dependence of the DSC curves of compression molded samples (Before starting each experiment, the samples were equilibrated at 80 ºC

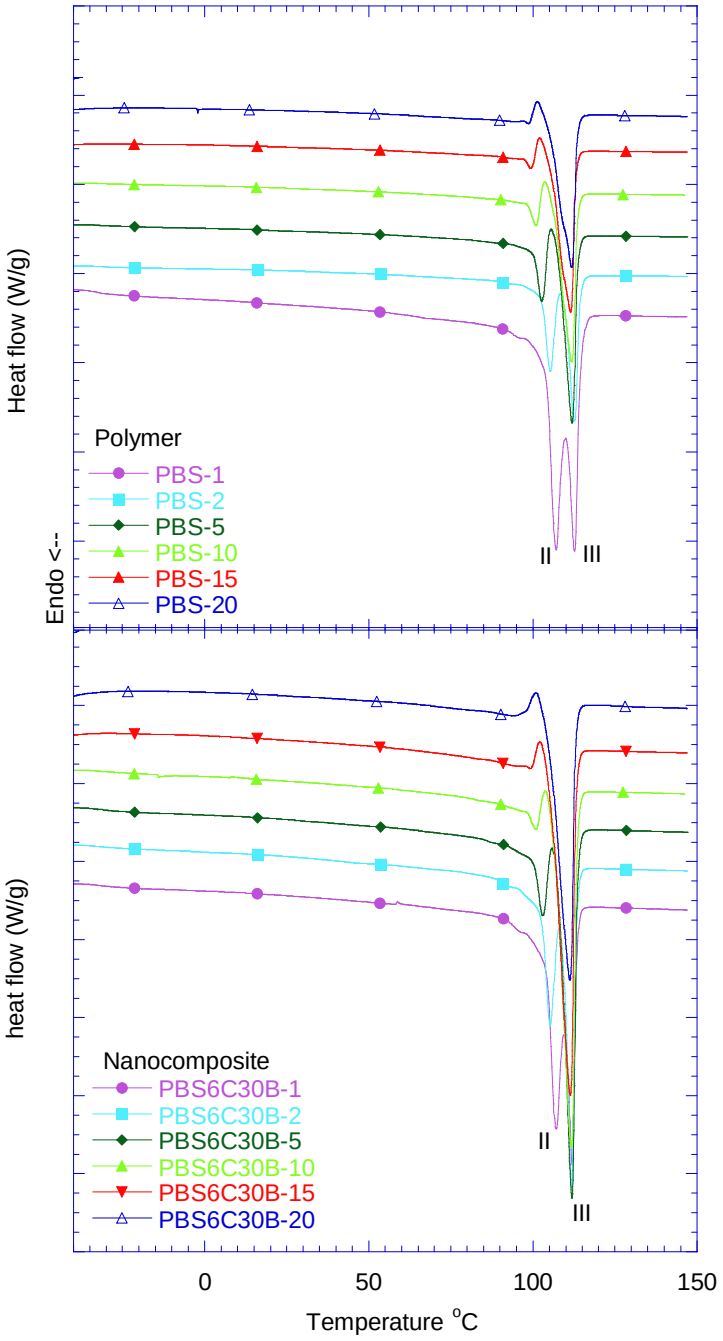

Figure 5.4 DSC curves of the samples after non-isothermal crystallization at different cooling rates

The same behaviour was also observed in the case of the nanocomposite sample, and all the endotherms are at the same temperatures as those of the polymer.

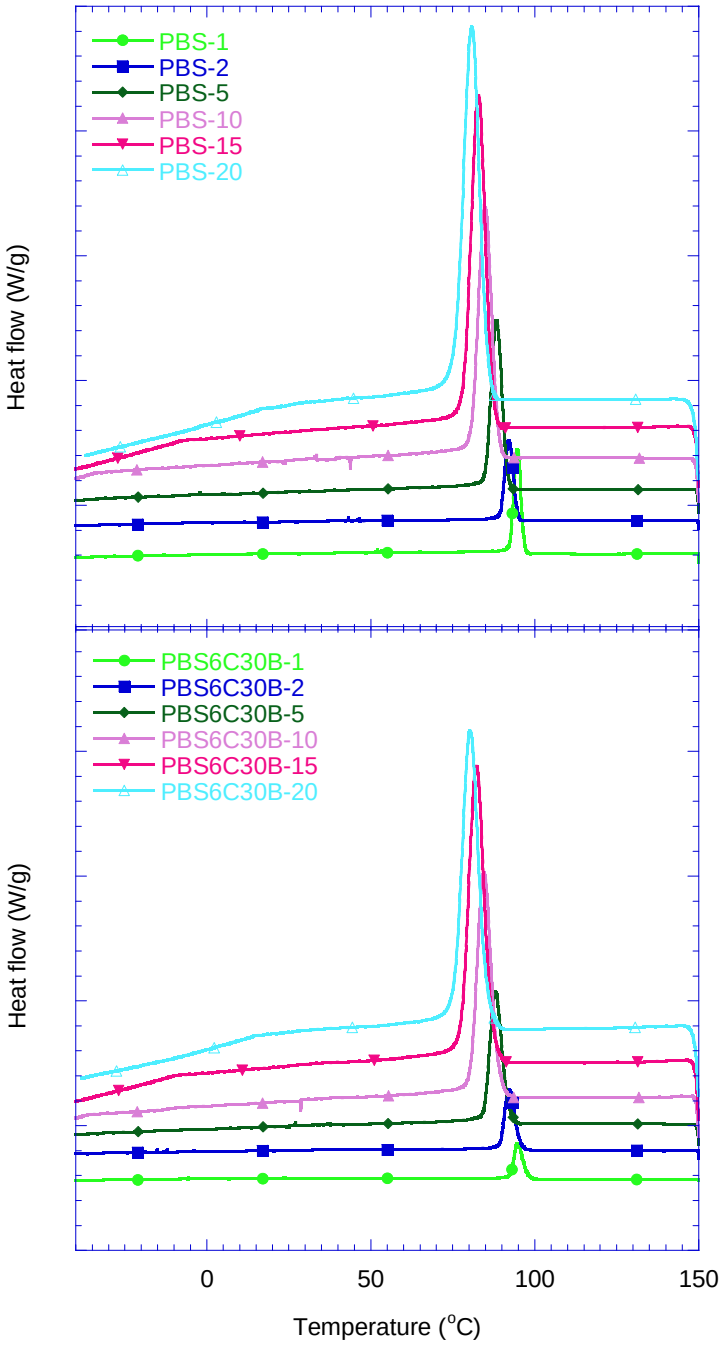

Figure 5.5 DSC cooling curves of the samples cooled from the melt at five different cooling rates

5.4 Crystallization behaviour

The crystallization exotherms of neat PBS and the PBSC30B nanocomposite at various cooling rates are presented in Figure 5.5. The crystallization onset (T_{on}) and peak (T_c) temperatures, as well as the crystallization enthalpies for the non-isothermal crystallization of the samples at different cooling rates, are listed in Table 5.1. The exothermic peak shifted to lower temperatures as the cooling rate increased for both the polymer and the nanocomposite. Thus crystallization occurred at higher temperatures with slower cooling rates. This is a common observation, since at the higher cooling rates the crystallization, which is kinetically driven, starts at lower temperatures because of supercooling. In the case of the neat PBS, the ΔH_{ex} (the degree of crystallinity) decreased with increasing the cooling rates, while that of the nanocomposite seems to be independent from the cooling rate. The degree of crystallinity of the nanocomposites is generally lower that that of the polymer (see Table 5.1). This is due to the high level of dispersion of the silicate layers in the PBS6C30B nanocomposite which hindered the local lamellar crystallization and led to the decrease in the degree of crystallinity. There is also a small decrease in T_c of the nanocomposite, and the only reason may be a change in peak width, which will be the result of changes in crystal size distribution.

5.5 Crystallization kinetics

The relative degree of crystallinity, X_T, defined in Eq. 1, is shown in Figure 5.6 as a function of temperature for PBS and the PBSC30B nanocomposite for different cooling rates (see Figure 5.5). All these curves have the same "S" shape. However, because of shorter crystallization times at higher cooling rates, the values of X_t are lower than those at lower cooling rates at the same crystallization temperatures (Figure 5.7). The half-crystallization time, $t_{1/2}$, for both the polymer and the nanocomposite, at various cooling rates was calculated (Eq. 2 and Figure 5.7). Table 5.2 shows how this time depends on the cooling rate for neat PBS and the PBSC30B nanocomposite; the value of $t_{1/2}$ decreases with increasing cooling rate. In general, the overall crystallization rate is determined by both the nucleation and the growth of the crystals. At temperatures close to the melting point of a material the crystallization rate mainly depends on nucleation, but the nucleation rate increases with decreasing temperature [6]. The $t_{1/2}$ value can be used to characterize the crystallization rate under isothermal conditions: the higher this value, the lower the crystallization rate. For non-

isothermal crystallization, $t_{1/2}$ can also be used to illustrate the crystallization rates [8]. The $t_{1/2}$ values for the nanocomposite are higher than those for the neat PBS.

Table 5.1 Characteristic parameters of non-isothermal crystallization from the melt

Sample	ϕ / °C min^{-1} [a]	T_{on} / °C [b]	T_c / °C [c]	ΔH_{ex} / Jg^{-1} [d]	Crystallinity / % [b]
PBS	1	100.5	94.7	145.5	69.3
	2	99.9	92.0	70.3	33.5
	5	96.2	88.3	77.4	36.9
	10	93.8	84.9	71.0	33.8
	15	92.7	82.9	71.1	33.9
	20	91.9	80.8	66.2	31.5
PBS6C30B	1	100.0	94.8	62.9	30.0
	2	99.3	92.1	61.5	29.3
	5	94.5	88.0	70.4	33.5
	10	93.0	84.5	68.4	32.6
	15	91.5	82.2	68.2	32.5
	20	90.2	80.3	52.6	25.0

[a] Cooling rate

[b] Crystallization onset temperature.

[c] Crystallization peak temperature.

[d] Enthalpy/heat of crystallization.

[e] Calculated using the 100% crystallinity value of PBS, 210J g^{-1} [11]

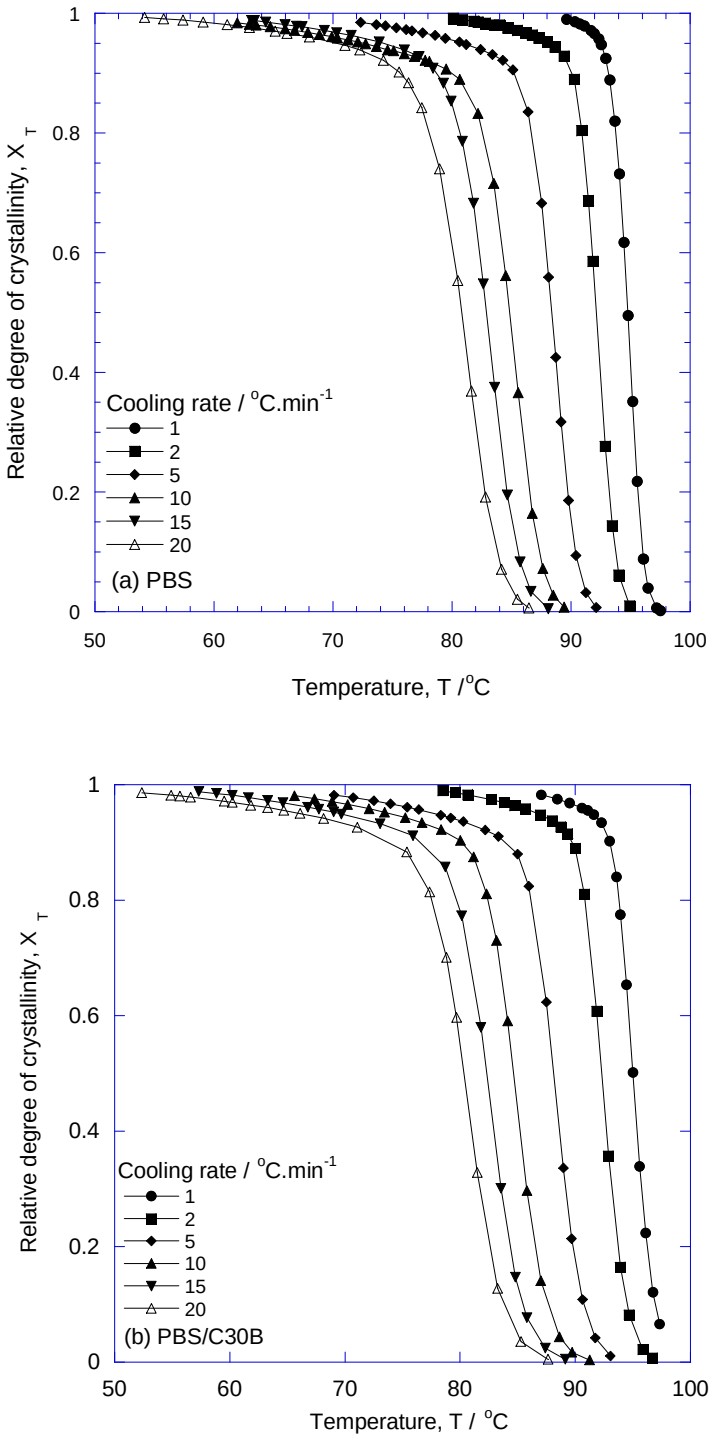

Figure 5.6 Temperature-dependent relative degree of crystallinity, X_T, as a function of temperature *(T)* for the non-isotheral crystallization of (a) neat PBS and (b) the PBS/C30B nanocomposite at five different cooling rates

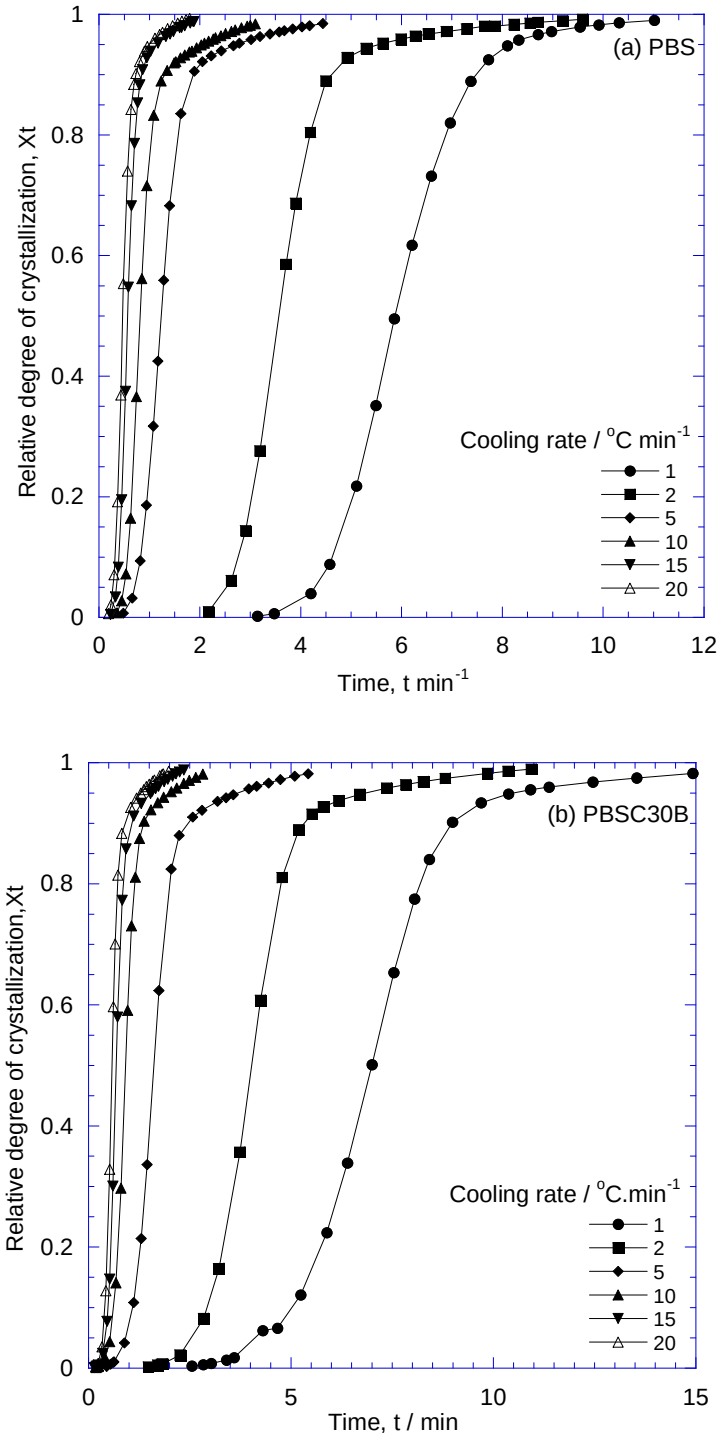

Figure 5.7 Equivalent time-dependent relative degree of crystallinity, X_T, as a function of crystallization time (t) of (a) PBS and (b) the PBS/C30B nanocomposite at five different cooling rates

According to Eq. 5 a plot of $\ln[-\ln(1-X_T)]$ versus $\ln\phi$ at a given temperature should give a straight line if the Ozawa equation is valid. Figure 5.8 shows non-straight lines for both PBS

and the PBSC30B nanocomposite, which means that the Ozawa model is not valid for our system. The reason for the curving in the Ozawa plots has been attributed to secondary kinetic processes [9], but may also be due to the inaccurate assumption of a constant heating function over the entire crystallization process. It is also apparent that the Ozawa analysis does not adequately describe the non-isothermal crystallization kinetics some polymers.

Table 5.2 Kinetic parameters based on the Avrami equation

Sample	ϕ / °C min[a]	n[b]	$\ln Z_t$[c]	$\ln Z_c$[d]	$t_{1/2}$[e]
PBS	1	9.10	-34.17	-34.17	5.33
	2	7.60	-26.81	-13.41	3.63
	5	4.90	-11.88	-2.38	1.24
	10	5.20	-10.95	-1.10	0.82
	15	5.00	-7.68	-0.51	0.57
	20	4.90	-7.51	-0.38	0.47
PBS6C30B	1	5.40	-22.95	-23.00	7.24
	2	5.70	-20.24	-10.12	4.15
	5	4.20	-11.90	-2.38	1.63
	10	4.20	-8.54	-0.85	0.93
	15	4.20	-7.57	-0.50	0.70
	20	4.70	-7.02	-0.35	0.58

[a] Cooling rate

[b] Avrami exponent

[c] Growth factor

[d] Jeziorny factor

[e] Crystallization half-time

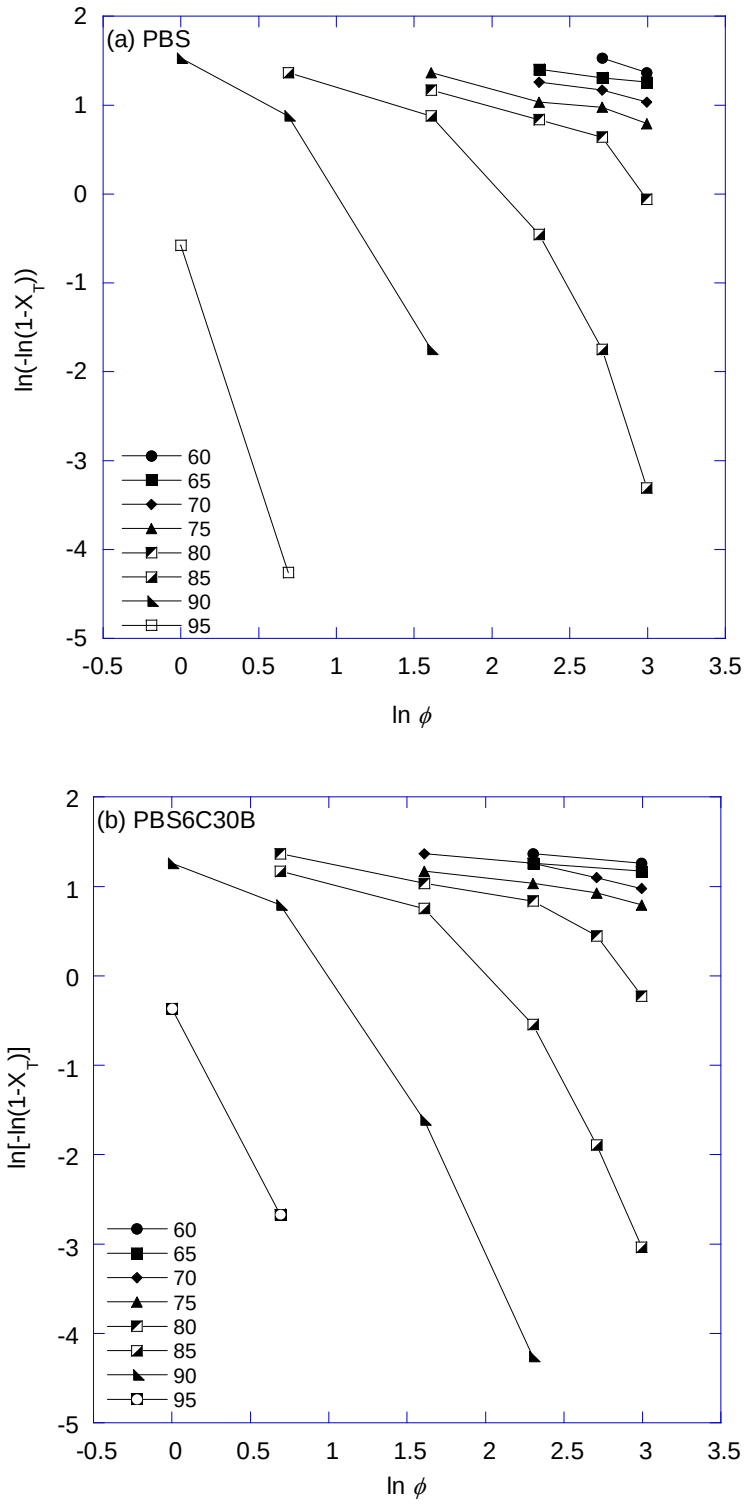

Figure 5.8 Plots of ln [-ln (1-*Xt*)] (*Xt* is the equivalent time-dependent relative degree of crystallinity) versus ln ϕ (ϕ is the cooling rate) for the non-isothermal crystallization of (a) PBS and (b) PBS/C30B

The Avrami equation, Eq. 6, was adopted here as an alternative approach. Using Eq. 6 in a double-logarithmic form and plotting ln [-ln(1-X_t)] against ln *t* for each cooling rate, should give a straight line. This plot is shown in Figure 5.9. In this case the line is not straight over the entire crystallinity range; there are regions where the modified Avrami analysis appears to be valid. For both samples the linear sections are almost parallel, but shift to shorter times with increasing cooling rates. The deviation is usually considered to be the result of secondary crystallization, which is caused by spherulite impingement in a later stage [10]. The Avrami parameters were calculated from the linear sections in Figure 5.9, and are presented in Table 5.2. The Avrami exponent, n, decreased in the polymer and nanocomposite with increasing the cooling rate, and all the values are higher than 3. Since the Avrami exponent is the sum of the order of the crystallisation process and the number of dimensions of the morphological unit, the observed n values suggest that well defined spherulitic structures cannot be formed at all the cooling rates used in this study. The values of n for the nanocomposites decrease non-linearly with an increase in cooling rate. The values of the total heat of crystallization, ΔH_{ex} (Table 5.1), for the neat PBS are higher than those of the nanocomposite. This suggests that the incorporation of C30B does not seem to significantly change the kinetics of the non-isothermal crystallization of PBS.

Table 5.3 Kinetic parameters based on the Liu equation

Sample	Kinetic parameters [a]	X_t [b] 20%	X_t [b] 40%	X_t [b] 60%	X_t [b] 80%
PBS	*F*(T)	3.53	3.69	3.88	4.17
	A	0.95	0.97	1.12	1.19
PBS6C30B	*F*(T)	3.89	4.06	4.34	4.63
	A	1.09	1.11	1.17	1.33

[a] *F*(T) refers a cooling rate to reach a defined degree of crystallinity and 'a' is the ratio of Avrami exponent to Ozawa exponent i.e., *n/m.*

[b] The relative degree of crystallinity as a function of time (20, 40, 60 and 80 % from Figure 5.7).

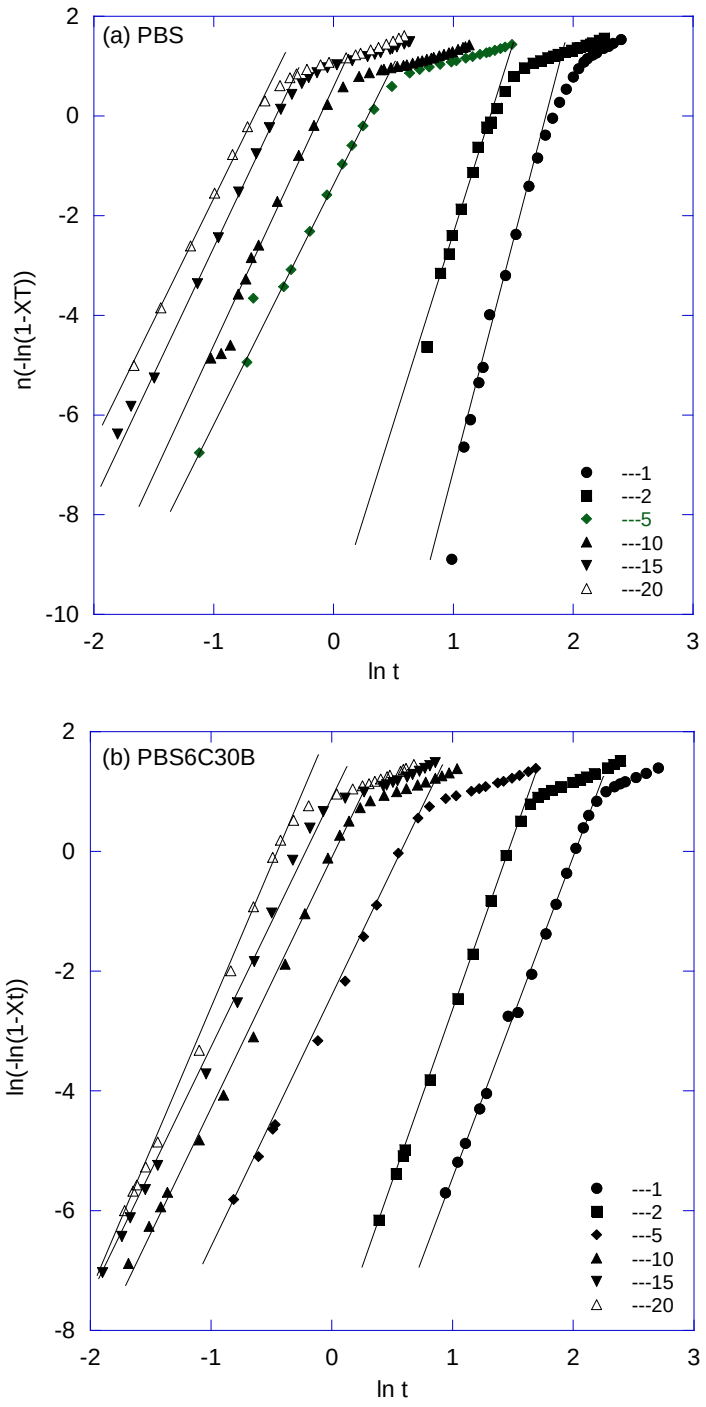

Figure 5.9 Plots of ln [-ln (1-*Xt*)] (*Xt* is the equivalent relative degree of crystallinity) versus ln *t* (*t* is the time) for non-isothermal crystallization of (a) PBS and (b) PBS/C30B

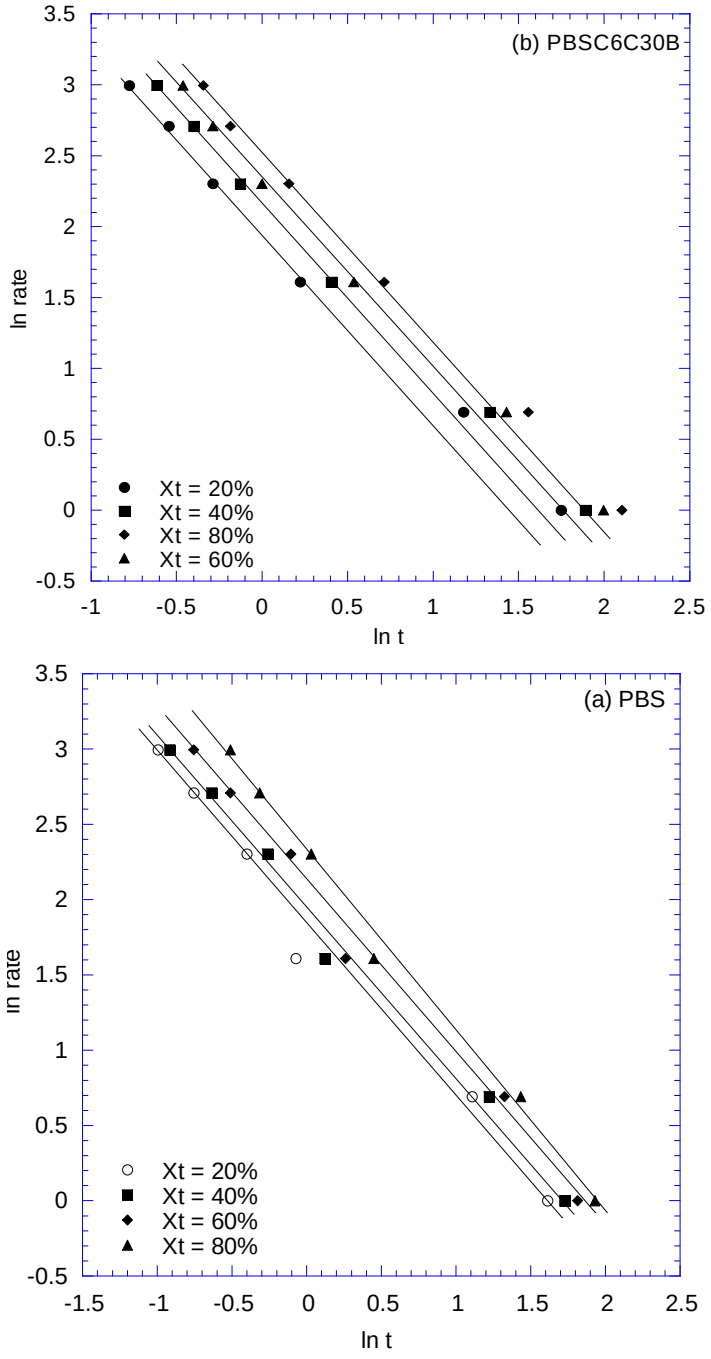

Figure 5.10 Plots of ln ϕ (ϕ is a cooling rate) versus ln *t* (*t* is the time) for (a) PBS and (b) PBS/C30B

At a given degree of crystallinity, plotting $\ln\phi$ versus ln *t* (Figure 5.10) yielded a linear relationship between $\ln\phi$ and ln *t* (Eq. 10). The values of *F*(T) and a could be obtained from the slopes and intercepts of these lines (see Table 5.3). The value of *F*(T) increased with increasing degree of crystallinity, indicating that at unit crystallization time, a higher cooling

rate should be applied to reach a higher degree of crystallinity. At the same relative degree of crystallinity, the value of $F(T)$ for the PBS/clay nanocomposite was higher than that of PBS. Therefore, to reach the same relative degree of crystallinity, the PBS/clay nanocomposite required a higher cooling rate, which indicates that the PBS/clay nanocomposite crystallized at a slower rate than PBS. This again supports the slower crystallization of PBS in the presence of C30B as discussed earlier.

5.6 Conclusions

We reported the effect of modified clay on the melting behaviour of PBS after different equilibrium crystallization conditions, as well as the non-isothermal crystallization behaviour and the crystallization kinetics. For both samples multiple melting behaviour was observed and may be associated with partial melting, re-crystallization, and re-melting phenomena. Neat PBS exhibited a higher melting temperature than the nanocomposite. These observations are believed to be due to the homogeneous dispersion of the C30B particles in the PBS matrix. The C30B particles in the PBS matrix might have hindered the local lamellar crystallization and led to the decrease in the overall degree of crystallinity and hence to the lower melting temperature.

The Ozawa equation did not provide an adequate description of the non-isothermal crystallization of PBS and its nanocomposite. In contrast, the Avrami analysis modified by Jeziorny and the method developed by Liu et al. were successful in describing the non-isothermal crystallization process and support the lower crystallization kinetics of PBS in the presence of C30B.

5.7 References

1. T. Ozawa. Kinetics of non-isothermal crystallization. Polymer 1971; 12:150-158 (DOI: 10.1016/0032-3861(71)90041-3).
2. M. Avrami. Kinetics of phase change I. General theory. Journal of Chemical Physics 1939; 7:1103-1112 (doi:10.1063/1.1750380).

3. A. Jeziorny. Parameters characterizing the kinetics of the non-isothermal crystallization of poly(ethylene terephthalate) determined by DSC. Polymer 1978; 19:1142-1144 (DOI:10.1016/0032-3861(78)90060-5).
4. T. Liu, J. Petermann. Multiple melting behaviour in isothermally cold-crystallized isotactic polystyrene. Polymer 2001; 42:6453-6461 (DOI:10.1016/S0032-3861(01) 00173-2).
5. Y. Kong, J.N. Hay. Multiple melting behaviour of poly(ethylene terephthalate). Polymer 2003; 44:623-633 (DOI:10.1016/S0032-3861(02)00814-5).
6. S.Y. Hobbs, C.F. Pratt. Multiple melting in poly(butylene terephthalate). Polymer 1975; 16:462-464 (DOI:10.1016/0032-3861(75)90258-X).
7. F.J. Medelling-Rodriguez, P.J. Phillips, J.S. Lin, R. Campos. The triple melting behaviour of poly(ethylene terephthalate): Molecular weight effects. Journal of Polymer Science Part B: Polymer Physics 1997; 35:1757-1774 (DOI: 10.1002/(SICI)1099-0488(199708)35:11<1757).
8. E.S. Yoo, S.S. Im. Melting behaviour of poly(butylene succinate) during heating scan by DSC. Journal of Polymer Science Part B: Polymer Physics 1999; 37:1357-1366 (DOI: 10.1002/(SICI)1099-0488(19990701)37:13<1357).
9. S. Sinha Ray, M. Bousmina. Crystallization behaviour of poly[(butylene succinate)-co-adipate] nanocomposite. Macromolecular Chemistry and Physics 2006; 207:1207-1219 (DOI: 10.1002/macp.200600163).
10. O. Yu-Chun, S. Ma-Yu, Y. Zhong-Zhen. Nonisothermal crystallization kinetics of in situ polyamide-6 blended with poly(phenylene oxide). Journal of Applied Polymer Science 1999; 73:767-775 (DOI: 10.1002/(SICI)1097-4628(19990801)73:5<767).
11. K. Chrissafis, K.M. Paraskevopoulos, D.N. Bikiaris. Thermal degradation mechanism of poly(ethylene succinate) and poly(butylene succinate): Comparative study. Thermochimica Acta 2005; 435:142–150 (DOI:10.1016/j.tca.2005.05.011).

CHAPTER 6

THERMAL AND THERMOMECHANICAL PROPERTIES OF POLY(BUTYLENE SUCCINATE) NANOCOMPOSITES

6.1 Overview

This chapter describes the thermal and thermomechanical properties of poly(butylene succinate) (PBS) and its nanocomposites. PBS nanocomposites with three different weight ratios of organically modified synthetic fluorine mica (OMSFM) were prepared by melt-mixing in a batch mixer at 140 °C. The structure and morphology of the nanocomposites were characterized by x-ray diffraction (XRD) analysis and transmission electron microscopy (TEM), that reveal the homogeneous dispersion of the intercalated silicate layers in the PBS matrix. The thermal properties of pure the PBS and nanocomposite samples were studied by both conventional and temperature modulated differential scanning calorimetry (DSC), which showed multiple melting behaviour of the PBS matrix. The investigation of the thermomechanical properties was performed by dynamic mechanical analysis. The results reveal a significant improvement in the storage modulus of neat PBS upon addition of OMSFM. The tensile modulus of neat PBS was also significantly increased with the addition of OMSFM, but the strength at yield and elongation at break of neat PBS systematically decreased with the loading of OMSFM. The thermal stability of the nanocomposites compared to that of the pure polymer sample was examined under both pyrolytic and thermo-oxidative environments. The thermal stability of PBS increased moderately in the presence of 3 wt. % of OMSFM, but there is no significant effect on further silicate loading in the oxidative environment. In the nitrogen environment, however, the thermal stability systematically decreased with increasing clay loading.

6.2 Nanocomposite structure

The structure of the polymer/layered silicate (PLS) nanocomposites was elucidated using XRD patterns and TEM observations. XRD patterns offer a convenient method to determine

the interlayer spacing of the silicate layers in the original layered silicate and in the intercalated PLS nanocomposites. TEM observations allow a qualitative understanding of the internal structure through direct visualization. Direct evidence of the intercalation of the polymer chains into the silicate galleries is provided by the XRD patterns in the range of 2θ = 1–10° as presented in Figure 6.1 for the OMSFM powder and the nanocomposite sheets. The mean interlayer spacing of the (001) plane ($d_{(001)}$) for the pure OMSFM powder obtained by XRD measurement is 2.08 nm (2θ = 4.2°). In the case of the PBS/clay nanocomposite with 3 wt.% nanoparticles (PBSCN3), the characteristic peak of OMSFM completely disappears, indicating the formation of an exfoliated structure. In the XRD pattern of the PBS/clay nanocomposite with 6 wt.% nanoparticles (PBSCN6), the intensity of the characteristic peak of OMSFM is significantly reduced and a sharp peak is observed at 2θ = 2.76°, corresponding to the (001) plane of the intercalated silicate layers dispersed in the PBS matrix, accompanied by two small peaks at 5.62° and 8.52°. After calculation, it is confirmed that these peaks are respectively due to the reflection from the (002) and (003) planes of the intercalated silicate layer in the PBS matrix. With increasing OMSFM content, the intensity of these peaks increased significantly, but their positions remained the same. This observation is due to the decrease in the percentage of intercalating polymer chains, and increased parallel stacking of the intercalated silicate layers with increasing OMSFM content.

The width of the XRD peak, β (measured by the full-width at half-maximum), is inversely proportional to the coherence length of scattering entities, D, and therefore reflects the coherent order of the silicate layers [1]. Because the width of the basal spacing of the OMSFM decreased after nanocomposite preparation with PBS, the coherency of the intercalated OMSFM layers was much higher than that of the un-intercalated OMSFM layers and increased with increasing OMSFM content. The XRD results indicate that the PBS chains were intercalated and had a strong effect on the crystal structure of OMSFM, The coherence length of the intercalated silicate crystallites also changed with increasing OMSFM content.

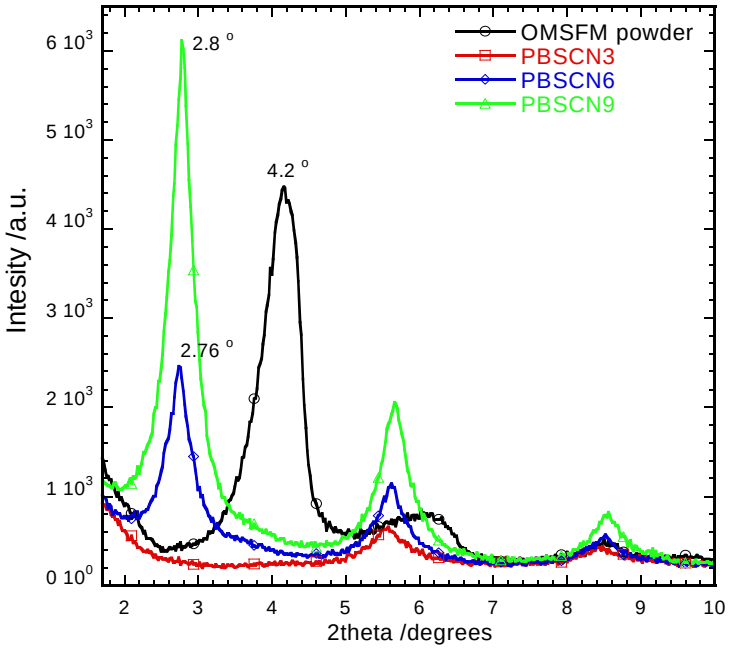

Figure 6.1 X-ray diffraction patterns of organically modified synthetic fluorine mica (OMSFM) and three different nanocomposites (PBSCNs)

The dispersability of the intercalated layered silicate particles in the PBS matrix was directly observed *via* TEM analyses. Figure 6.2 shows the TEM bright field images of various PBSCNs corresponding to the XRD patterns as shown in Figure 6.1, in which dark entities are the cross section of the intercalated silicate layers. The figures show both larger views, illustrating the dispersion of the silicate particles within the PBS matrix, and a higher magnification, permitting the observation of discrete silicate layers. Figure 6.2a is a bright field TEM image of PBSCN3. Although the XRD pattern of PBSCN3 is featureless, the stacking of some silicate layers is readily observable, and this is more discernible with the high magnification TEM image as presented in Figure 6.2a'.

It is very difficult to make a final conclusion about the structure of the nanocomposite exhibiting the featureless diffraction pattern on the basis of the XRD alone. In general, many factors other than layer disorder, such as intercalate composition and silicate concentration, may contribute to a featureless diffraction pattern [2]. Figures 6.2b and c represent the bright field TEM images of PBSCN6 and PBSCN9. The TEM images for both PBSCNs reveal that there are some intercalated stacked and disordered and/or exfoliated silicate-layers coexisting in the nanocomposites. The stacked intercalated silicate layers are responsible for the strong XRD diffractions observed in Figure 6.1 for PBSCN6 and PBSCN9, whereas the disordered

and delaminated silicate layers had no periodic stacking and thus remained XRD silent. These kind of mixed intercalated and exfoliated structures originate from the chemical and size inhomogeneities of the silicate layers. Typically the larger in-lateral-size silicate layers create a stacked intercalated structure, whereas the smaller layers tend to exfoliate [3].

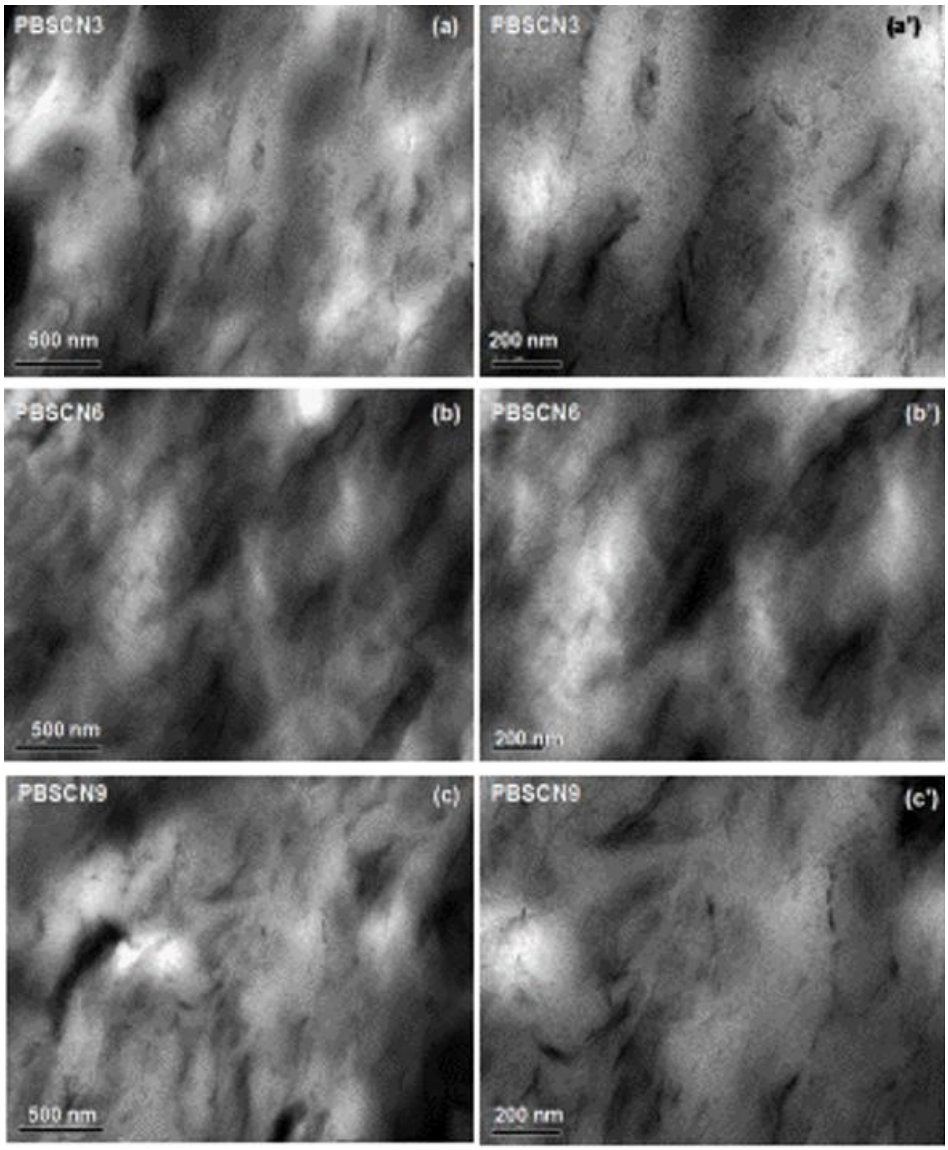

Figure 6.2 Bright field transmission electron microscopy images of various nanocomposites at two different magnifications in which dark entities are the cross section of the intercalated/delaminated silicate layers

6.3 Thermal properties

To understand the effect of OMSFM loading on the melting behaviour of the neat PBS sample, DSC analyses of compression moulded samples were conducted at a heating rate of

20 °C min^{-1} and the heating curves of the pure polymer and three different nanocomposite samples are shown in Figure 6.3. To have identical thermal history of all the samples, the samples were kept at 60 °C for 6 h under vacuum, before starting each set of experiments. It is clear from the figure that all the samples show three endothermic melting peaks for PBS, labelled as I, II, and III from low to high temperature and one recrystallization peak in between the last two melting peaks.

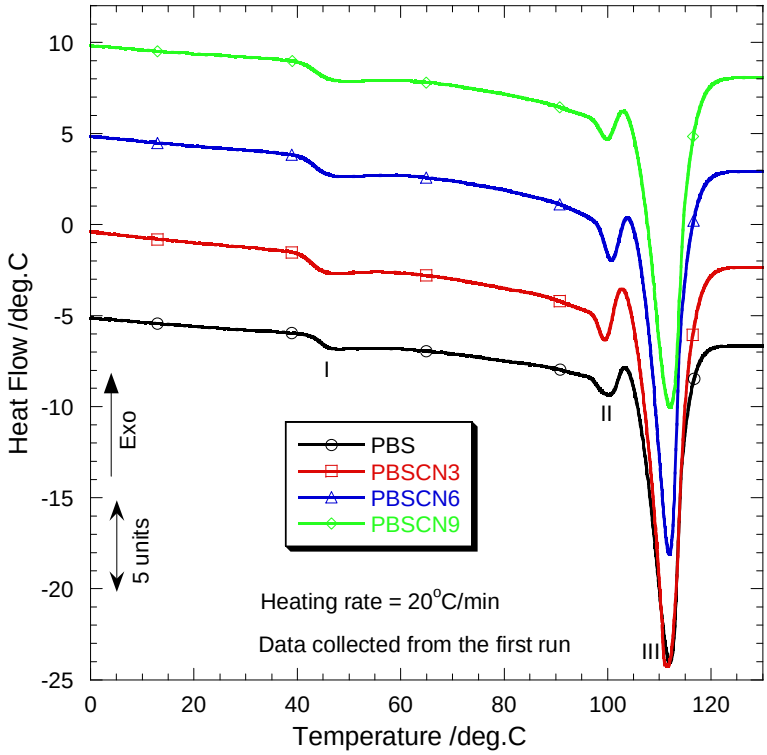

Figure 6.3 First heating DSC curves of the compression molded samples of neat PBS and the three different nanocomposites

There are several models that explain the multiple melting behaviour of thermoplastic semicrystalline polymers, of which the most important one is the presence of melting, re-crystallization, and re-melting phenomena [4-6]. According to this model, the first step is the melting and recrystallization of the lower melting crystallites with lower thermal stability. This is followed by the melting of the crystallites with higher thermal stability formed through the re-crystallization of the crystallites molten at lower temperatures.

To verify the presence of melting, re-crystallization, and re-melting phenomena, both the pure polymer and the nanocomposite (here we chose PBSCN6 as a model system) samples were

scanned at different heating rates of 2, 5, 10, 15 and 20 °C min^{-1}. The results are presented in Figure 6.4. In the case of the PBS sample (Figure 6.4a), the endotherm 'III' is shifted towards a higher temperature with increasing the heating rate, while the endotherm 'I' becomes more prominent and systematically moves to a lower temperature, and endotherm 'II' appears between these two endotherms. Another interesting feature is that the re-crystallization process is becoming more important with increasing heating rate. This observation indicates that the melting and recrystallization processes are operative at the same time for the higher temperature endotherm. At a very low heating rate, the sample passes through the re-crystallization process slowly, so there is more than enough time for the molten sample to reorganize into new crystals. For this reason only endotherm 'III' is well defined at a very slow heating rate of 2°C min^{-1}. However, at a higher heating rate (more than 5°C min^{-1}), the sample passes through the recrystallization region so rapidly that there is not enough time for the molten sample to reorganize into new crystals. For this reason, the reorganization process is largely inhibited as the heating rate increases and at the same time the number of perfect crystals decreases, which finally contributes to the decrease in the peak temperature of endotherm 'III'. These observations indicate that the presence of melting, re-crystallization, and melting phenomena are actually responsible for the multiple melting behaviour of the PBS sample. The PBSCN6 sample shows the same type of behaviour; however, all the melting endotherms are at lower temperatures compared to the neat PBS sample. Two possible effects may be responsible for the shift of melting endotherms towards lower temperatures in the case of the PBSCN6 sample. The first is the decrease in the matrix molecular weights after nanocomposite preparation with OMSFM. However, the GPC results (Table 6.1) show that there is no degradation of the PBS matrix after nanocomposite preparation. Therefore the matrix molecular weights are not responsible for the shift of melting endotherms towards lower temperatures. A second reason is the restricted movement of the polymer chains. Because of the homogeneous dispersion of the intercalated silicate layers in the PBS matrix (TEM observations), the silicate layers act as obstacles for the mobility and flexibility of the polymer chains to fold and join the crystallization growth front. That means the overall per cent of crystallinity of the PBS matrix decreases in the presence of OMSFM and, as a result, all the enothermic peaks were less intense and shifted towards lower temperatures compared to neat the PBS.

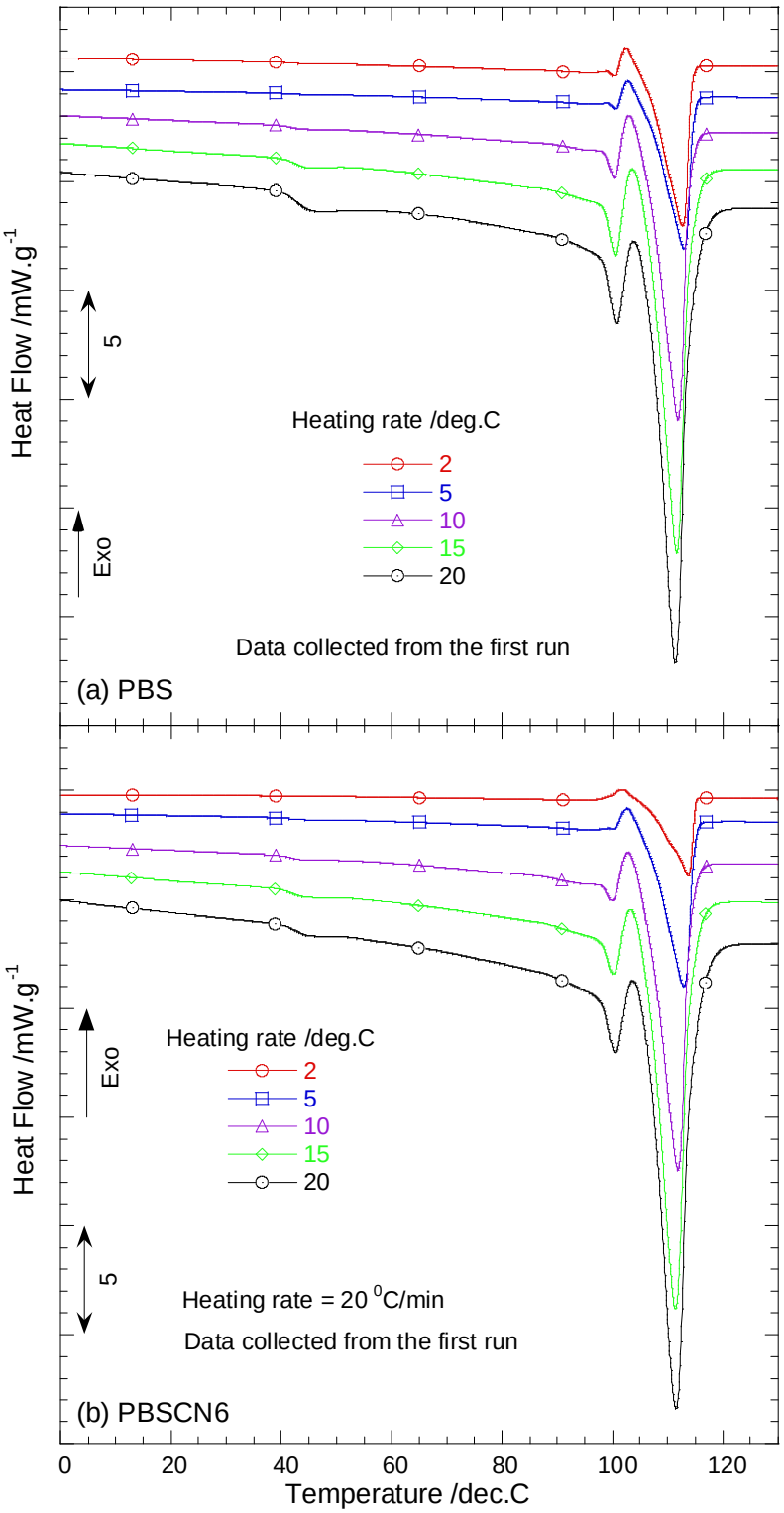

Figure 6.4 Heating rate dependence of DSC curves of compression moulded samples of neat PBS and PBSCN6

Table 6.1 GPC results of neat PBS and various nanocomposites

Sample	M_w x 10^{-3} g/mol	M_w/M_n
PBS	**112**	**2.1**
PBSCN3	**113**	**2.2**
PBSCN6	**111**	**2.2**
PBSCN9	**114**	**2.1**

To support the above melting phenomena of PBS, temperature modulated DSC (TMDSC) was used. TMDSC generally applies a sinusoidal temperature oscillation (modulation) during heating in a conventional DSC, and causes the total heat flow (as obtained from the conventional DSC) to be separated into heat capacity related (reversible) and kinetic related (non-reversible) components. Therefore, TMDSC allows us to see if a re-crystallization process occurs as soon as PBS begins to melt.

Parts a and b of Figure 6.5 show the TMDSC curves of the neat PBS and PBSCN6 samples that were heated at a heating rate of 2°C min^{-1} (annealed samples were used) from -60°C. For both samples the total heat flow (middle curve) is separated into a well defined reversible heat flow (bottom curve) and a non-reversible heat flow (top curve). For the neat PBS sample, the following behaviour is observed: Firstly, a well-distinguished re-crystallization signal is recorded in the three curves, and at the same time a melting signal is observed in the non-reversible curve. Secondly, the signal intensity of the re-crystallization exotherm in the non-reversible signal is enhanced significantly compared to the exotherm recorded in the reversible and the total heat flow curves. This observation may be due to the continuous partial melting and perfection of crystals at temperatures before their final melting. The non-reversible curve of the PBSCN6 sample shows a 'four-fingers' like behaviour i.e. crystallization – melting – re-crystallization – re-melting phenomena. We believe that this behaviour may be due to the presence of short chain segments. These chain segments remain attached to the crystal surfaces and they set up a local equilibrium of crystallization – melting – re-crystallization – remelting. Because of these phenomena all the crystals are molten in the reversible heat flow. For this reason, melting is more important in the reversible heating. Although the reversible and the total heat flow curves of the PBSCN6 sample show the same behaviour as observed in the case of the neat PBS sample, all endothermic and exothermic

peaks are shifted towards lower temperatures. This is again due to the restricted movement of the polymer chains in the nanocomposite.

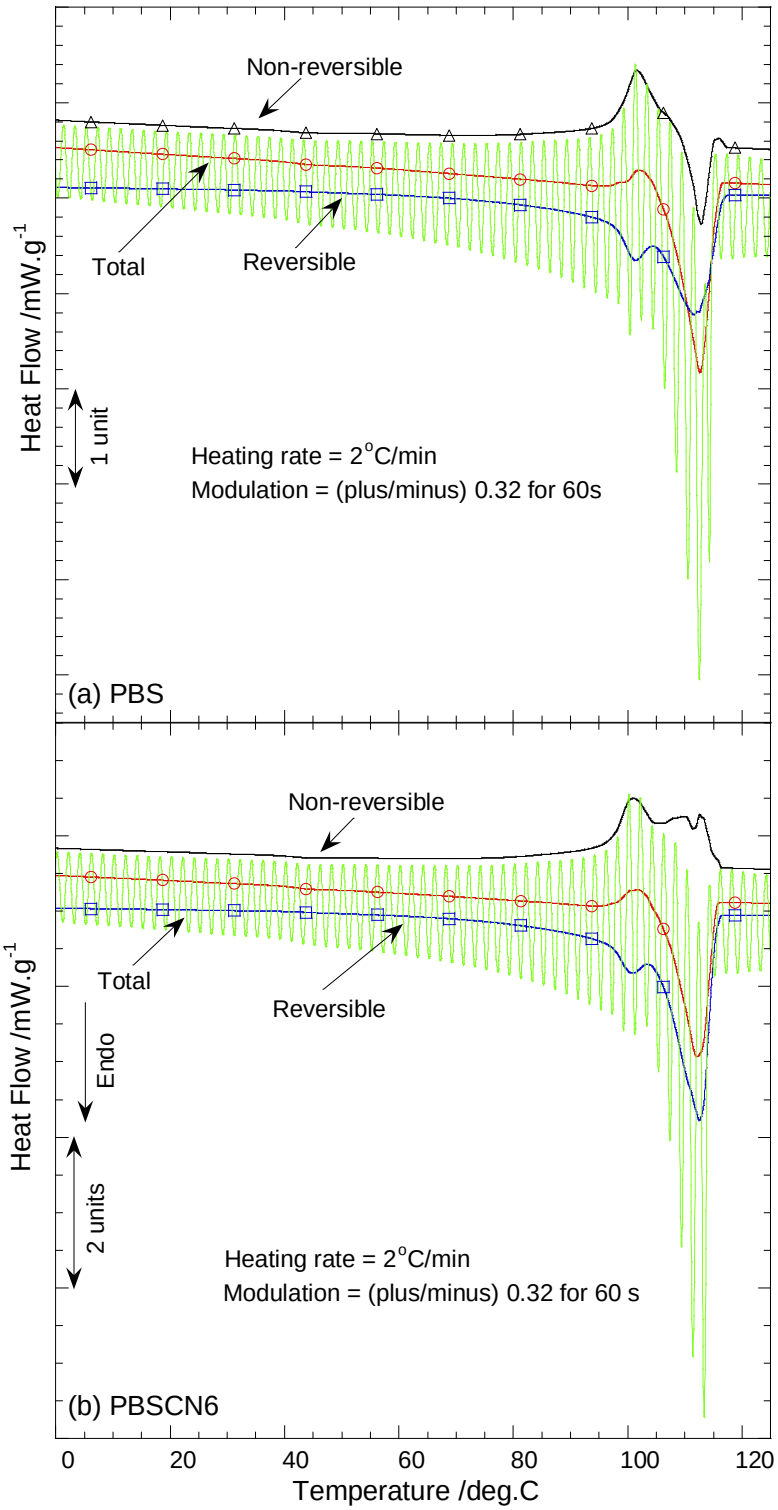

Figure 6.5 First heating TMDSC curves of compression moulded samples of neat PBS and PBSCN6. Heating rate 2°C min^{-1} with an amplitude of ± 0.32 °C, and a period of 60 s

The above results and discussion, in the case of both samples, clearly confirm that the multiple melting behaviour of the PBS matrix originates from the melting and recrystallization of the low melting crystallites with lower thermal stability. The higher melting endotherm corresponds to the melting of the crystallites with higher thermal stability formed through the recrystallization of the crystallites formed after melting at lower temperatures.

To study the influence of cooling rate during non-isothermal crystallization on the melting behaviour of PBS, all the samples were heated at a rate of 20°C min^{-1} directly from -60 °C as soon as the cooling has finished. Parts 'a' and 'b' of Figure 6.6 represent the subsequent melting behaviour of PBS and the PBSCN6 nanocomposite samples that were non-isothermally crystallized from the melt (150 °C) at cooling rates ranging from 2 to 20 °C min^{-1}. The total heat of fusion (ΔH_{en}) of the two melting peaks of the PBS, estimated by integration of the area under the endothermic region of the DSC curves, decreased with the addition of OSFM (see Table 6.2), indicating that the degree of crystallinity of PBS is decreased by inorganic phase incorporation [7]. An interesting observation is that, for both samples, two melting endotherms and one small re-crystallization exotherm appear after they have been crystallized non-isothermally from the melt at a rate of 20°C min^{-1}. But when the compression molded samples were heated at the same heating rate (see Figure 6.3), they show triple melting endotherms. This result indicates that the crystals, associated with melting endotherm I in Figure 6.3, do not form during non-isothermal crystallization at all cooling rates in Figure 6.6.

In the case of neat PBS, endotherms 'II' and 'III' appear perfect when the sample was crystallized non-isothermally from the melt at a cooling rate of 20°C min^{-1}. However, with decreasing cooling rate, the endotherm 'II' systematically shifts towards a higher temperature, whereas the endotherm 'III' moves in the opposite direction, and both endotherms become less resolved. At the very slow cooling rate of 2°C min^{-1}, both endotherms merge into one broad melting endotherm. This observation indicates that with decreasing the cooling rate, the crystal growth associated with both melting endotherms become equally important and controls the total melting behaviour. The nanocomposite sample also shows the same type of behaviour as PBS, except for an increase in peak sizes of the nanocomposite. This is due to

the effect of clay on the crystal size after non-isothermal crystallization. From the lower heat of fusion values of the nanocomposite we can conclude that the clay reduced the crystal size of the PBS in the nanocomposite.

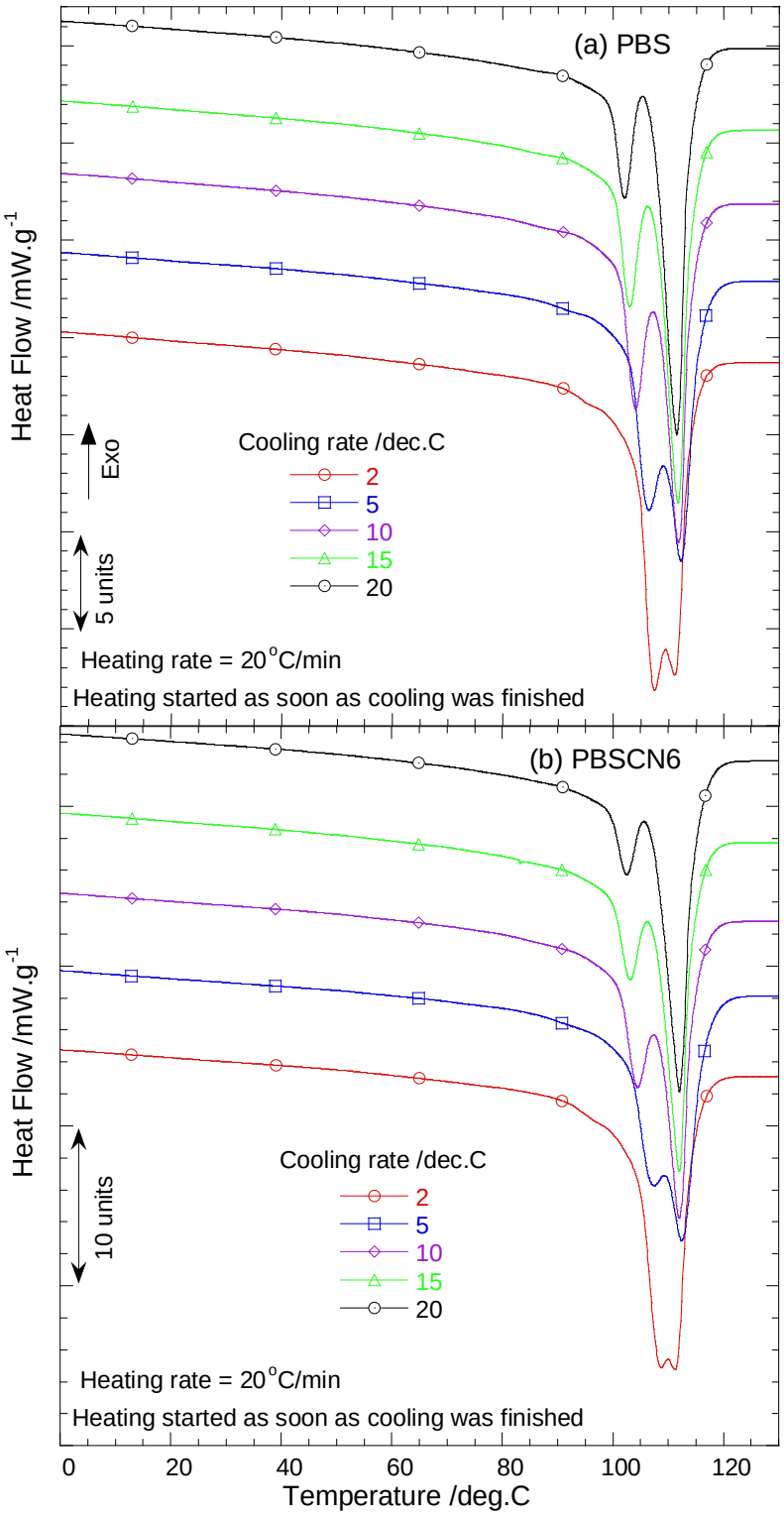

Figure 6.6 Melting behaviour of PBS and the PBSCN6 samples after non-isothermal crystallization at different cooling rates.

Table 6.2 Cooling rate dependence of the total heat of fusion (ΔH_{en}) obtained from the two melting peaks of PBS estimated by integration of the area under the endothermic region of the DSC curves

Sample	Cooling rate / °C min^{-1}	ΔH_{en} / J g^{-1}
PBS	**2**	**120.2**
	5	**116.3**
	10	**115.1**
	15	**107.5**
	20	**85.9**
PBSCN6	**2**	**96.8**
	5	**84.2**
	10	**83.9**
	15	**84.2**
	20	**81.9**

6.4 Dynamic mechanical analysis (DMA)

DMA measures the response of a given material to an oscillatory deformation (here in tension-torsion mode) as a function of temperature. DMA results are expressed by three main parameters: (a) the storage modulus (*G*') corresponding to the elastic response to the deformation; (b) the loss modulus (*G*"), corresponding to the plastic response to the deformation; and (c) tan δ, that is, the (*G*"/*G*') ratio, useful for determining the occurrence of molecular mobility transitions such as the glass transition. We used DMA analysis to track the temperature dependence of *G*', *G*", and tan δ of neat PBS upon nanocomposite formation with three different loadings of OMSFM. Figure 6.7 shows the temperature dependence of *G*', *G*", and tan δ for neat PBS and the corresponding nanocomposites. At low temperatures both the polymer and the nanocomposites are in a glassy state. PBS is characterized by an apparent glass transition (T_g) at about -38 °C, that was revealed by a steep decrease in G' followed by a rubbery plateau. The matrix T_g was not affected significantly by OMSFM incorporation. However, over the entire measuring temperature range, G' of all PBSCNs was always higher than that of the neat PBS. G' of neat PBS dramatically increased upon the addition of 3 wt. % of OMSFM. The G' of the PBSCNs systematically increased with increasing the OMSFM

content. This behaviour may be due to the very high degree of intercalation of polymer chains into the silicate layers of OMSFM in the case of PBSCN3 (as observed in the XRD patterns and TEM images), which leads to a large surface area for interactions between the filler surface and the polymer matrix. The polymer chains inside the silicate galleries are immobilized and the effect of immobilization on the polymer chains may be the main factor responsible for this dramatic increase in G' in the case of PBSCN3.

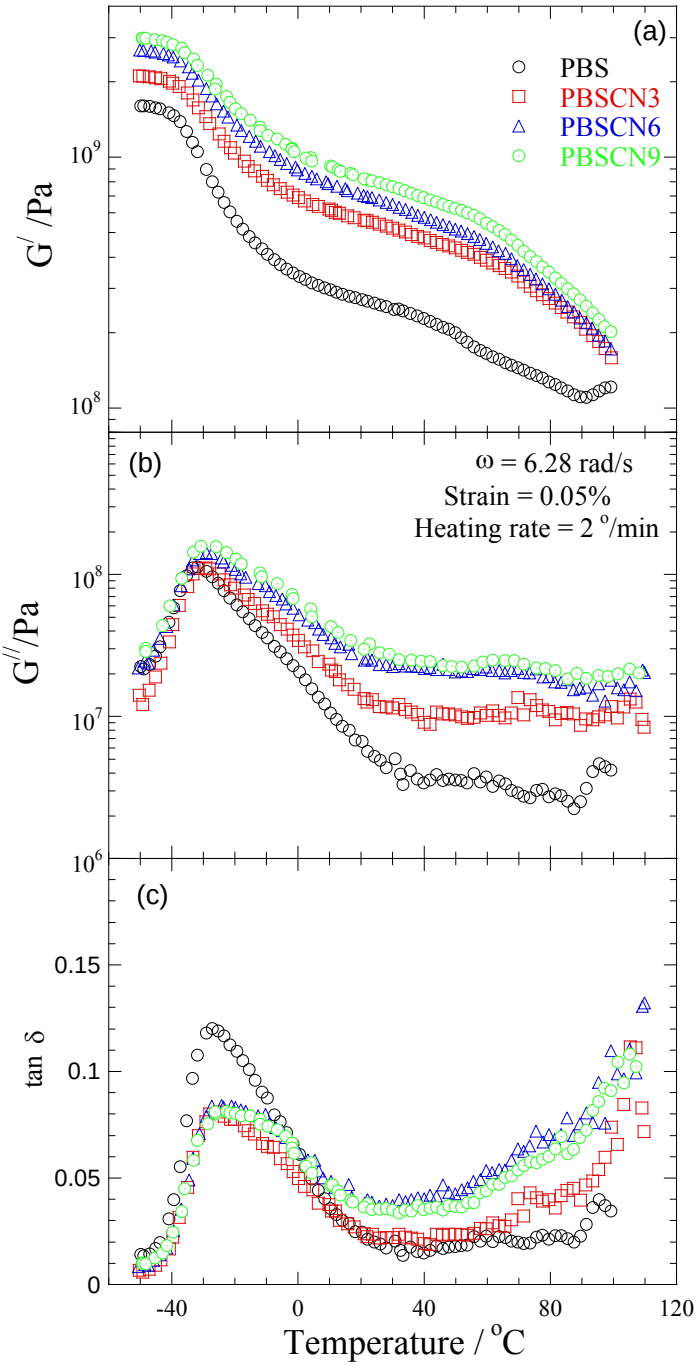

Figure 6.7 Temperature dependence of storage modulus (G'), loss modulus (G"), and tan δ of neat PBS and PBSCN6 samples.

The incorporation of OMSFM in the PBS matrix resulted not only in a substantial increase in elasticity, but also in internal frictions, as revealed by a quite similar substantial increase in G". However, the presence of OMSFM does not lead to a significant shift and broadening of the tan δ curves for all PBSCNs compared to that of neat PBS. This behaviour has been ascribed to the unrestricted segmental motions in the organic-inorganic interface neighbourhood of intercalated PBSCNs [8].

6.5 Tensile properties

The tensile properties of neat PBS and the three different PBSCNs are reported in Figure 6.8. From these figures, it is clear that the tensile modulus of PBS systematically improved with OMSFM loading. However, the yield strength and the elongation at break of the PBS systematically decreased with the addition of OMSFM. This behaviour may be due to the addition of OMSFM, leading to increased brittleness of the PBS matrix. The significant increase in the modulus for such low clay concentrations cannot be attributed simply to the introduction of the higher modulus inorganic filler layers. A theoretical approach assumes a layer of affected polymer on the filler surface, with a much higher modulus than the equivalent bulk polymer [9]. This affected polymer can be thought of as the region of the polymer matrix that is physic-sorbed onto the silicate surface, and is thus stiffened through its affinity for and adhesion to the filler surfaces. Obviously, for such high aspect ratio fillers as our layered silicates, the surface areas exposed to the polymer are large, and the significant increases in the modulus at low filler content are not surprising. This behaviour is also ascribed to the resistance exerted by the clay itself and to the orientation and aspect ratio of the intercalated silicate layers. Additionally, the stretching resistance of the oriented backbone of the polymer chain in the gallery also contributed to enhancing the modulus.

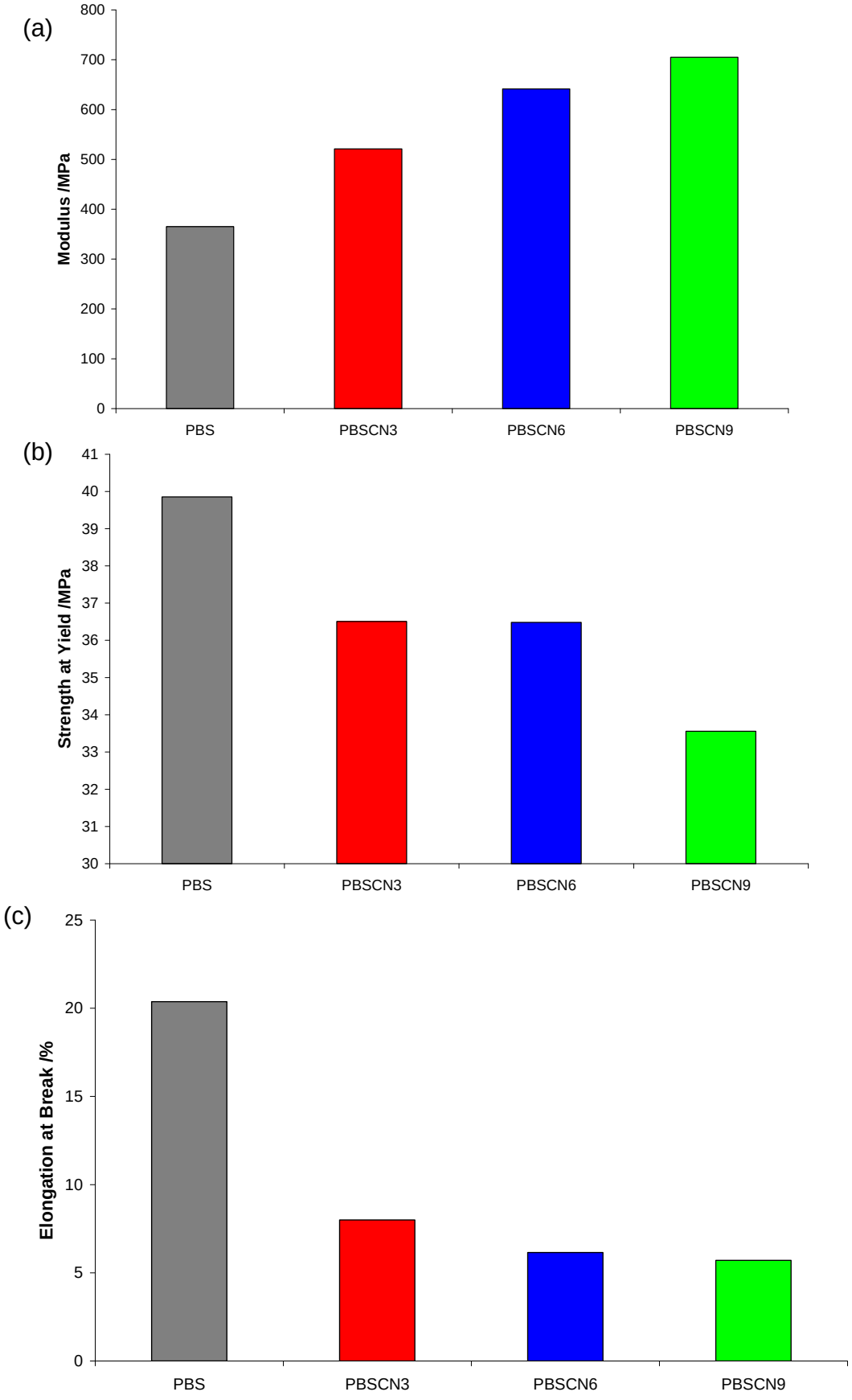

Figure 6.8 Tensile properties of neat PBS and the various nanocomposites: (a) modulus, (b) yield strength, and (c) elongation at break

6.6 Thermogravimetric analysis (TGA)

The TGA curves of the neat PBS and the three different nanocomposites obtained under pyrolytic and thermo-oxidative conditions are presented in Figure 6.9. It is clear from the figure that with the addition of 3 wt.% of OMSFM, the stability of PBS significantly increased in both environments. The higher thermal stability of the PBSCN3 can be attributed to the homogeneous dispersion of the intercalated silicate layers which by nature has a much higher thermal stability [10]. When further increasing the filler content, a decrease in thermal stability was observed. This behaviour is explained by the relative extent of exfoliation/delamination as function of the amount of OMSFM. With increasing the OMSFM loading, the stability of the PBSCNs remains the same in the oxidative environment because of the lower permeability of the oxygen. This can be attributed to the exfoliated and intercalated (mixed) morphology of the nano-clay in the polymer matrix, as shown by the TEM and XRD results. In the nitrogen environment the thermal stability of PBSCN9 is lower than that of the other nanocomposite samples. This is because of the more reactive hydroxyl groups in the organically modified nano-clay that produce reactive species and accelerated the thermal degradation of the polymer.

6.7 Conclusions

In the present study we have systematically investigated the effect of different loadings of organically modified synthetic fluorine mica on the thermal and thermomechanical properties of PBS. XRD patterns and TEM observations show the homogeneous dispersion of intercalated silicate layers in the PBS matrix. This may be due to the moderate interaction between the CO groups present in the PBS matrix with the hydroxyl groups present in the surfactant. For both neat PBS and nanocomposite samples the observed multiple melting behaviour is associated with melting, re-crystallization, and re-melting phenomena. The lower melting temperatures and heats of fusion of the nanocomposite samples are due to the homogeneous dispersion of intercalated silicate layers in the PBS matrix. The homogeneous dispersion of the intercalated silicate layers hinders local lamellar crystallization and leads to a decrease in the overall degree of crystallinity and hence to a lower melting temperature. The homogeneous dispersion of silicate layers in PBS leads to a significant improvement in the temperature dependence of the storage modulus; there is, however, a very moderate improvement in the loss modulus. The nanocomposites were thermally more stable in an

environment compared to a nitrogen environment. This was probably due to the formation of exfoliated and intercalated (mixed) morphology of the nano-clay in the polymer matrix which inhibited the diffusion of oxygen into the matrix.

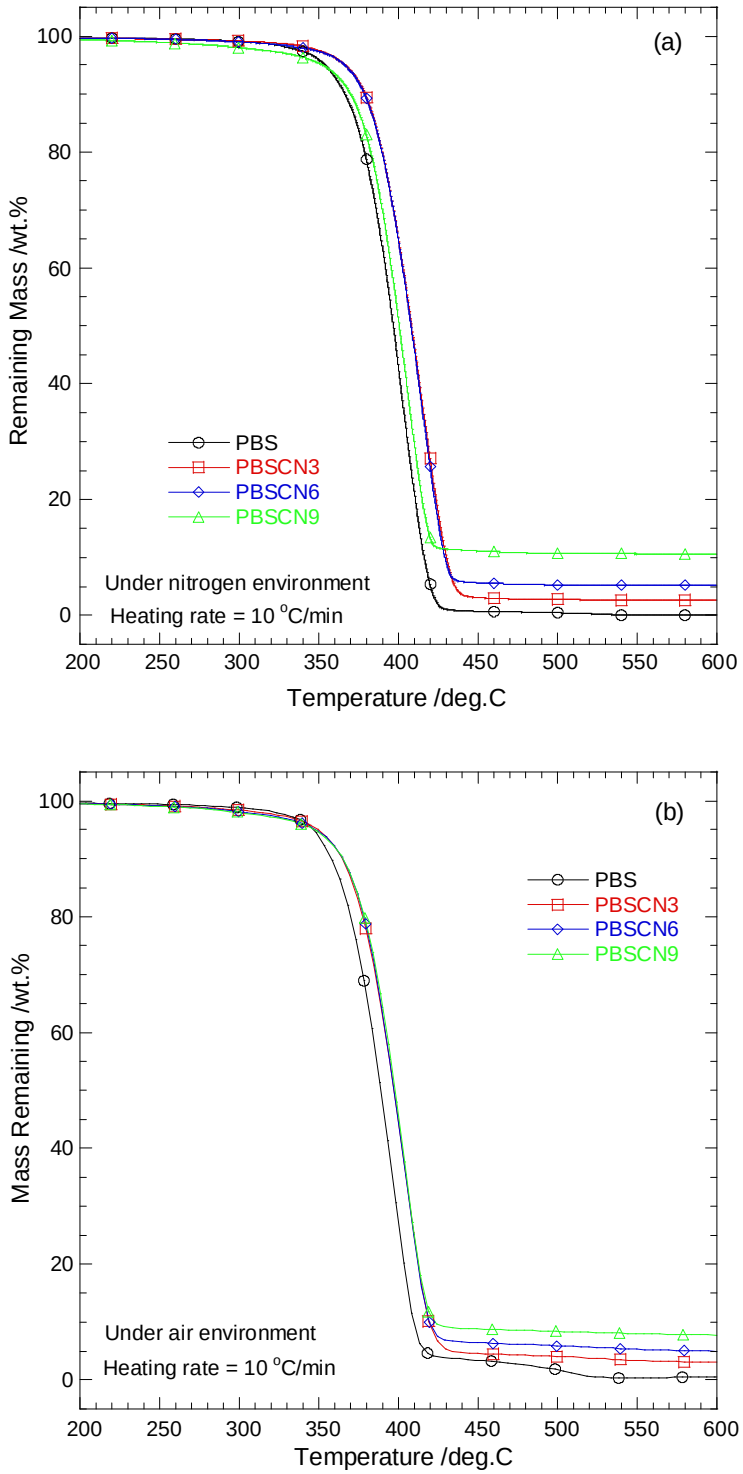

Figure 6.9 TGA curves of neat PBS and the nanocomposite samples: (a) under nitrogen atmosphere and (b) under air atmosphere

6.8 References

1. V.A. Dritis, C. Tchoubar. X-ray Diffraction by Disordered Lamellar Structures: Theory and Applications to Microdivided Silicates and Carbons. Springer-Verlag: New York (1991) p.21-22.
2. B.D. Cullity. Principles of X-ray Diffraction. Addison-Wesley: Rading, MA (1978).
3. S. Sinha Ray, K. Yamada, M. Okamoto, A. Ogami, K. Ueda. New polylactide-layered silicate nanocomposite: nanoscale control over multiple properties. Macromolecular Rapid Communications 2002; 23:943-947 (DOI: 10.1002/1521-3927(200211)23: 16<943).
4. Y. Kong, J.N. Hay. Multiple melting behaviour of poly(ethylene terephthalate). Polymer 2003; 44:623-633 (DOI:10.1016/S0032-3861(02)00814-5).
5. S.Y. Hobbs, C.F. Pratt. Multiple melting in poly(butylene terephthalate). Polymer 1975; 16:462-464 (DOI:10.1016/0032-3861(75)90258-X).
6. F.J. Medelling-Rodriguez, P.J. Phillips, J.S. Lin, R. Campos. The triple melting behaviour of poly(ethylene terephthalate): molecular weight effects. Journal of Polymer Science Part B: Polymer Physics 1997; 35:1757-1774 (DOI: 10.1002/(SICI)1099-0488(199708)35:11<1757).
7. S. Sinha Ray, M. Bousmina. Crystallization behaviour of poly[(butylene succinate)-co-adipate] nanocomposite. Macromolecular Chemistry and Physics 2006; 207:1207-1219 (DOI: 10.1002/macp.200600163).
8. S. Sinha Ray, P. Maiti, M. Okamoto, K. Yamada, K. Ueda. New polylactide-layered silicate nanocomposites. 1. Preparation, characterization and properties. Macromolecules 2002; 35:3104–3110 (DOI: 10.1021/ma011613e).
9. D. Shia, C.Y. Hui, S.D. Burnside, E.P. Giannelis. An interface model for the prediction of Young's modulus of layered silicate-elastomer nanocomposites. Polymer Composites 1998; 19:608-615 (DOI: 10.1002/pc.10134).
10. S.T. Lim, Y.H. Hyun, H.J. Choi, M.S. Jhon. Synthetic biodegradable aliphatic polyester/montmorillonite nanocomposites. Chemistry of Materials 2002; 14:1839-1844 (DOI: 10.1021/cm010377j).

CHAPTER 7

SUMMARY AND REMARKS

New environmental polices, societal concerns, and growing environmental awareness triggered the search for new products and processing methods that are benign with the environment. Biodegradable polymers are considered as an alternative to the existing petroleum-based plastics. The morphologies and properties of some of the biodegradable polymers, and the nanocomposites prepared by introducing organically modified layered silicates into these polymers, have been discussed in this thesis. The following important observations were made and discussed:

a) Highly dispersed silicate particles accelerated the nucleation and crystal growth of PES by offering a large surface area and also by stopping the super-cooling phenomenon of the PES matrix during non-isothermal crystallization.
b) There was a significant improvement in the thermal stability of the PES after nanocomposite formation.
c) The Cloisite 30B nano-clay particles in the PBS matrix seemed to have hindered the local lamellar crystallization which led to a decrease in the overall degree of crystallinity and hence to a lower melting temperature.
d) The Ozawa equation did not provide an adequate description of the non-isothermal crystallization of PBS and its nanocomposite, while the Avrami analysis modified by Jeziorny and the method developed by Liu et al. were successful in describing the non-isothermal crystallization process and support the lower crystallization kinetics of PBS in the presence of Cloisite 30B.
e) With different loadings of OMSF, different morphologies were achieved, i.e. exfoliated, mixed and intercalated morphologies.
f) The homogeneous dispersion of silicate layers in PBS led to a dramatic improvement in the temperature dependence of the storage modulus and a very moderate improvement in the loss modulus.

The above improved properties are generally achieved at low silicate content (3 to 6 wt. %). These improved properties are very important to obtain fully crystallized PES nanocomposite based products or parts in an injection moulding cycle. The crystallization kinetics is also

important in the manufacturing industries for they will help to know how fast or slow materials will cool down. In summary, nanocomposites with various types of organically modified silicate layers will have to be looked at in future as OMSF and OMMT have not been researched for other properties. Many properties such as biodegradability, gas barrier properties and heat distortion temperature of these nanocomposites are also important.